University of Stavanger

Faculty of Science and Technology

MASTER'S THESIS

Study program/ Specialization: Petroleum Engineering / Reservoir Engineering	Spring semester, 2015 Open
Writer: Inger Karin Dirdal	…… (Writer's signature)
Faculty supervisor: Steinar Evje	
Thesis title: A mathematical model for flow of gas-liquid mixture in a vertical pipe	
Credits (ECTS): 30	
Key words: Two-phase flow Mathematical model Numerical solution Taylor bubble Ascend velocity	Pages: 97 + enclosure: 6 Stavanger, 15.06.2015

University of Stavanger
The Faculty of Science and Technology

Master Thesis in Petroleum Engineering

A mathematical model for flow of gas-liquid mixture in a vertical pipe

by

Inger Karin Dirdal

Spring 2015

ABSTRACT

A one-dimensional mathematical model for the ascend velocity to a Taylor bubble consisting of gas in a two-phase flow of gas and liquid in vertical pipes is derived. This model illustrates different effects of two-phase flow in pipes from a numerical approach. The model is based on the conservation laws of mass and momentum for an initial gas slug located on the closed of bottom in a pipe which is filled with stagnant liquid. The model is investigated at laboratory scale where assumptions as incompressible fluids, no viscosity terms, no acceleration effects and equal phase pressure are made. By use of the assumptions was the conservation of mass for liquid reduced to following expression.

$$\partial_t \alpha_l + \partial_x h(\alpha_l) = 0$$

Where the sum of volume fractions are given as $\alpha_g + \alpha_l = 1$. The derivation lead to an expression of the superficial velocity of liquid depending on the liquid volume fraction (α_l), gravitational acceleration (g), density difference between liquid and gas ($\Delta\rho$) and friction between fluids and wall (f_g and f_l) as well as interfacial tension (C), as the expression below indicates.

$$h(\alpha_l) = u_{ls} = -\frac{\alpha_l^2(1-\alpha_l)^2}{\alpha_l^2 f_g + (1-\alpha_l)^2 f_l + C}\Delta\rho g$$

The numerical solutions are found by implementing the derived model of the superficial liquid velocity into a MATLAB script for computing the solution. The numerical solutions is compared with an experimental case in addition to previous research on ascending Taylor bubbles of gas in pipes with liquid. The model corresponds well with results from previous experiments and observations made during performance of experiments. It gives a good estimation of the ascend velocity of the Taylor bubble, pressure, differential pressure and illustrate the characteristic nose shape of the Taylor bubble. The numerical solution is seen to be sensitive to how the friction terms are defined. The model also responds well with the result from previous research regarding the velocity of the ascending Taylor bubble independence of the gas layers length and shows good response on changes in interfacial tension.

ACKNOWLEDGEMENTS

I would like to express my utmost gratitude to my advisor Professor Steinar Evje, for his excellent guidance where good advices, support and patience have been invaluable.

I also grateful to senior engineer Herimonja Andrianifaliana Rabenjafimanantsoa who let me observe his experiments of ascending Taylor bubble. The opportunity to observe the different effects of ascending Taylor bubbles has been very useful during thesis.

Through this thesis I have become familiar with both LaTeX and MATLAB. I have found both of them to be quite useful software and I want to thank Steinar for all his help with my MATLAB works in addition to introducing me for LaTeX . I also want to thank fellow student, Kaia Olsen, for help and support with LaTeX as well as good company during writing of the thesis.

I also want to thank my family for support and motivation through this thesis. Especially my mother, Asbjørg Dirdal, for proofreading this thesis.

Contents

List of Figures

List of Tables

1 INTRODUCTION

1.1 Background

In two-phase flows of gas and liquid, the fluids can distribute themselves in many different ways. How the fluids are distributed during flow is a relevant mechanism in the industry today. In the petroleum industry, one can find two-phase flows in production and transportation of hydrocarbons, down in the reservoir and in gas kicks during drilling of wells. Gas kicks occurs when a well is drilled into a high-pressure zone containing gas. Due to the lower pressure in the well, the gas will flow in and rise upwards as a slug flow. This slug flow is characterized by a large continuous bubble of gas, also known as Taylor bubble. The Taylor bubble occupies large parts of the cross section of the pipe and are bullet shaped with a film of liquid between the bubble and the wall [15]. When the gas is detected in the well bore, the blow out preventer (BOP)must be closed and the flow controlled, either by circulate the gas out through a choke or by pumping fluid into the well and force the gas into the formation. If the flow is not controlled and BOP not closed a blow-out may occur [11, 23]. Therefore it is necessary to know how the gas will ascend and related effects to avoid hazardous effects as blow-out.

Two-phase slug flow of ascending Taylor bubble of gas in liquid have been a widely studied subject over the years, in order to get known with the different effects of ascending Taylor bubble and the related parameters. Laboratory experiments, modelling based on fundamental flow concepts and development of relationship between different parameters that affects the flow from fitting of data from experiments, have all been used to study the ascending Taylor bubble.

By laboratory experiments, several researchers have tried to find how different parameters affect the ascending Taylor bubble, and relate them to observed effects. Important parameters that have been shown to affect the flow are the inner diameter of pipe (D), density and viscosity of liquid (ρ_l and μ_l), gravitational acceleration (g) and interfacial tension (σ_{gl}) [15]. Relations for the velocities of the Taylor bubble based on experimental data have been proposed by different researchers [4, 5, 16]. While others have considered the effect of thickness of the liquid film [15, 17]. Investigations of dimensionless ratios of parameters relevant to flow and development of relationships between them and the effects from ascending Taylor bubble are also considered to get a full understanding of ascending Taylor bubbles [24, 26]. Modelling of two-phase flow of gas and liquid have been experimented on to find out how different effects of the ascending Taylor bubbles

may be determined by an analytical approach [10, 13, 21, 27]

1.2 Objectives

- In this thesis is a mathematical model derived to describe an ascending Taylor bubble of gas through stagnant liquid in a vertical conduit in one dimension. The model of consideration is based on the mathematical model for two-phase flow from Evje and Flåtten [6], which has been designed based on fundamental laws for flow of fluids in pipes, the laws of conservation of mass and momentum. The model is derived to investigate an ascending Taylor bubble at a laboratory scale and to illustrate the observed effects during performance of the laboratory experiments on ascending gas in a vertical pipe.

- A MATLAB code where the derived model is implemented computes the numerical solution. The numerical solution needs to be tested to see how changes in different parameters affect the model in order to find the sensitivity of the different terms and parameters the model is based on. This creates the need of a Base case of the model that can be compared with changes in different parameters to get known with the sensitivity. Especially, the sensitivity of changes in friction terms will be considered.

- Observation of performed laboratory experiment and previous research are considered in section 3, to get the full impression of how an ascending Taylor bubble behaves and important parameters that influence the ascending gas, to ensure that the behaviour of the model corresponds with the theory. Also, the sensitivity of the model to the different terms will be compared with the results from the previous research.

2 FUNDAMENTALS

The mathematical model for flow of two fluids are based on several general principles and fundamental concepts as well as observed parameters from experiments. This section will therefore consist of description of the general principles and fundamental concepts that are relevant for this thesis.

2.1 Conservation

Physicals expressions that are related to flow of fluids are fundamental in development of analytical description of fluid flow [25]. For almost all fluid flow are there three fundamental laws of physics named conservation of mass, Newton's second law of motion (also known as conservation of momentum) and Thermodynamics first law (conservation of energy, which will not be considered in this thesis), that can be applied [25]. The most important concepts in this thesis are the laws of conservation of mass and momentum, which the two fluid flow model in this thesis is based on.

2.1.1 Conservation of mass

The law of mass conservation states that mass cannot be created or destroyed [25]. Therefore, the sum of the net flux of mass, rate of accumulation of mass within the controlled volume element and taking in consideration of injection or production as a source or sink term respectively, will be equal to zero when summed up.

$$\{rate\,of\,accumulation\} + \{net\,flux\} + \{source/sink\} = 0$$

This can easily be illustrated by considering a one-dimensional flow of a fluid in a pipe with constant cross section as shown in figure (2.1). The mass conservation for this type of system will be as followed:

$$\frac{\partial}{\partial t}\rho + \frac{\partial}{\partial x}(\rho u) + \Omega = 0$$

where ρ is mass density and u is velocity of the fluid. The first term is the rate of accumulation, the second term is net flux and the last term Ω is the source/sink term. This is called the continuity equation. If there is no accumulation of mass, the mass that flows into the controlled volume element will be equal to the mass that flows out of the system.

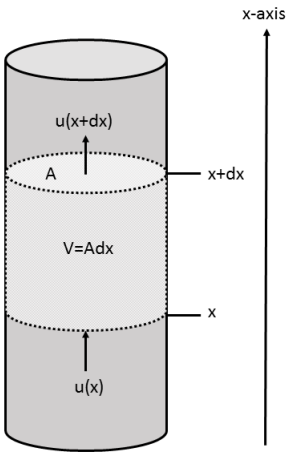

Figure 2.1: *Illustration of flow in a pipe with constant cross section*

In this thesis is a two-phase flow of gas and liquid in one-dimension considered. The derivation of the mass conservation equation will stay the same, except there will be a mass conservation equation for each of the two fluids. There will be no injection or production of fluids, which excludes the source/sink term. Since a one-dimensional flow is considered, it is necessary to include the fluid phase fraction in the rate of accumulation and net flux for the fluid phase in the corresponding conservation of mass equation. In addition a term that consist of rate of mass transfer to the fluid phase must be included [2].

$$\frac{\partial}{\partial t}(\rho_f \alpha_f) + \frac{\partial}{\partial x}(\rho_f \alpha_f u_f) = \beta_f$$

Here refers the subscript f to the fluid phase f, α_f is the phase fluid fraction, while β_f is the rate of mass transfer to the fluid phase f.

Throughout this thesis, it is assumed that no mass transfer will occur between the two phases and no source/sink term. This can be called an immiscible flow of two fluids and will lead to the equations (2.1) and (2.2) for conservation of mass for gas and liquid respectively.

$$\frac{\partial}{\partial t}(\rho_g \alpha_g) + \frac{\partial}{\partial x}(\rho_g \alpha_g u_g) = 0 \tag{2.1}$$

$$\frac{\partial}{\partial t}(\rho_l \alpha_l) + \frac{\partial}{\partial x}(\rho_l \alpha_l u_l) = 0 \tag{2.2}$$

2.1.2 Conservation of momentum

The other main concept is the conservation of momentum principle which is based on Newton's second law of motions [25]. The conservation law of momentum states that the

sum of the rate of accumulation of momentum and the rate of flux of momentum within a controlled volume element is equal the sum of forces acting on the controlled volume element [2].

$$\{sum\,of\,forces\} = \{net\,flux\,of\,momentum\} + \{rate\,of\,accumulation\,of\,momentum\}$$

The forces acting on the fluid in the controlled volume element are due to external forces, friction forces on the control volume and the force on a fluid from the other fluid [2].

$$\frac{\partial}{\partial t}(\rho u) + \frac{\partial}{\partial x}(\rho u^2) = F$$

Where F is the net force in the controlled volume element.

The forces relevant throughout this thesis, the two phase flow in vertical pipe as illustrated in figure (2.1), will be some gravitational forces that are relevant to the external force mentioned above. There will also be friction on the control volume from the fluids on the pipe wall. In addition are there some friction forces between the two fluids, which is an interfacial drag force that represents the force interaction between the two fluid and some viscous forces. As for the conservation of mass, requires the conservation of momentum two equations, one for each of the fluids present.

$$\partial_t(nu_g) + \partial_x(nu_g^2) + \alpha_g \partial_x P_g = -f_g u_g - C(u_g - u_l) - ng + \partial_x(\mu_g \partial_x u_g) \tag{2.3}$$

$$\partial_t(mu_l) + \partial_x(mu_l^2) + \alpha_l \partial_x P_l = -f_l u_l + C(u_g - u_l) - mg + \partial_x(\mu_l \partial_x u_l) \tag{2.4}$$

Where $n = \alpha_g \rho_g$ and $m = \alpha_l \rho_l$. $\partial_t(\rho_f \alpha_f u_f)$ represents the change in momentum, $\partial_x(\rho_f \alpha_f u_f^2)$ is the change in kinetic energy (flux), $\alpha_f \partial_x P_f$ is the change in fluid phase pressure, $\rho_f \alpha_f g$ is the gravitational force, $f_f u_f$ is the friction force between the fluid and the wall, $C(u_g - u_l)$ is the interfacial tension between the two fluids and $\partial_x(\mu_f \partial_x u_f)$ is viscous forces. These formulations of the conservation of momentum for gas and liquid are similar to the formulation by Prosperetti and Tryggvason [19].

2.2 Flow of gas-liquid in a pipe

When gas and liquid both are present in a pipe, the motion of fluids will be driven by either buoyancy forces, external forces as a pressure gradient or a combination of these forces [10]. If the gas is introduced at the bottom of a vertical pipe containing stagnant liquid, it will start to rise up in the well due to density differences between gas and liquid, buoyancy. How the gas and liquid are distributed in the pipe when the gas rises is called

flow regimes. The gas can be distributed as a layer, small bubbles, large bubbles or as a column of gas with liquid around it. It is the time and space distribution of gas and liquid flow, in other words the flow velocity that determines which flow regimes that will dominate the flow [22].

2.2.1 Flow regimes

In addition to distinguish between laminar (layered flow) and turbulent flow (chaotic flow) as it is done in single phase flows, it has to be distinguish between different flow regimes when two phase flow is considered [22]. There are different flow regimes for horizontal flow and vertical flow. Only the latter one is relevant in this thesis. Figure (2.2 a) illustrates the possible flow regimes. They are slug flow, churn flow, dispersed bubble flow and annular flow [22]. As seen from the figure, the gas and liquid phase will flow more separately at low velocities, and becomes more mixed as velocity increase.

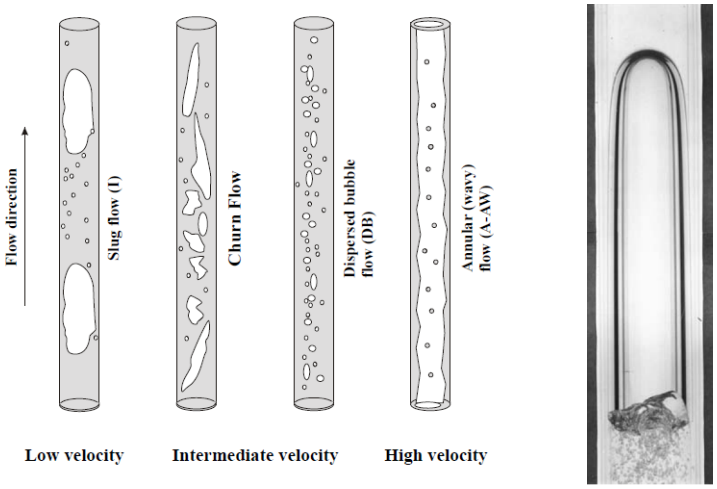

(a) *Flow regimes* [22]

(b) *Taylor bubble* [24]

Figure 2.2: *Illustration of flow regimes in a vertical two-phase flow in addition to an illustration of an ascending Taylor bubble of air in a pipe filled with water*

The flow regime of gas and liquid flow considered in this thesis is gas slug. According to E. W. Liewellin et al can a gas slug also be called Taylor bubble or long bubble [15]. As the figure (2.2 b) illustrates, the gas bubble will rises up and fill a large part of the inner cross section of the pipe, while the liquid will fall and form a film at the wall of the pipe. There may be a tail of small bubbles, also called dispersed flow, following the large gas bubble. The Taylor bubble can be further divided into different regions that

are characteristics shape for this type of gas bubbles. At the front of the bubble is a region called the bubble nose. The bubble nose will have a characteristic shape, which is hemispherical. A large cylindrical part, which may fill up large parts of the cross section surrounded by a liquid film, follows the bubble nose. This region of the Taylor bubble can be called the body. Behind the body region is the back of the bubble. This region may vary in morphology. It can be flat, concave or hemispheroidal and it can have ripples. As mentioned, may there be a liquid slug region that follows the Taylor bubble. It consist of a gas emulsion which is created by turbulence at the bubble wake that creates small gas bubbles by tearing up some parts of the Taylor bubble [15][23].

2.3 Concepts of multiphase flow

As seen in the previous sections, there are several general concepts that are necessary to describe multiphase flows in pipes. The basics equations for conservation of mass (2.1) and (2.2) in addition to the conservation of momentum (2.3) and (2.4) contains some variables as fluid fractions, velocities, liquid film thickness, pressures and frictions, which needs to be considered.

2.3.1 Fluid fractions

In two-phase flow of gas and liquid are parts of the volume element filled with gas while the rest is filled with liquid. As explained in section (2.2) the distribution of gas and liquid can vary. It is useful to know the fluid phase fractions, α, during flow of the fluids. This is a ratio of the fluid phase amount and can be considered either as an volume, area or line average [22]. The definition of fluid fraction as an area average is given in equation (2.5).

$$\alpha_f = \frac{A_f}{A} \tag{2.5}$$

Where A the area of flow and A_f is the area containing fluid f. The sum of the phase volume fractions will be equal to one.

$$\sum_f \alpha_f = 1 \tag{2.6}$$

The figure (2.3) illustrates a cross section in a pipe containing a Taylor bubble at the cylindrical body part in a slug flow, where the inner cross section is filled with gas and the outer filled with liquid. Based on figure (2.3), the gas and liquid fraction can be

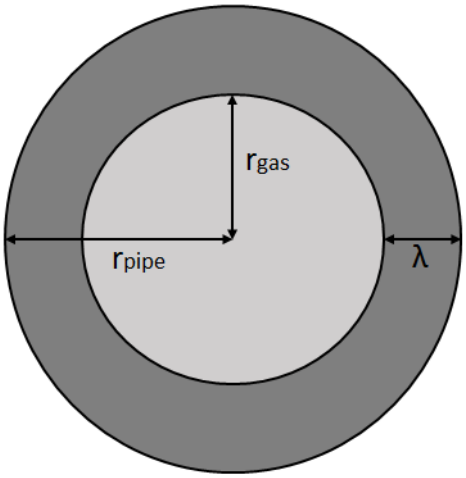

Figure 2.3: *Illustration of distribution of gas and liquid in a cross section of a pipe, with radius of pipe (r_{pipe}), radius upto gas-liquid interface (r_{gas}) and thickness of the outer liquid film (λ) indicated in the figure*

defined by area averages based on the definition given in equation (2.5). The resulting area averages of gas and liquid is given in equations (2.7) and (2.8) respectively.

$$\alpha_g = \frac{A_g}{A_{pipe}} = \frac{A_g}{A_g + A_l} = \frac{D_g^2}{D_{pipe}^2} \tag{2.7}$$

$$\alpha_l = \frac{A_l}{A_{pipe}} = \frac{A_l}{A_g + A_l} = \frac{D_{pipe}^2 - (D_{pipe} - D_g)^2}{D_{pipe}^2} \tag{2.8}$$

Where D_g and D_{pipe} are the diameter to the gas-liquid interface and pipe respectively. Here it is assumed that the interface between gas and liquid is circular. By this two-phase gas-liquid system equation (2.6) can be expressed as equation (2.9).

$$\alpha_g + \alpha_l = 1 \tag{2.9}$$

It is easy being deceived when trying to estimate gas and liquid fractions during two-phase flow in pipes. As C. Brennen shows by figure (2.4), a mixture of individual bubbles that ascends as shown in the left picture will have a gas fraction at approximately 1% but it seems to be much higher, and will increase to approximately $4,5\%$ and over 15% for the photographs towards right [2]. By considering the case given in figure (2.3), an observation is that even with thin liquids film the liquid volume fraction will be higher than expected. This is due to the liquid film surrounds the gas at a large radius, which will give a large cross section of fluid. Figure (2.5) illustrate how the gas fraction is affected by the thickness of the liquid film. The plot rises from the calculation of the gas volume fraction (α_g) by equation (2.7) at the given dimensionless thickness of the

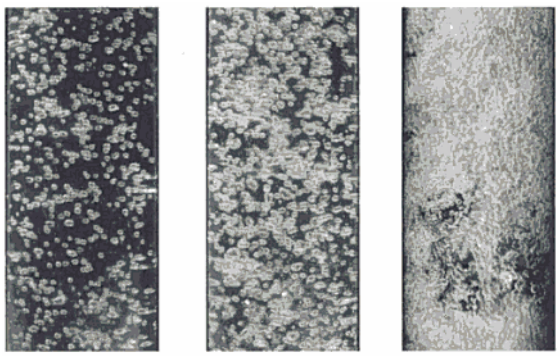

Figure 2.4: *Illustration of air-water flow in a pipe by C. Brennen* [2]

liquid film (λ') given by $\frac{D_{pipe}-D_g}{\frac{D_{pipe}}{2}}$. As seen from the figure, the volume fraction of gas will quickly decrease when the thickness of the liquid film is thin but increasing, but the decrease in gas volume fraction will decline at thicker liquid films.

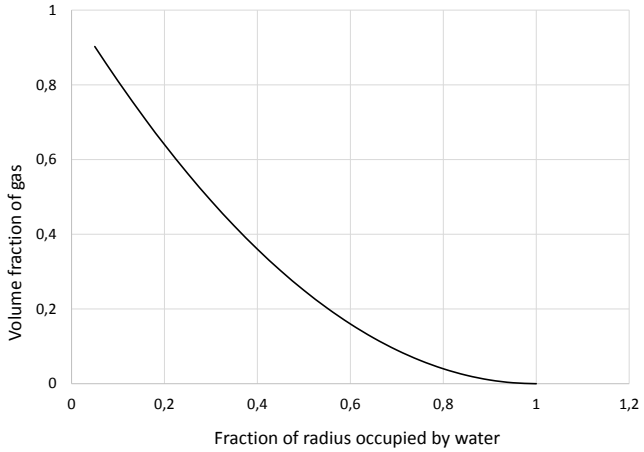

Figure 2.5: *Illustration of how the volume fraction of gas* (α_g) *changes when the thickness of liquid film* (λ) *increases*

2.3.2 Velocities of the fluids

In multiphase flows of fluids, there are several ways of expressing the velocities of the fluids. The superficial velocity of a fluid, u_{fs}, is a relationship between the volumetric flow and the cross section of the pipe as given in equation (2.10). It is an expression of the velocity to a fluid as if it was the only fluid present [22].

$$u_{fs} = \frac{q_f}{A} \tag{2.10}$$

Where q_f represents the volumetric flow rate of a fluid. The real velocity of a fluid phase is expressed with the fraction of the flowing phase area. This is referred to as phase

velocity, u_f, of a flowing fluid [22].

$$u_f = \frac{q_f}{A_f} \tag{2.11}$$

The superficial and phase velocities can be related to each other through the fluid fractions.

$$u_{fs} = \alpha_f u_f = \alpha_f \frac{q_f}{A_f} = \frac{q_f}{A} \tag{2.12}$$

The mixture velocity, u_{mix}, is achieved by adding the superficial velocities of the fluids. This gives an expression of the real average velocity the flow of fluid inhibits [22]. If the fluids present are gas and liquid, the expression of mixture velocity will be as given in equation (2.13).

$$u_{mix} = u_{gs} + u_{ls} \tag{2.13}$$

The velocity of an ascending gas bubble in a pipe filled with liquid is dependent on several parameters, which will be considered in section (3.2) where previous research on two-phase flow of gas and liquid looked into.

2.3.3 Liquid film

In section (2.2) were falling liquid films introduced as phenomenon in two-phase slug flow. The figure (2.3) illustrates a film of liquid surrounding gas where the thickness of the liquid film defined as λ. A relation between the thickness of the liquid film and radius of the pipe, r_{pipe}, is shown in equation (2.14). This ratio is called the dimensionless thickness of the liquid film, λ'.

$$\lambda' = \frac{\lambda}{r_{pipe}} \tag{2.14}$$

As mentioned, the thickness of the liquid film will affect the volume fractions, figure (2.5), which will affect the velocities of the fluids, hence the thickness of the liquid film is an important variable. In section 3.2.3, several theories from previous research are looked into, where some models are proposed to determine the thickness of the falling liquid film.

2.3.4 Pressure

In the conservation of momentum equations (2.3) and (2.4), the forces can be related to the pressure drops that occurs during flow of fluids in pipes. The total pressure gradient

for flow in pipes is given by equation (2.15) for a steady-state situation (independent of time).

$$\frac{dp}{dx} = (\frac{dp}{dx})_f + (\frac{dp}{dx})_h + (\frac{dp}{dx})_a \tag{2.15}$$

Where $(\frac{dp}{dx})_f$ is the frictional pressure gradient, $(\frac{dp}{dx})_h$ is the hydrostatic pressure gradient and $(\frac{dp}{dx})_a$ is the acceleration pressure gradient [22]. The frictional pressure drop depends on the flow regime present and is related to the friction present in the flow (the frictions present in the flow will be considered in section 2.3.5). While the hydrostatic pressure is related to density of fluids, gravitational acceleration and height of fluid column $P_{hydrostatic} = \rho g x$. The hydrostatic pressure gradient in liquid is much higher than in gas due to the low density in gases ($\rho_g << \rho_l$). The acceleration pressure gradient depends on variation in velocity which may occur when there are changes in the cross section of the pipe or changes in the density of gas [22].

2.3.5 Friction

As mentioned in section (2.1.2), forces related to friction will be present during flow of fluids in pipe, equations (2.3) and (2.4). Considering two phase flow of gas and liquid in pipes there will be friction between the two fluids (C), friction between gas and wall (f_g) and friction between liquid and wall (f_l), which are given as force versus length.

The friction between the phases can be related to interfacial tension, which sometimes can be referred to as surface tension, depending on if it is between phases or between the vapour phase and its corresponding liquid respectively. It can be related to the difference in molecular density in the different phases [22], where the molecular density in gases are much lower than in liquids which again are lower than in solids. The interfacial tension has an effect of how the phases will distribute themselves when they are in contact with each other and influence the velocities (flow regimes). They are affected by temperature and pressure [22]. The friction between fluids and wall are named shear stress. The wall shear stress is due to a non-moving wall, which often is rough and will slow the velocity of the fluid.

In addition to the tensions, the fluids contain an inner friction, an inner resistance against flow. This is known as viscosity of a fluid (μ). The viscosity of a liquid is larger than for a gas due to the high molecular density in liquid, which will increase the inner friction. The gas has a lower viscosity due to the low molecular density.

2.4 Discretization of volume element and differential equations

The mass and momentum conservation equations are differential equations which needs converted into linear equations in order to be solved numerically. This is achieved by discretization of the differential equations to make them algebraic, followed by linearization of the algebraic equations to make them linear. The process will result in a large set of linear equations to be solved [14]. This section is based on lecture notes and course compendium from the course *PET565:Core scale modelling and interpretation* [9], in addition to some confirming theory from Ben-Artzi and Falcovitz and Kleppe [1, 14]

2.4.1 Grid

The first step in the discretization process is to discretize the volume element into a grid. The volume element considered must be divided into blocks of equal length (Δx) with the computational points as center in the block cells ($\{x_i\}_{i=1}^{M}$), this can be called a uniform grid in space [1, 9, 14]. Figure (2.6) is an illustration of a one-dimensional uniform grid in space. Since it is also of interest to see the changes in time, a discretization in time

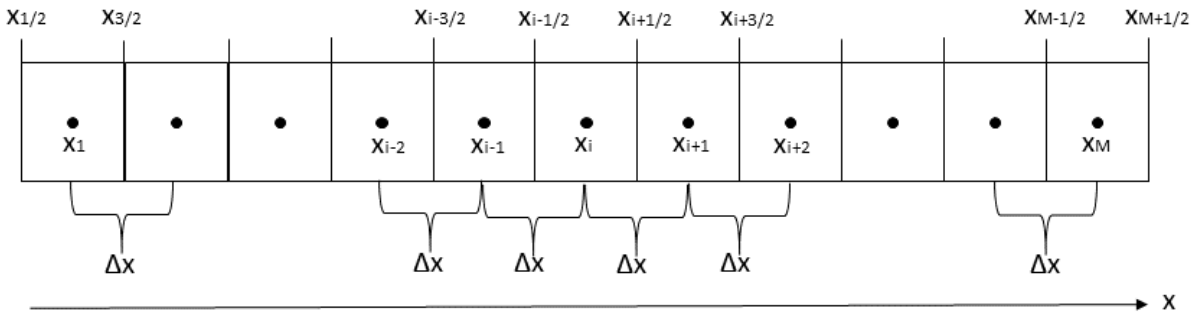

Figure 2.6: *Illustration of a one dimensional uniform grid in space in x-direction, based on a figure from the compendium by Kleppe* [14]

is required. The time interval is divided into a number of timesteps (N_{step}) with equal length (Δt), which gives the discretization of time as $\{t^n\}_{n=1}^{N}$ [1, 9, 14]. Figure (2.7) is an illustration of a one-dimensional uniform grid in space and time. The numerical solutions will be computed at all the computational points located in the center of the grid blocks and at each time step [14]. It is important to use appropriate size of grid during numerical simulations and investigations. If the number of cells are very large, the simulation will be very accurate but take long time. If the number of cells are to low the simulation will be very fast but not accurate.

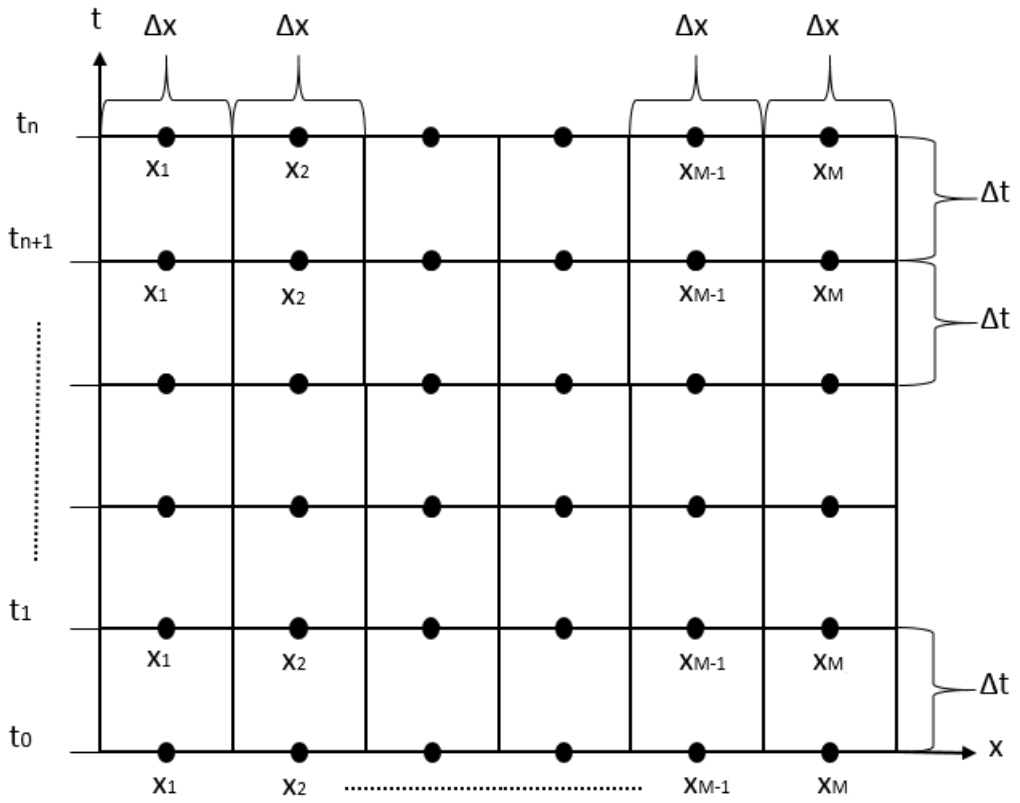

Figure 2.7: *Illustration of a uniform grid in space (x-direction) and time, based on the figure* (2.6) *but expanded to include the second dimension, time*

2.4.2 Discrete scheme

The discretization procedure consist as indicated above of several steps. In this section will discretization of a differential equation be illustrated, and the procedure is based on the lecture notes and course compendium from the course *PET565: Core scale modelling and interpretation* [9]. The equation (2.16) is a differential equation.

$$\partial_t \varepsilon + f(\varepsilon)_x = 0 \tag{2.16}$$

By restricting this differential equation to one grid block can the differential equation by the use of discretization, be converted into one algebraic equation for each grid block.

$$\frac{\partial}{\partial t}\varepsilon \mid_{x_i,t} + \frac{\partial}{\partial x} f(\varepsilon) \mid_{x_i,t} = 0 \tag{2.17}$$

When the discrete form of equation (2.17) is to be found are the figures (2.6) and (2.7) useful to have in mind. The equation (2.18) is the discrete form of the differential equation (2.16).

$$\frac{\varepsilon_i^{n+1} - \varepsilon_i^n}{\Delta t} + \frac{F_{i+\frac{1}{2}}^n - F_{i-\frac{1}{2}}^n}{\Delta x} = 0, \quad i = 1, ..., M \text{ and } t \,\epsilon\, [t^n, t^{n+1}] \tag{2.18}$$

Where $F_{i\pm\frac{1}{2}} \approx f(x_{i\pm\frac{1}{2}})$. Since the variables are only known at the cell center needs the terms $F_{i\pm\frac{1}{2}}$ to be considered further. A central based flux discretization is where the two nearby cells is averaged, gives an unconditionally unstable scheme [9]. Therefore is a correction term used together with the central based discretization terms to make it conditionally stable [9].

$$\begin{aligned} F^n_{i+\frac{1}{2}} &= \frac{f(\varepsilon^n_i) + f(\varepsilon^n_{i+1})}{2}) - \frac{a}{2}(\varepsilon^n_{i+1} - \varepsilon^n_i) \\ F^n_{i-\frac{1}{2}} &= \frac{f(\varepsilon^n_i) + f(\varepsilon^n_{i-1})}{2} - \frac{a}{2}(\varepsilon^n_i - \varepsilon^n_{i-1}) \end{aligned} \tag{2.19}$$

Where a is a parameter with conditions $a > 0$ and $max_\varepsilon|f'(\varepsilon)| \leq a$, which makes the parameter a an upper bound for the speed [9]. By this derivation will equation (2.20) be the discretized form of the differential equation (2.16).

$$\frac{\varepsilon^{n+1}_i - \varepsilon^n_i}{\Delta t} + \frac{1}{2}\frac{f(\varepsilon^n_{i+1}) - f(\varepsilon^n_{i-1})}{\Delta x} - \frac{a}{2\Delta x}(\varepsilon^n_{i+1} - 2\varepsilon^n_i + \varepsilon^n_{i-1}) = 0 \tag{2.20}$$

Some rearranging of the discretized equation leads to:

$$\varepsilon^{n+1}_i = \varepsilon^n_i - \frac{\Delta t}{2\Delta x}\{f(\varepsilon^n_{i+1}) + f(\varepsilon^n_{i-1}) - a(\varepsilon^n_{i+1} - 2\varepsilon^n_i + \varepsilon^n_{i-1})\} \tag{2.21}$$

The discretized equations can be solved either implicit or explicit. In the derivation above is an explicit approach used. Since the discretized equations once the solution at time step n is known, computes the solution at the next time step $n + 1$, are the explicit schemes easiest to solve, due to it only contains one unknown, ε^{n+1}_i [14]. However, there are stability problems, which gives rise of a stability condition. The implicit method is the most complicated, but there is no stability condition [14]. A large set of linear equations are needed in order to solve an implicit scheme.

For computation of the numerical solution is it necessary to define the initial condition in the considered element which is the values at all the computational points at the initial time, $(x, t = 0)$. In addition to the conditions at the boundary of the volume element, $(x = 0, t)$ and $(x = M, t)$, needs to be specified, as if there are inflow or production at the boundaries or if the boundaries are sealed off [14].

2.4.3 Stability

There may be other parameters than the size of grid can cause stability problems that will restrict the values of the parameters. As described, the differential equations will be replaced by difference equations, which consist of algebraic approximations instead of differential operators. Stability problems may exist in these types of equations. The

computational error of the solution increases as the computations moves on, which may give unphysical solutions that can exceed the boundaries [7]. As mentioned, explicit solution procedure will exhibit stability problems. Therefore is a stability criterion as in equation (2.22) needed [9].

$$0 \leq a\frac{\Delta t}{\Delta x} \leq 1 \tag{2.22}$$

2.5 Riemann problems

Some functions consist of one or more discontinuities (jumps) in their initial data. These types of data can be referred to as Riemann data [1, 8]. A solution where the discontinuity can be connected either by an continuous solution or a shock solution is desirable. In order to illustrate a Riemann problem and its solution is the same function as in equation (2.16) which is repeated in equation (2.23) where $f(\varepsilon) = \frac{1}{2}\varepsilon^2$ and the function f is assumed to be convex (a non-linear function). This function f is referred to as the "Burgers equation" [1]. Two cases of initial states given in equations (2.24) and (2.29) are considered to illustrate how respectively a solution of a decreasing and increasing discontinuity can be obtained. As seen in both sets of initial data there are a discontinuity in the data around $x = 0$. The solution procedures are based on lecture notes and course compendium in the course *PET565: Core scale modelling and interpretation* [8] in addition to some confirming theory from Ben-Artiz and Falcovitz [1].

$$\frac{\partial}{\partial t}\varepsilon + \frac{\partial}{\partial x}f(\varepsilon) = 0, \quad f(\varepsilon) = \frac{1}{2}\varepsilon^2, \quad f'(\varepsilon) = \varepsilon \quad f''(\varepsilon) > 0 \tag{2.23}$$

2.5.1 Shock wave solution

The initial condition given in equation (2.24) is an decreasing discontinuity where $\varepsilon_l > \varepsilon_r$.

$$\varepsilon(x, t = 0) = \varepsilon_0(x) = \begin{cases} \varepsilon_l = 1, & if\ x < 0 \\ \varepsilon_r = 0, & if\ x > 0 \end{cases} \tag{2.24}$$

The characteristics that are associated with this function at $x = 0$ are

$$x = f'(\varepsilon_l)t = f'(1)t \quad and \quad x = f'(\varepsilon_r)t = f'(0)t \tag{2.25}$$

which gives $f'(1) > f'(0)$, the characteristics are crossing and will meet at some time.

The Rankine-Hugoniot jump condition (2.26), which is a relation for the speed of a function at a discontinuity [1, 8].

$$s = \frac{f(\varepsilon_l) - f(\varepsilon_r)}{\varepsilon_l - \varepsilon_r} \tag{2.26}$$

For the conditions given in equation (2.24), will the Rankine-Hugoniot condition (2.26) give a speed of $s = \frac{1}{2}$ as seen from the derivation below.

$$s = \frac{\frac{1}{2}\varepsilon_l^2 - \frac{1}{2}\varepsilon_r^2}{\varepsilon_l - \varepsilon_r} = \frac{\frac{1}{2} - 0}{1 - 0} = \frac{1}{2}$$

The Lax entropy condition (2.27), is a criterion for when a discontinuous solution (shock solution) is the correct solution to a Riemann problem [1, 8].

$$f'(\varepsilon_l) > s > f'(\varepsilon_r) \tag{2.27}$$

From the calculated Rankine-Hugoniot speed it is seen that Lax entropy condition is fulfilled.

$$f'(1) > \frac{1}{2} > f'(0)$$

This leads to following solution of equation (2.23) with the initial condition as given in equation (2.24)

$$\varepsilon(x,t) = \begin{cases} 1, & if\ \frac{x}{t} \leq s = \frac{1}{2} \\ 0, & if\ \frac{x}{t} > s = \frac{1}{2} \end{cases} \tag{2.28}$$

This jump solution, which satisfied the Lax entropy condition can be referred to as shock wave solution [1, 8].

2.5.2 Rarefaction wave solution

The initial condition in equation (2.29) gives an increasing discontinuity where $\varepsilon_l < \varepsilon_r$.

$$\varepsilon(x, t = 0) = \varepsilon_0(x) = \begin{cases} 0, & if\ x < 0 \\ 1, & if\ x > 0 \end{cases} \tag{2.29}$$

The characteristics which are associated with this function at $x = 0$ are

$$x = f'(\varepsilon_l)t = f'(0)t \quad and \quad x = f'(\varepsilon_r)t = f'(1)t \tag{2.30}$$

which gives $f'(1) > f'(0)$. These characteristics can be referred to as spreading characteristics and will not satisfy the Lax entropy condition (2.27). Therefore must a continuous solution also known as a rarefaction wave solution be looked for [1, 8].

This is done by considering a solution similar to the function $\varepsilon(x,t)$ and find conditions where $\varepsilon(x,t)$ is a solution. The similarity solution considered here depends on $\frac{x}{t}$ as

shown in equation (2.31), which is the same as considered in the lecture notes and course compendium in the course *PET565: Core scale modelling and interpretation* [8], where a solution was derived.

$$\varepsilon(x,t) = \varphi(\frac{x}{t}) \tag{2.31}$$

To be sure that the function $\varepsilon(x,t)$ is a solution one has to express equation (2.23) with the new similar function in equation (2.31).

$$\begin{aligned} \frac{\partial}{\partial t}\varepsilon(x,t) = \frac{\partial}{\partial t}\varphi(\frac{x}{t}) = \varphi'(\frac{x}{t}) \times (-\frac{x}{t^2}) \\ \frac{\partial}{\partial x}\varepsilon(x,t) = \frac{\partial}{\partial x}\varphi(\frac{x}{t}) = \varphi'(\frac{x}{t}) \times \frac{1}{t} \\ \frac{\partial}{\partial x}f(\varepsilon(x,t)) = \frac{\partial}{\partial x}f(\varepsilon(x,t)) \times \frac{\partial}{\partial x}\varepsilon(x,t) = \\ \frac{\partial}{\partial x}f(\varphi(\frac{x}{t})) \times \frac{\partial}{\partial x}\varepsilon = f'(\varphi(\frac{x}{t})) \times \varphi'(\frac{x}{t}) \times \frac{1}{t} \end{aligned} \tag{2.32}$$

By implementing the expressions in equation (2.32) into equation (2.23) give:

$$\varphi'(\frac{x}{t}) \times (-\frac{x}{t^2}) + f'(\varphi(\frac{x}{t})) \times \varphi'(\frac{x}{t}) \times \frac{1}{t} = 0 \tag{2.33}$$

The equation (2.33) gives two possible solutions as shown in equation (2.34).

$$\begin{aligned} f'(\varphi(\frac{x}{t})) = \frac{x}{t} \quad and \quad \varphi'(\frac{x}{t}) \neq 0 \\ or \\ \varphi'(\frac{x}{t}) = 0 \end{aligned} \tag{2.34}$$

The second option is only possible when φ is constant, which is when $\nu_l = \nu_r$. As the initial data (2.29) shows is this not the case here, which excludes that possibility. It can be solved by rearrange the first expression in equation (2.34) for $\varphi(\frac{x}{t})$.

$$\varphi(\frac{x}{t}) = (f')^{-1}\frac{x}{t} \tag{2.35}$$

From the use of the characteristics in equation (2.30) on equation (2.35) one can find $\varphi(\frac{x}{t})$ for $f'(\varepsilon_l) \leq \frac{x}{t} \leq f'(\varepsilon_r)$.

$$\begin{aligned} \varphi(\frac{x}{t}) = (f')^{-1}(\frac{x}{t}) = (f')^{-1}(f'(\varepsilon_l)) = \varepsilon_l \\ \varphi(\frac{x}{t}) = (f')^{-1}(\frac{x}{t}) = (f')^{-1}(f'(\varepsilon_r)) = \varepsilon_r \end{aligned}$$

The solution of the function given in equation (2.23) with the initial condition given in equation (2.29) is given in equation (2.36).

$$\varepsilon(x,t) = \varphi(\frac{x}{t}) = \begin{cases} \varepsilon_l = 0, \quad if \ \frac{x}{t} \leq f'(\varepsilon_l) \\ (f')^{-1}(\frac{x}{t}), \quad if \ f'(\varepsilon_l) < \frac{x}{t} < f'(\varepsilon_r) \\ \varepsilon_r = 1, \quad if \ \frac{x}{t} \geq f'(\varepsilon) \end{cases} \tag{2.36}$$

As seen from the solution, there will be a continuous transition for the data in between $f'(\varepsilon_l) < \frac{x}{t} < f'(\frac{x}{t})$, not a shock wave as for the solution in equation (2.28). This type of solution is referred to as a rarefaction wave solution [1, 8].

3 EXPERIMENTAL BACKGROUND

Much research has been done on ascending Taylor bubbles in pipes and according to Flavia Viana et al, the research can be dated all the way back to Gibson in 1913 [24]. In order to get known with the physical effects to make the mathematical model accurate, are experiments performed by Herimonja Andrianifaliana Rabenjafimanantsoa ("Benja") at the University of Stavanger observed, in addition to some investigation of previous research on two-phase slug flow in pipes are considered.

3.1 Observations of experiments

The experiments performed by Benja of ascending air in stagnant liquid, are similar to the experiments performed by Thomas Paz [18] and Kristine Høyland Tjelta and Ingeborg Elin Kvamme [23] in their bachelor thesis. Experimental set-ups are illustrated in figures (3.1) and (3.2). The first figure is a picture of the lower part of the experimental equipment, while the second figure is an older illustration experimental set-up but it gives a better overview with the indicated pressure measurement, air valve and size of the experiment. One should notice that in the second figure, the columns are separated, while in the recent experiments are a connection placed between them as seen in figure (3.1).

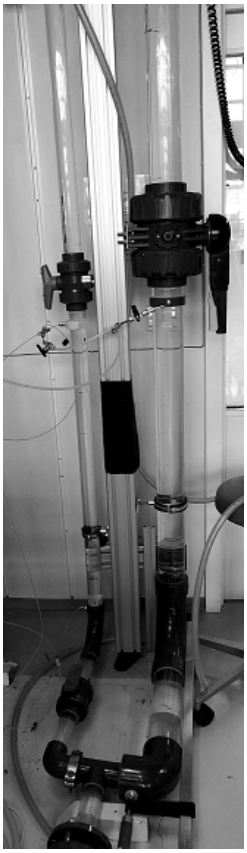

Figure 3.1: *Picture of the bottom of the column used in Benja's experiments*

The air is injected below the black valve in the right column in figure (3.1) and will form a layer separated from the liquid column above (which is open to atmosphere), by a valve. Below the layer of air is the pipe filled with water. As the valve is opened, the gas will start to ascend upwards driven by buoyancy. A quick rise of the air-water surface at the top of the pipe was observed in addition to some oscillation. The water will not have much passage to pass by due to the cross section is occupied by air. This leads to the observed quick rise of the air-water surface at the top of the pipe. Another explanation may be due to rapid expansion and compression of the air caused by pressure difference in air and water phases, which may cause the rise and oscillation in the air-water surface [18].

Not long after the air starts to ascend, it will form into a Taylor bubble, and a passage for the water in the form of a falling liquid film is created. The creation of the falling water film slows down the rapid increase of the air-water surface at the top, but it will still increase. This may be due to the volume of air in the Taylor bubble, which ascends faster than the volume of water is being displaced by the liquid film. The rising of the air-water surface continues but the instant the air bubble passes through the air-water surface, will the surface decrease to a level below the initial water-air surface.

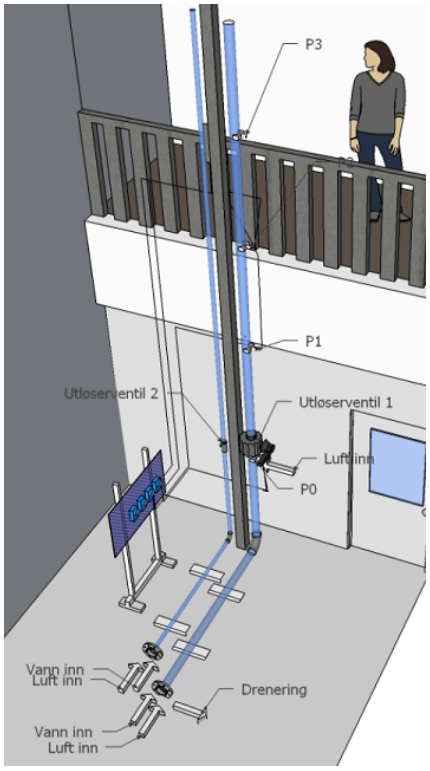

Figure 3.2: *Illustration of experimental equipment from Paz bachelor thesis* [18]

The velocity of the ascending Taylor bubble will be highest in the center at the top of the bubble, due to the friction forces by the liquid film, which flows in opposite direction at the edges of the bubble. As the Taylor bubble ascends, a tail of dispersed small bubbles of air will follow with decreasing bubble size. These bubbles ascends with lower velocity. The velocity decreases as the bubble size decreases. This tails grows as the Taylor bubble ascends which can be explained by the existence of turbulence at the bubble wake which may form smaller bubbles by the cost of tearing of some of the Taylor bubble volume [23]. The length of the ascending Taylor bubble was much longer than the length of the initial gas layer. The reason for this may be due to the outer area occupied by the water film, in addition to some expansion of the gas caused by decreasing pressure as the bubble ascends. It seems like the length of the bubble becomes shorter as it ascends, which may be caused by the formation of the tail.

A mathematical model in one dimension relevant for the experiments performed by Benja will be derived. The purpose of the model is to illustrate the observed parameters during experiments, as the velocity of the ascending Taylor bubble and saturation distribution in the pipe, which will give an impression of the shape of the bubble as well as the tail of the dispersed gas and thickness of the liquid film around the bubble. In addition, the pressure and pressure differences in the pipe as the gas ascends will be considered.

3.2 Previous research

Through research over the years have ascending slug flows, especially Taylor bubbles, been investigated by several researches. The ascend velocity is shown to be dependent on the density (ρ_l) and viscosity of the liquid (μ_l), the interfacial tension between gas and liquid (σ_{gl}), gravitational acceleration (g) and the internal diameter of the pipe (D). These parameters have been related to the velocity through theory and often considered in different ratios by combining them into dimensionless groups [10, 12, 13, 15, 21, 24, 26, 27]. The most common dimensionless ratios are Froude number (Fr), Morton number (Mo) and Eötvös number (Eo), but some researchers have also worked with the Inverse viscosity number (N_f), Weber number (We) and Reynolds bubble number (Re_b). These ratios have been defined differently by the previous researchers. The main difference between their definitions have been due to the large difference in the density between gas and liquid, which has either resulting in neglecting the ratio $\frac{\rho_l - \rho_g}{\rho_l}$ since it is approximately equal to one. Kang et al showed through their research that the ratios $\frac{\rho_l}{\rho_g}$ and $\frac{\mu_l}{\mu_g}$ had small effect on the dimensionless ratios [13]. These are most common forms and are shown in the equations (3.1)-(3.6).

The Froude number is a ratio of inertial (where viscous and interfacial forces are of less importance) and gravitational forces, which result in a dimensionless velocity [15]. The expression relates the velocity of the bubble (v_b) to the gravitational acceleration, diameter of the pipe in addition to the Froude number.

$$Fr = \frac{v_b}{\sqrt{gD}} \tag{3.1}$$

The gravitational acceleration, viscosity and density of the liquid and interfacial tension are combined into a dimension less ratio called the Morton number. This is a ratio of viscous and interfacial forces [15].

$$Mo = \frac{g\mu_l^4}{\rho_l \sigma_{gl}^3} \tag{3.2}$$

The ratio of buoyancy and interfacial tension forces is represented by the Eötvös number [15].

$$Eo = \frac{\rho_l g D^2}{\sigma_{gl}} \tag{3.3}$$

By combining the Eötvös and Morton number is a ratio called the dimensionless inverse viscosity [15] or buoyancy Reynolds number found [10, 24].

$$N_f = \frac{\rho_l}{\mu_l}\sqrt{gD_{pipe}^3} \tag{3.4}$$

The bubble Reynolds number is an ratio of inertial and viscous forces in the liquid [15]

$$Re_b = \frac{\rho v_b D}{\mu} \tag{3.5}$$

The Weber number relates the inertial forces with the interfacial forces [13].

$$We = \frac{\rho v_b^2 D}{\sigma_{gl}} \tag{3.6}$$

3.2.1 Velocity by determine a constant value for the Froude number

Several constants has been suggested as constant value for Froude number in equation (3.1) to find an expression of the velocity expressed by a constant, gravitational acceleration and the inner diameter of the pipe. Dumitrescu suggested through his research $0,351$ [5, 15], as a value for the constant Froude number, equation (3.7). He used a theoretical approach where it was assumed to be a hemispherical shape of the Taylor bubble nose in addition to laminar flow in the falling liquid film. In addition did Dumitrescu find another value by an experimental approach to be $0,346$ [5, 15, 26].

$$v_b = 0,351 \times \sqrt{gD} \tag{3.7}$$

Some years later, Davies and Taylor did experiments where they proposed a constant for the Froude number in equation (3.1). They experimented with a pipe sealed at the top and open to atmosphere at the bottom. The tube was filled with water and they measured the velocity of the ascending air bubble as the water were drained. They observed that the constant for the Froude number rises a little with increased inner diameter of the pipe but it was nearly constant. The three diameters they looked at where $1,23cm, 2,16cm$ and $7,94cm$ and observed values for constant Froude numbers ranging between respectively $0,283 - 0,2899, 0,316 - 0,331$ and $0,33 - 0,346$ [4]. They assumed that variation was due to viscosity, and explained their assumption with, when the inner diameter of pipes increases will the Reynolds number increase, equation (3.5) [4]. With high Reynolds number, they expected that viscosity effects could be negligible [4]. Davies and Taylor also found a value of the constant Froude number by a theoretical approach that were $0,328$, equation (3.8), which is close to the observed constant during flow in the pipe with a diameter of $7,94cm$ and a little lower than the value defined by Dumitrescu in equation (3.7) [4].

$$v_b = 0,328 \times \sqrt{gD} \tag{3.8}$$

Nicklin et al studied two-phase gas and liquid flow in vertical pipes where they investigated slug flow in both stagnant and moving liquid [16]. They found that the ascend velocity to

gas slug is relative to movement of liquid in front of the slug. If the liquid were stationary they agreed with the constant proposed by Dumitrescus, given in equation (3.7), for the ascend velocity of the gas slug. If the liquid were moving either upwards or downwards in the tube, they needed to add a component to the equation. When there was movement of liquid in an upwards direction they found that the component that needed to be added were larger than the average velocity of the liquid. For liquid moving downwards, they found it harder to find a constant for the component due to unsymmetrical bubble [16].

Rader et al studied experimentally the factors affecting ascending velocity of large bubble through drilling fluid during gas kick by the use of laboratory models and a $1828,8\,m$ deep well [20]. The factors they found that affected the ascending velocity of a bubble where the viscosity of liquid, density of liquid and gas, rate of gas expansion, liquid velocity, angle of deviation from vertical orientation and inner and outer radius of annulus. While factors with little or no effect on the ascending velocity of gas were the length of the bubble, surface tension between the fluids and eccentricity of annulus [20].

3.2.2 Relations between the dimensionless ratios

Instead of finding a constant for the Froude number to estimate the velocity several researchers have made use of the dimensionless ratios given in the equations (3.1)-(3.6). The dimensionless ratios are calculated from the results of their experiments and plotted them against each other in logarithmic scale to find a trend in the data.

E. T. White and R. H. Beardmore did experiments on the rise velocity of air bubbles in different liquids in pipes and investigated of how several physical parameters affect the ascend velocity of gas. From the experiments they did, as Davies and Taylor, find diameter of the pipe to have an effect on the ascend velocity of the gas, especially in thin pipes. In addition were the inclination of the pipe looked at where they observed that with increased deviation from vertical increased the ascend velocity of gas. The angles they investigated were from vertical upto $20°$ [26]. They also found the length of the bubble to have no effect on the ascend velocity of the gas bubble. Their results showed that the terminal velocity (a constant speed achieved when the bubble has stopped accelerating) of the gas bubble was reached after less than 2 pipe diameters distance [26]. They also found that the Froude number depends on the dimensionless inverse viscosity and the Eötvös number, $Fr(N_f, Eo)$, and noticed that either one or more of the effects of viscosity, surface tension and inertial could be neglected within different areas. For high N_f, Eo and low Fr could the viscosity effect, surface tension and inertial effects respectively be

neglected [26].

Viana et al used all available data from experiments from the literature (225) in addition to new experiments at PDVSA Intevep (Petróleos de Venezuela, S.A.) (7) on the ascend velocity of gas bubble in stagnant fluids in pipes [24]. They suggested that the ascend velocities of Taylor bubbles are not affected by the length of the bubbles, as indicated earlier [20, 24, 26]. Viana et al agreed with White and Beardmore that the Froude number is a function of dimensionless inverse viscosity and Eötvös number [24, 26]. A universal correlation for the ascend velocity of the gas was found by processing the data into Froude numbers, dimensionless inverse viscosity and Eötvös number in log-log plots and by double logistic dose curve fitting of data [24]. This universal correlation was found to apply for all data within the range of $Eo > 6$ [24].

When Funada et al refers to the universal correlation, defined by Viana et al, as a solution of the ascend velocity without understanding due to fact that it is not developed by the fundamentals of flow but by processing data [12]. Funada et al studied the ascend velocity of Talyor bubbles by a theoretical approach. They derived a formula for the velocity of an ascending ellipsoidal gas bubble in a tube containing viscous liquid, by assuming that the liquids motion (the falling liquid film) is irrational/neglected. They fitted the derived formula to the data of Viana et al where they found that the surface tension influenced the shape of the nose on the ascending gas bubble, due to ratios from the fitting depended more of the Eötvös than the dimensionless inverse viscosity [12].

From this previous research it is indicated that it is hard to find an expression of the ascend velocity of Taylor bubbles in pipes based on fundamental fluid dynamics. However, it is important to notice that the velocity of an ascending Taylor bubble depends on several parameters [4, 5, 20, 24, 26].

- Diameter of the pipe
- Viscosity of the liquid
- Gravitational acceleration
- Density of the liquid
- Interfacial tension

There are some disagreement on the effects of viscosity and interfacial tension on the ascend velocity of a Taylor bubble. As described there are some proposed regions where

either one or more effects could be neglected to find the ascend velocity [24, 26]. If the liquid in the pipe is flowing or not seems to influence the velocity of the ascending Taylor bubble [16, 20]. While it seemed like the length of the ascending Taylor bubble had no effect [20, 24, 26]. Expressions relating the ascend velocity of Taylor bubble with diameter of pipe, gravitational acceleration and a constant Froude number were proposed by Davies and Taylor and Dumitrescu. In the proposed constant Froude number, it can be assumed that the viscosity and interfacial tension are indirectly included. The relation between velocity of ascending gas bubble and Froude number, equation (3.1), with proposed constants [4, 5], in addition to several measured results from previous experiments [4, 18, 24] are later used to find a velocity to aim the numerical solution at.

3.2.3 Liquid film

As mentioned in section (2.2.1), a falling film of liquid will form at the wall around the ascending Taylor bubble of gas. The thickness of this film is of interest in order to get a more accurate mathematical model to illustrate the two-phase slug flow in a pipe.

Nogueira et al investigated ascending Taylor bubbles in vertical tubes containing liquid through laboratory experiments. They looked in to the flow in the nose region in addition to the annular film at both stagnant and flowing liquids [17]. They found that for higher viscosities are the nose curvature lower and therefore stated that viscous forces influence the shape of the nose region. When the film thickness decreased did the axial velocity of the liquid increase, with maximum velocity at the gas-liquid interface. They found the liquid film to be fully developed at a distance behind the nose. By looking into the shear stress in the falling liquid film they found that by decreasing viscosity did also the shear stress decrease and at higher liquid rates with low viscosity were the shear stress lower. They concluded with that the nose shape, liquid film thickness and shear wall stress are influenced by viscosity [17].

Taha and Cui investigated slug flow in vertical tubes through a numerical study. They found that the thickness of the liquid film decreases when the dimensionless inverse viscosity is increased (N_f). In addition, they observed that as the interfacial tension increased did the thickness of the liquid film decrease, and found the shape of the bubble to be related to viscosity of the liquid and interfacial tension [21].

Through computational fluid dynamics simulation did Zheng et al research slug flows hydrodynamic characteristics, which as previous mentioned depends on viscous, interfacial and inertial forces [27]. They found that when viscosity is the dominating force, which

makes the inverse viscosity an important parameter. The thickness of the falling liquid film decreases and the velocity in the liquid film increases as the dimensionless inverse viscosity increases [27]. In addition, the thickness of the falling liquid film did decrease as the dimensionless distance to the nose is increased. While in interfacial tension dominated flow, where the Eötvös number is an important parameter, an increase in interfacial tension (lowered Eötvös number) gave a thicker falling liquid film and increased curvature of the bubble nose. In inertia-dominated flow where viscous and interfacial forces are neglected, which will give a falling liquid film without interfacial shear. In such flows will the ascending Taylor bubble not be dependent on superficial velocities and length of the bubble and variation in the dimensionless thickness of the liquid film represented the shape of the ascending Taylor bubble [27].

Numerical experiments performed by Feng on gas bubbles driven by buoyancy in a pipe filled with viscous liquid, gave results agreeing with Taha and Cui and Zheng that the dimensionless inverse viscosity affects the thickness of the falling liquid film by decrease in film thickness as the dimmensionless inverse viscosity increases [10].

Through a numerical study did Kang et al investigate Taylor bubble ascending through stagnant liquids by tracking the interface explicitly with velocity of the front interpolated from the regular finite difference grid. This method is called the front tracking method [13]. Kang et al found that both the density- and the viscosity ratio had small effects on the shape of the ascending Taylor bubble, all the dimensionless ratios (bubble Reynolds number, Weber number and Froude number), thickness of the falling liquid film and the length of the wake. They found the squared dimensionless inverse viscosity (which they refer to as Archimedes number, Ar), to affect the shape of the Taylor bubble, shear wall stress and thickness of the liquid film which is in agreement with Taha and Cui [13, 21]. With an increase in the squared dimensionless inverse viscosity, they found a reduction in the length in addition to an increase of the thickness of the Taylor bubble and the shear wall stress was reduced. Due to the thicker Taylor bubble will the falling liquid film reduce in the thickness. From these results, they found a correlation between the dimensionless thickness of the film and dimensionless inverse viscosity [13].

$$\frac{\lambda}{D} = 0,32Ar^{-0,1} = 0,32(N_f^2)^{-0,1} \tag{3.9}$$

E. W. Llewellin et al performed laboratory experiments where they looked into the thickness of the falling liquid film around a Taylor bubble of gas to the quantify the physical controls and proposed two models under the assumption of neglecting interfacial tension between gas and liquid [15]. From the result of their experiments, they agreed with

Nogueira et al and Feng that the dimensionless inverse viscosity can be related to the thickness of the falling liquid film [10, 15, 17]. They saw a sigmoidal trend between the dimensionless thickness of the film and the logarithm of the dimensionless inverse viscosity. They found that the dimensionless thickness of the liquid film is independent of the dimensionless inverse viscosity for $N_f \lesssim 10$ and $N_f \gtrsim 10^4$ where the dimensionless thickness of the film will be around $\lambda' \approx 0,33$ and $\lambda' \approx 0,08$ respectively [15]. In the interval between these dimensionless inverse viscosity values, $10 \lesssim N_f \lesssim 10^4$, will the dimensionless thickness of the film decrease as the dimensionless inverse viscosity increase [15].

One of the models they proposed is an empirical model, equation (3.10), which is based on their experimental data in combination with the data from Nogueira et al research [17] and is valid for the dimensionless inverse viscosity in the range of $10^{-1} \lesssim N_f \lesssim 10^5$ [15].

$$\lambda' = a + b \times tanh(c - d \times log_{10} N_f) \tag{3.10}$$

Where $a+b$ and $a-b$ are expressions for the low-N_f and high-N_f asymptotic values of the dimensionless thickness of the liquid film respectfully, transition between the asymptotes is described by c while d gives an indication of how abrupt the transition between the asymptotes is. The constants have following values $a = 0,204$, $b = 0,123$, $c = 2,66$ and $d = 1,15$ [15].

The other model E. W. Llewellin proposed is based on analyses of theory from Brown, Viana el al and Dukler and Bergelin [15]. They proposed for laminar flow in film, which corresponds to the dimensionless inverse viscosity, $N_f < 1372$ a relationship based on analysis of Brown and Viana et al [15]. While the theory for larger dimensionless inverse viscosity where the transition from laminar to turbulent flow in the film occurs $N_f > 1372$ is based on Dukler and Bergelin theory on falling films. They adapted this theory to apply for a falling thin film (which were concluded to only be valid for the dimensionless inverse viscosity $N_f > 200$) around a Taylor bubble [15]. This model is valid in the range of dimensionless inverse viscosity between $0,1 < N_f < 20\,000$ [15].

Llewellin et al also did some research where interfacial tension not were neglegted. The results from this research showed, in agreement with Taha and Cui, that the thickness of the falling liquid film became thinner as the interfacial tension increased [15]

From this review of previous laboratory and numerical experiments, it is seen that the thickness of the falling liquid film is dependent on:

- Viscosity of the liquid [10, 13, 15, 17, 21, 27].
- Interfacial tension [15, 21, 27].

The thickness of the liquid film has been related to the dimensionless inverse viscosity, equation (3.4), by increase in N_f will the thickness of the liquid film decrease [10, 13, 15, 21, 27]. The proposed correlations by Kang et al and Llewellin et al, equations (3.9) and (3.10), will be used to estimate the aimed thickness of the falling liquid film in this thesis. Interfacial tension has also some influence on the thickness of the falling liquid film, but there are some disagreement in the affection. By Zheng et al will an increased interfacial tension give an increase in the thickness of the liquid film [27], while for Llewellin et al and Taha and Cui will an increase in interfacial tension give an decrease in the falling liquid film [15, 21].

Based on these sections by observing performance of the experiments in addition to considering previous laboratory and numerical experiment have an impression of what the model should illustrate and important parameters been achieved.

4 THE MATHEMATICAL MODEL

The mathematical model that will be considered in this thesis is derived from a general model that has been studied before by several others [6]. It is a simplified model based on a basic one dimensional two-fluid model of gas (g) and liquid (l), for flow in pipelines, where mass conservation and momentum conservation equations are used as foundation of the model. The model will be used to simulate an ascending Taylor bubble of gas in a pipe filled with stagnant liquid.

4.1 General model for two-phase flow in pipes

As described in section 2.1, two mass conservation and two momentum conservation equations will be necessary to describe the two-phase flow. The variables that are conserved, mass densities (m_g and m_l) and mass fluxes (I_g and I_l), are defined in equation (4.1), which is the vector of conserved variables, U [6].

$$U = \begin{bmatrix} \rho_g \alpha_g \\ \rho_l \alpha_l \\ \rho_g \alpha_g u_g \\ \rho_l \alpha_l u_l \end{bmatrix} = \begin{bmatrix} m_g \\ m_l \\ I_g \\ I_l \end{bmatrix} \tag{4.1}$$

Here are ρ_f and u_f fluid density and phase velocity respectively for phase f, and α_f is volume fraction of fluid phase f with the total volume fraction, as defined in equation (2.6), equal to one as shown in equation (4.2).

$$\alpha_g + \alpha_l = 1 \tag{4.2}$$

By rearranging equation (4.1) fluid phase velocities can be obtained, as defined in equation (2.11).

$$u_g = \frac{U_3}{U_1}, \; u_l = \frac{U_4}{U_2} \tag{4.3}$$

The conservation of mass equations (4.4) for gas and (4.5) liquid are identical to those defined in section 2.1.1, equations (2.1) and (2.2).

$$\frac{\partial}{\partial t}(\rho_g \alpha_g) + \frac{\partial}{\partial x}(\rho_g \alpha_g u_g) = 0 \tag{4.4}$$

$$\frac{\partial}{\partial t}(\rho_l \alpha_l) + \frac{\partial}{\partial x}(\rho_l \alpha_l u_l) = 0 \tag{4.5}$$

While the conservation of momentum are given in equations (4.6) and (4.7) for gas and liquid respectively [6].

$$\frac{\partial}{\partial t}(\rho_g \alpha_g u_g) + \frac{\partial}{\partial x}(\rho_g \alpha_g u_g^2) + \Delta p \frac{\partial}{\partial x}(\alpha_g) + \alpha_g \frac{\partial}{\partial x}(p) = Q_g + M_g^D \tag{4.6}$$

$$\frac{\partial}{\partial t}(\rho_l \alpha_l u_l) + \frac{\partial}{\partial x}(\rho_l \alpha_l u_l^2) + \Delta p \frac{\partial}{\partial x}(\alpha_l) + \alpha_l \frac{\partial}{\partial x}(p) = Q_l + M_l^D \tag{4.7}$$

Where the source term due to gravity and friction effect is represented by Q_f and M_f^D represent interfacial drag force for the fluid phase f. The total interfacial drag force is zero as equation (4.8) outlines [6]. The capillary effects are represented by Δp.

$$M_g^D + M_l^D = 0 \tag{4.8}$$

It is also necessary to include some equations of states (EOS) for the gas and liquid phase since the density of the phase will vary when there is a column of fluid due to the change in pressure. These thermodynamic relations are simplified and given by equation (4.9) for gas and equation (4.10) for liquid [6].

$$\rho_g = \frac{p}{a_g^2} \tag{4.9}$$

$$\rho_l = \rho_{l,0} + \frac{p - p_0}{a_l^2} \tag{4.10}$$

Where p_0 is atmospheric pressure, that is $1\,bar = 10^5\,Pa$, and a_g and a_l are sound velocity in gas and liquid respectively. The values are approximately $a_g^2 = 10^5\ m^2/s^2$ and $a_l^2 = 10^6\,m^2/s^2$ [6]. An important observation to make here is that the pressure will not influence the density to liquid as much as gas since the liquid density is most dependent of the liquid density at atmospheric pressure.

The phase volume fractions can be related to conserved variable by relating equation (4.1) with equation (4.2), and as seen from the equations (4.9) and (4.10) are densities related to pressure as shown in [6].

$$\frac{m_g}{\rho_g(p)} + \frac{m_l}{\rho_l(p)} = 1 \tag{4.11}$$

In order to get rid of the fractions in equation (4.11), can it be multiplied with the densities of gas and oil which leads to following equation.

$$m_g \rho_l(p) + m_l \rho g(p) = \rho_g(p)\rho_l(p) \tag{4.12}$$

By inserting equations (4.9) and (4.10) into equation (4.12) pressure can be related to mass densities, sound velocities, the density of liquid at atmospheric pressure and the atmospheric pressure.

$$m_g\left(\rho_{l,0}+\frac{p-p_0}{a_l^2}\right)+m_l\frac{p}{a_g^2}=\frac{p\rho_{l,0}}{a_g^2}+\frac{p^2-pp_0}{(a_g a_l)^2} \tag{4.13}$$

Which can be rewritten to the following expression.

$$p^2+p(\rho_{l,0}a_l^2-m_g a_g^2-m_l a_l^2-p_0)=m_g a_g^2(\rho_{l,0}a_l^2-p_0) \tag{4.14}$$

This means that pressure is a polynomial of second degree. The pressure is only a function of the mass densities of gas and oil, $p(m_g, m_l)$ due to $\rho_{l,0}, a_g, a_l$ and p_0 are defined constants for the specific gas, liquid and the known reference pressure. Hence the equation be written as

$$p^2+pB(m_g,m_l)+C(m_g)=0 \tag{4.15}$$

where $B(m_g,m_l)=\rho_{l,0}a_l^2-m_g a_g^2-m_l a_l^2-p_0$ and $C(m_g)=m_g a_g^2(\rho_{l,0}a_l^2-p_0)$. The pressure difference (Δp) in the equations (4.6) and (4.7), is a term which is chosen in order to make the model well defined [6].

4.2 Derivation of the simplified model

The mathematical model described in the previous section can be simplified to be used on a smaller scale. The conservation of mass equations are as shown below the same as in the general model, equations (4.4) and (4.5), which the equation below indicates.

$$\partial_t(n)+\partial_x(nu_g)=0 \tag{4.16}$$

$$\partial_t(m)+\partial_x(mu_l)=0 \tag{4.17}$$

Where $n=\alpha_g\rho_g$ and $m=\alpha_l\rho_l$ are the mass density of gas and liquid respectively. While the conservation of momentum equations will differ from the general model.

$$\partial_t(nu_g)+\partial_x(nu_g^2)+\alpha_g\partial_x P_g=-f_g u_g-C(u_g-u_l)-ng+\partial_x(\mu_g\partial_x u_g) \tag{4.18}$$

$$\partial_t(mu_l)+\partial_x(mu_l^2)+\alpha_l\partial_x P_l=-f_l u_l+C(u_g-u_l)-mg+\partial_x(\mu_l\partial_x u_l) \tag{4.19}$$

The difference with this model with respect to the conservation of momentum equations, are that some choices have been made for the terms on the right hand side of the equations

(4.6) and (4.7). Instead of having gravity and friction forces included in the sink/source term (Q_g and Q_l) as in equations (4.6) and (4.7) they are separated in the new equation. The gravitational forces are represented by the terms ng and mg, which indicates that flow in vertical direction is of consideration. While the friction terms are represented by f_g as friction between gas and pipe wall, f_l as friction between liquid and pipe wall and C as the interfacial tension between gas and liquid. In addition has the pressure difference term (Δp) been removed from the expression and a viscosity term ($\partial_x(\mu\partial_x u)$) has been added.

As earlier, the sum of the volume fractions will be equal to one.

$$\alpha_l + \alpha_g = 1 \tag{4.20}$$

4.2.1 Assumptions to simplify the model

In order to achieve a simplified model are several assumptions made. The capillary pressure between gas and liquid is assumed to be zero. This means that the pressure of the gas phase will be equal to the pressure of the liquid phase.

$$P_l = P_g = P \tag{4.21}$$

As in explained in the sections 2.3.4 and 4.1, are the phase densities dependent of pressure, $\rho_g = \rho_g(P)$ and $\rho_l = \rho_l(P)$. In order to simplify this model when studying on laboratory-scale with a vertical conduct approximately 5 meters high, it is assumed that the fluids are incompressible and viscosity terms are zero. Incompressible fluids means no change in density with respect to change in time or height. This assumption eliminates the densities due to they are constant and common terms in the equations of conservation of mass, (4.16) and (4.17), which will reduce the expressions as indicated below.

$$\partial_t \alpha_g + \partial_x(\alpha_g u_g) = 0 \tag{4.22}$$

$$\partial_t \alpha_l + \partial_x(\alpha_l u_l) = 0 \tag{4.23}$$

By adding the conservation of mass equations, (4.22) and (4.23), and use that the constraint that sum of volume fractions are equal to one, equation (4.20), a conservation of mass equation for the whole system is achieved.

$$\partial_t(1) + \partial_x(\alpha_g u_g + \alpha_l u_l) = \partial_x(u_{mix}) = 0 \tag{4.24}$$

This indicates that the mixture velocity (u_{mix}), defined in section 2.3.2, equation (2.13), in other words the total velocity, is constant. By implementing the boundary condition

of no flow at the bottom of the pipe (at $x = 0$), will lead to the constant value of the total velocity in the system is zero ($u_{mix} = 0$). Therefore can the superficial velocity to liquid be set to equal magnitude as the superficial velocity to gas. However, the flows will be in opposite directions as the negative sign in front of the superficial liquid velocity indicates.

$$u_{mix} = 0,\ u_{gs} = \alpha_g u_g = -\alpha_l u_l = -u_{ls} \tag{4.25}$$

Remark 1 *This indicates that the superficial velocities are equal. As seen from equation (2.12), will this only balance the flow such that the amount gas ascending is balance with the amount of liquid flowing downwards. Note that this does not mean that the phase (real) velocities of gas and liquid are equal.*

The conservation of momentum equations, (4.18) and (4.19), are also reduced by using the following assumptions:

- Incompressible fluids, $\rho(P) = \rho$
- Equal phase pressure (zero capillary pressure) $P_g = P_l = P\,(P_c = P_g - P_l = 0)$
- Viscosity term is ignored, which eliminates $\partial_x(\mu\partial_x(u))$ (Viscosity effects are accounted for by the friction terms on the right hand side of the conservation of momentum equations. This will be considered in section 4.2.5)
- No acceleration effects. This assumption eliminates the flux of momentum ($\partial_t(mu)$) and the rate of accumulation of momentum ($\partial_x(mu^2)$), which is an reasonable assumption since the terminal velocity is reached quickly after release [26].

Therefore can the conservation of momentum equations (4.18) and (4.19) be simplified to the following equations.

$$\alpha_g \partial_x P = -f_g u_g - C(u_g - u_l) - \rho_g \alpha_g g \tag{4.26}$$

$$\alpha_l \partial_x P = -f_l u_l + C(u_g - u_l) - \rho_l \alpha_l g \tag{4.27}$$

4.2.2 Phase velocities and superficial velocities

It is of interest to find expressions of phase velocities. A more detailed derivation is included in Appendix 9.1. The equations (4.26) and (4.27) are solved for u_g and u_l

respectively.

$$u_g = -\frac{\alpha_g \partial_x P + \rho_g \alpha_g g - C u_l}{C + f_g} \tag{4.28}$$

$$u_l = -\frac{\alpha_l \partial_x P + \rho_l \alpha_l g - C u_g}{C + f_l} \tag{4.29}$$

As seen from the expression does both of them consist of both velocity terms u_g and u_l. Therefore is the expression of u_l implemented into equation (4.28) and the expression of u_g inserted into equation (4.29), to achieve expressions of phase velocities that does not depend on the velocity of the other phase.

$$u_g = -\frac{\alpha_g \partial_x P + \rho_g \alpha_g g + C\frac{\alpha_l \partial_x P + \rho_l \alpha_l g}{C + f_l}}{C + f_g - \frac{C^2}{C + f_l}} \tag{4.30}$$

$$u_l = -\frac{\alpha_l \partial_x P + \rho_l \alpha_l g + C\frac{\alpha_g \partial_x P + \rho_g \alpha_g g}{C + f_g}}{C + f_l - \frac{C^2}{C + f_g}} \tag{4.31}$$

As seen in the expressions above, they consist of two parts. One part that is dependent on pressure and one gravity dependent part. By some rearranging and use of the constraint of volume fractions, equation (4.20), can the equations (4.32) and (4.33) be achieved.

$$u_g = -\frac{\alpha_g f_l + C}{C f_g + C f_l + f_g f_l}\partial_x P - \frac{\alpha_g \rho_g f_l + (\alpha_l \rho_l + \alpha_g \rho_g) C}{C f_g + C f_l + f_g f_l} g \tag{4.32}$$

$$u_l = -\frac{\alpha_l f_g + C}{C f_g + C f_l + f_g f_l}\partial_x P - \frac{\alpha_l \rho_l f_g + (\alpha_l \rho_l + \alpha_g \rho_g) C}{C f_g + C f_l + f_g f_l} g \tag{4.33}$$

From these two equations can the superficial phase velocities which are used in the conservation of mass equations, (4.22) and (4.23), be found by using the relation described in section 2.3.2, equation (2.12).

$$u_{gs} = -\frac{\alpha_g^2 f_l + \alpha_g C}{C f_g + C f_l + f_g f_l}\partial_x P - \frac{\alpha_g^2 f_l + \alpha_g C}{C f_g + C f_l + f_g f_l}\rho_g g - \frac{\alpha_g \alpha_l (\rho_l - \rho_g) C}{C f_g + C f_l + f_g f_l} g \tag{4.34}$$

$$u_{ls} = -\frac{\alpha_l^2 f_g + \alpha_l C}{C f_g + C f_l + f_g f_l}\partial_x P - \frac{\alpha_l^2 f_g + \alpha_l C}{C f_g + C f_l + f_g f_l}\rho_l g + \frac{\alpha_g \alpha_l (\rho_l - \rho_g) C}{C f_g + C f_l + f_g f_l} g \tag{4.35}$$

4.2.3 Pressure

An expression for $\partial_x P$ is needed to eliminate the number of unknowns in the model. It can be found by adding the superficial velocities together and assuming that the total velocity

is zero, $u_{mix} = u_{gs} + u_{ls} = 0$ as indicated by equation (4.25). During the derivation it is observed that the last terms in u_{gs} and u_{ls} in equations (4.34) and (4.35) cancel each other. A more detailed derivation is found in Appendix 9.2.

$$\partial_x P = -\frac{\frac{\alpha_g^2 F_l + \alpha_g C}{C f_g + C f_l + f_g f_l}\rho_g + \frac{\alpha_l^2 F_g + \alpha_l C}{C f_g + C f_l + f_g f_l}\rho_l}{\frac{\alpha_g^2 f_l + \alpha_g C}{C f_g + C f_l + f_g f_l} + \frac{\alpha_l^2 f_g + \alpha_l C}{C f_g + C f_l + f_g f_l}} g \tag{4.36}$$

which can be rewritten to equation (4.37).

$$\partial_x P = -\frac{\lambda_g \rho_g + \lambda_l \rho_l}{\lambda_g + \lambda_l} g = -\frac{\lambda_g \rho_g + \lambda_l \rho_l}{\lambda_t} g \tag{4.37}$$

where λ_g, λ_l and λ_t are defined as following:

$$\lambda_g = \frac{\alpha_g^2 F_l + \alpha_g C}{C f_g + C f_l + f_g f_l} \tag{4.38}$$

$$\lambda_l = \frac{\alpha_l^2 F_g + \alpha_l C}{C f_g + C f_l + f_g f_l} \tag{4.39}$$

$$\lambda_t = \lambda_g + \lambda_l = \frac{\alpha_g^2 f_l + \alpha_l^2 f_g + C}{C f_g + C f_l + f_g f_l} \tag{4.40}$$

It is also of interest to find the expression of pressure, $P(x)$. This is obtained by consider equation (4.37) and integrate over the section of consideration.

$$\int_x^L \partial P = -\int_x^L \frac{\lambda_g \rho_g + \lambda_l \rho_l}{\lambda_t} g \partial x \tag{4.41}$$

This leads to

$$P(x) = P(x = L) + g \int_x^L \frac{\lambda_g \rho_g + \lambda_l \rho_l}{\lambda_t} dx \tag{4.42}$$

where $P(x = L) = 1\, atm \approx 10^5\, Pa$

4.2.4 Superficial velocities

By implementing equation (4.37) into the superficial velocity equation of gas and liquid, equation (4.34) and (4.35) respectively, and using definitions of λ_g, λ_l and λ_t expressions (4.38)-(4.40) in the superficial velocities may the pressure dependency be eliminated. This derivation will only be shown for the superficial velocity of liquid since the derivation of the superficial velocity of gas will be the same and is shown in Appendix 9.3.

$$u_{ls} = \frac{\lambda_g \rho_g + \lambda_l \rho_l}{\lambda_t} \lambda_l g - \lambda_l \rho_l g + \frac{\alpha_g \alpha_l (\rho_l - \rho_g) C}{C f_g + C f_l + f_g f_l} g \tag{4.43}$$

By using the relation between λ_g, λ_l and λ_t in equation (4.40), the first fraction can be rewritten by expressing λ_l with λ_g and λ_t.

$$u_{ls} = \frac{\lambda_g(\rho_g - \rho_l) + \lambda_t \rho_l}{\lambda_t} \lambda_l g - \lambda_l \rho_l g + \frac{\alpha_l \alpha_g (\rho_l - \rho_g) C}{C f_g + C f_l + f_g f_l} g \tag{4.44}$$

This equation above can be reduced by defining $\Delta\rho = \rho_l - \rho_g$, to following expression:

$$u_{ls} = -\frac{\lambda_l \lambda_g}{\lambda_t} \Delta\rho g + \frac{\alpha_l \alpha_g C}{C f_g + C f_l + f_g f_l} \Delta\rho g \tag{4.45}$$

By implementing the relations for λ_g, λ_l and λ_t defined in equation (4.38)-(4.40) in order to reduce the expression further.

$$u_{ls} = -\frac{\frac{(\alpha_l^2 f_g + \alpha_l C)(\alpha_g^2 f_l + \alpha_g C)}{(C f_g + C f_l + f_g f_l)^2}}{\frac{\alpha_l^2 f_g + \alpha_g^2 f_l + C}{C f_g + C f_l + f_g f_l}} \Delta\rho g + \frac{\alpha_l \alpha_g C}{C f_g + C f_l + f_g f_l} \Delta\rho g \tag{4.46}$$

After some calculation where $C f_g + C f_l + f_g f_l$ is observed to be a common term and reduce the expression to one fraction is the equation (4.47), obtained.

$$u_{ls} = -\frac{\alpha_l^2 \alpha_g^2}{\alpha_l^2 f_g + \alpha_g^2 f_l + C} \Delta\rho g \tag{4.47}$$

By using the relationship between the phase volume fractions in equation (4.20), the superficial phase velocity of liquid may be expressed with only the volume fraction of liquid.

$$u_{ls} = -\frac{\alpha_l^2 (1 - \alpha_l)^2}{\alpha_l^2 f_g + (1 - \alpha_l)^2 f_l + C} \Delta\rho g \tag{4.48}$$

As mentioned earlier is the derivation of the superficial gas velocity, u_{gs}, the same as for the superficial velocity of liquid, u_{ls} and the result is shown in equation (4.49).

$$u_{gs} = \frac{\alpha_g (1 - \alpha_g)^2}{\alpha_l^2 f_g + \alpha_g^2 f_l + C} \Delta\rho g \tag{4.49}$$

Hence, the derivation led to expressions with reduced number of unknowns. The superficial velocities expressed by friction parameters (f_g, f_l and C) and fluid volume fractions (α).

4.2.5 Conclusion

The derivation from the conservation of mass equations (4.16) and (4.17), and conservation of momentum equations (4.18) and (4.19) for gas and liquid respectively, lead to by

several assumptions, a simplified model for velocities of gas and liquid flows in vertical pipes, equations (4.49) and (4.48), for gas and liquid respectively.

Some choices for the friction parameters (f_g, f_l and C) have to be made. The frictions are assumed to be dependent of the viscosities (a fluids inner resistance against flow), fluid volume fractions and some constants that determines the strength of the frictions. The proposed expressions for friction between the gas and wall (f_g), friction between liquid and wall (f_l) and interfacial tension (C) are indicated below.

$$f_g = I_g \mu_g \alpha_g = I_g \mu_g (1 - \alpha_l) \tag{4.50}$$

$$f_l = I_l \mu_l \alpha_l \tag{4.51}$$

$$C = II \mu_l \alpha_l \tag{4.52}$$

where I_g, I_l and II are constants that determines the strength of the frictions.

Remark 2 *As mentioned are the friction expression only proposed expressions. The fluid volume fraction (α) is included to avoid friction of a phase when it is not present and relate it to amount of the phase present. The previous research showed that the velocity of ascending gas is related to the viscosity (μ), which make it reasonable to assume that it should be included in the friction terms as it is a measure of the fluids inner friction against flow.*

In addition, to simplify the expressions further are some gravity terms defined.

$$\gamma_g = \rho_g g, \ \gamma_l = \rho_l g, \ \Delta\gamma = \gamma_l - \gamma_g \tag{4.53}$$

As a result of the assumed expression of friction terms and the defined gravity terms, are two functions defined. The function $g(\alpha_g)$ is the superficial velocity function for gas and the function $h(\alpha_l)$ is the superficial velocity function for liquid, only expressed as a function of the corresponding volume fraction.

$$g(\alpha_g) = u_{gs} = \frac{\alpha_g (1 - \alpha_g)^2}{\alpha_g (1 - \alpha_g) I_l \mu_l + (1 - \alpha_g)^2 I_g \mu_g + II \mu_g} \Delta\gamma \tag{4.54}$$

$$h(\alpha_l) = u_{ls} = -\frac{\alpha_l (1 - \alpha_l)^2}{\alpha_l (1 - \alpha_l) I_g \mu_g + (1 - \alpha_l)^2 I_l \mu_l + II \mu_l} \Delta\gamma \tag{4.55}$$

Which gives new expressions of the conservation of mass equations (4.22) and (4.23).

$$\partial_t \alpha_g + \partial_x g(\alpha_g) = 0 \tag{4.56}$$

$$\partial_t \alpha_l + \partial_x h(\alpha_l) = 0 \tag{4.57}$$

The function $h(\alpha_l)$, equation (4.55) is implemented into a MATLAB script for finding a numerical solution. As described in section 2.4, in order to find a solution is a discrete scheme necessary to implement into MATLAB. The discrete scheme used in this thesis is taken from the course *PET565:Core scale modelling and interpretation*, named "solCentral". This scheme was used to study a Buckley-Leverett model by a central based discretization with a correction term included, equation (2.19) [9]. The only change that had to be considered was that in this thesis are there no inflow at the bottom of the pipe.

5 THE BASE CASE

By use of the mathematical model derived in the previous section, equation (4.55), is a slug flow of two-phases, air as gas and water as liquid, in a vertical pipe of $5\,m$ height and diameter of $0,08\,m$, simulated in MATLAB. Based on earlier research and observations from experiments as considered in section 3, there are some indication of how the variables should be determined to make the model as accurate as possible. In addition must the parameters that defines the grid of the model be determined carefully to achieve stability and accuracy as described in section 2.4. On this background is a Base case of the model constructed.

5.1 Initial fluid distribution

The initial distribution of fluids in this simplified gas-liquid model is a volume of gas approximately at the bottom of the pipe with a little layer of liquid beneath it and a large liquid column above. This layer of gas is chosen to be $0,4\,m$, which is large enough to ensure that the physical properties occurring during the flow will be observed in the results. As shown in previous research does not the length of the Taylor bubble impact the velocity of the ascending gas bubble significantly [5, 16, 20, 24, 26]. The length of the little layer of liquid beneath the gas and the large liquid column above the gas layer are respectively $0,05\,m$ and $3,55\,m$. The pipe is open to atmosphere at the top, and therefore it will contain gas above the liquid column. The expression below, equation (5.1), indicates mathematically the distribution of liquid initially in the pipe, where α_l is the liquid volume fraction and x is the height of pipe in meters.

$$\alpha_l(x, t=0) = \alpha_{l,0} = \begin{cases} 1, & if\ 0 < x < 0,05 \\ 0, & if\ 0,05 \leq x \leq 0,45 \\ 1, & if\ 0,45 < x \leq 4,0 \\ 0, & if\ 4,0 < x \end{cases} \tag{5.1}$$

This is also illustrated in figure (5.1) where a graphical illustration of the initial fluid distribution in the pipe is presented.

As seen from the figure (5.1), the initial data will consist of three discontinuities, Riemann problems. The discontinuities are located at the three gas-liquid surfaces at $0,05\,m$, $0,45\,m$ and $4,0\,m$, and arises by the quick changes in saturation. Since the liquid velocity function, $h(\alpha_l)$, is not a typical convex function, cannot the theory for computing

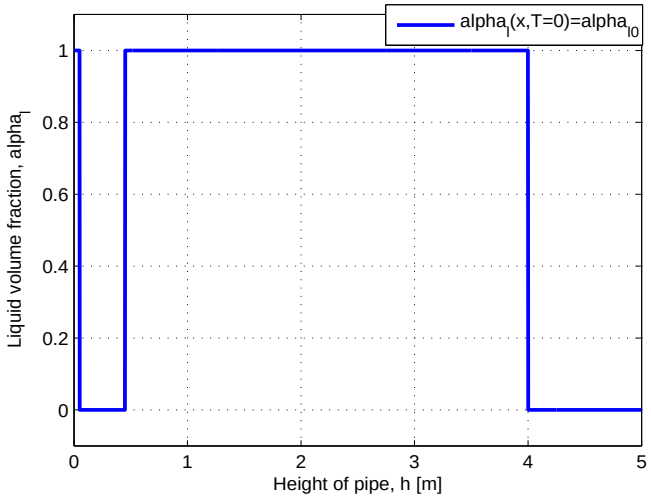

Figure 5.1: *Initial saturation distribution of liquid (water), α_{l0}, in the pipe*

solution of Riemann problem as described in section 2.5, be used directly. When the numerical solution of the model is simulated through MATLAB it will be observed if there exist a rarefaction wave and/or shock wave solution for the discontinuities.

5.2 The behaviour of the ascending Taylor bubble

The Base case is constructed with the parameters defined in table (5.1). The numerical solutions of the Base case at different times ($T = 4$, 8 and 14 s) are shown in figure (5.2). The left figures illustrate the liquid velocity function, $h(\alpha_l)$, and are equal for all times (time independent). While the right figures give an impression of how the gas will ascend by the changes in fluid saturation distribution in the pipe as the time passes by.

From the numerical solution, it is observed that a Taylor bubble of gas is formed very quickly after the release of gas. This corresponds well with the performance of the experiments by Benja, as the Taylor bubble was seen to form quickly after opening of the valve. Figure (5.2 a), shows the numerical saturation distribution in the pipe four seconds after the release of the gas. The gas slug is characterised by a sharp front (discontinuity) where the liquid saturation (α_l) decreases from 1 to approximately $0,5$ in almost no difference in height of the pipe, which indicates a shock wave solution. The next part of the function is more curved, and represents the nose of the Taylor bubble. Here it is observed that the saturation of liquid gradually decreases from $0,5$ to approximately $0,2$ as one go further down in the pipe (from approximately $1,6\,m$ to $1,1\,m$), which gives a rarefaction wave solution. As figure (2.2 b) shows corresponds this gradual decrease with

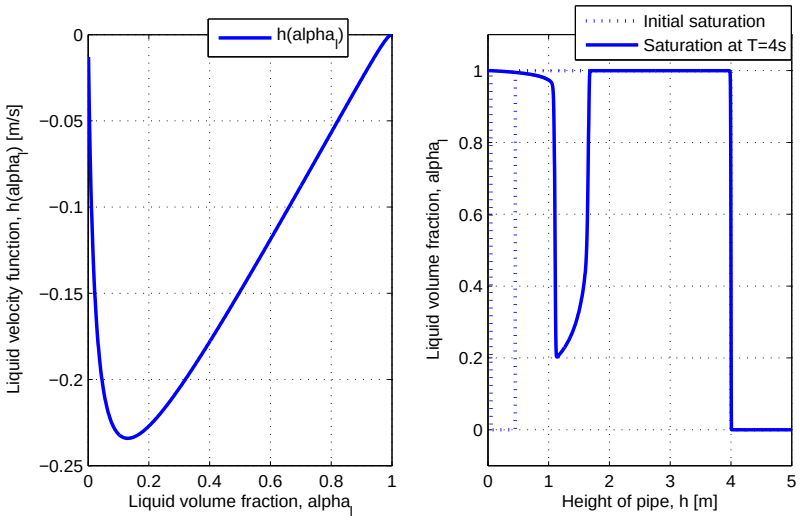

(a) Time, T=4s

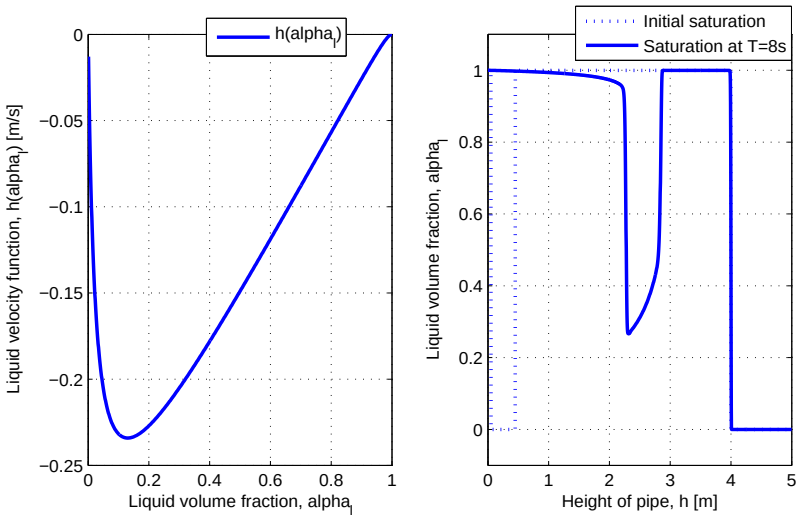

(b) Time, T=8s

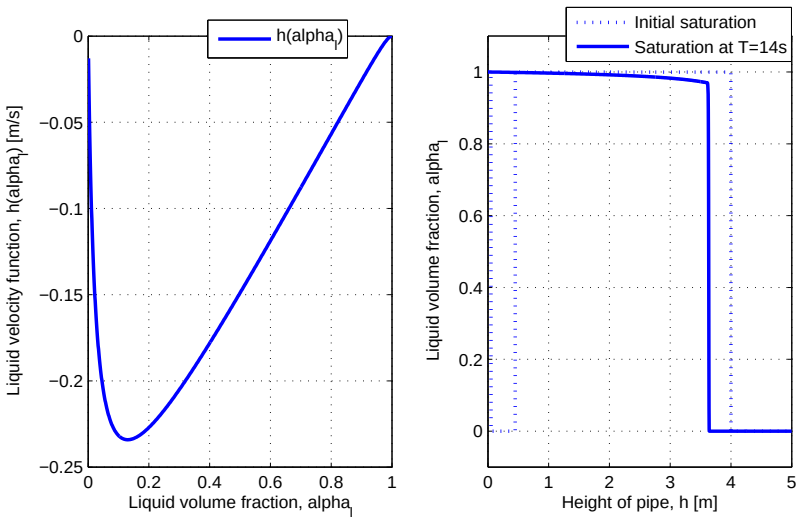

(c) Time, T=14s

Figure 5.2: *Base Case, illustration of the saturation distribution at different times*

Table 5.1: *Variables for input in MATLAB for the Base case*

Parameter description		Unit	Value
Number of cells	N		2000
Length of pipe	L	m	5
Length of cells	$\Delta x_{N=2000}$	m	$0,0025$
Number of time step	$NSTEP$		80
Length of timestep	$\Delta t_{T=14}$	s	$0,175$
Stability	a		20
Density liquid	ρ_l	kg/m^3	1000
Density gas	ρ_g	kg/m^3	1
Gravity constant	g	m/s^2	$9,81$
Viscosity liquid	μ_l	$Pa \times s$	$1,2 \times 10^{-3}$
Viscosity gas	μ_g	$Pa \times s$	5×10^{-5}
Friction constants	I_l	$1/m^2$	60×10^2
	I_g		60×10^7
	II		60×10^4

the shape of the nose. The saturation distribution around the body of a Taylor bubble should be almost constant as a fully developed liquid film from previous research was found to be formed a distance behind the nose [17], but as seen in figure (5.2 a) this is not the case as the rarefaction wave solution continues to the bottom of the ascending Taylor bubble. This means that the numerical solution shows the discontinuity at the top of the gas layer given in the initial data at $x = 0,45\,m$, will give an shock wave solution followed by a rarefaction wave solution of the Riemann problem.

After the rarefaction wave follows a new shock wave at $x \approx 1,1\,m$. Here is there an increasing jump in liquid saturation from $0,2$ to $0,9$. A rarefaction wave follows afterwards which reflects the tail of the gas slug that increases in the liquid saturation back to the bottom of the pipe. This is the transition from the back of the Taylor bubble which represents the discontinuity in the bottom of the gas layer located at $0,05\,m$ in the initial data, where the numerical solution will be a shock wave followed by a rarefaction wave.

The rarefaction wave that reflects the tail corresponds well with the observation made during the performance of the experiments by Benja, where gas bubbles with decreasing size followed the Taylor bubble. These were observed to have decreasing velocity as the size of the bubble decreased and were still ascending through the liquid column after the Taylor bubble had passed through the system. This effect is also reflected in the

numerical solution. In figure (5.2 c) which shows the saturation distribution in the pipe after time $T = 14\,s$, has the Taylor bubble passed through the system, but as observed are there still gas present that decreases in saturation in the pipe down to $x \approx 1\,m$. The numerical solution also indicates that the length of the tail increases as the Taylor bubble ascend. This effect can be explained by the shock wave at the back of the Taylor bubble has a higher velocity than the rarefaction wave that follows, which means that the length of the rarefaction wave increases.

Figure (5.2 b) shows the same trend in shock wave and rarefaction wave solution as described for figure (5.2 a) for the ascending Taylor bubble. The discontinuity at the top of the pipe at $x = 4$, does not give a shock wave solution or a rarefaction wave solution. This discontinuity will be considered in the next section, 5.3.

By investigation of the figure (5.2 a,b) it is observed that the Taylor bubble increases in length as it starts to ascends in the pipe compared with the initial length of the gas layer. This is also confirmed by the use of data cursor in MATLAB. Initially the gas layer has a length of $0,4\,m$ and after 4 and $8\,s$ it has increased to approximately $0,6\,m$. In addition there is a small increase between 4 and $8\,s$. The reason for this increase in length is due to the falling liquid film around the bubble. In order to obtain the mass conservation, the ascending gas must become longer as it becomes thinner. From the experiments performed by Benja, it was also observed that the gas slug seemed to be longer compared to the initial layer.

5.3 Gas-liquid surface at the top of the pipe

Based on the experiments performed by Benja it was expected that the gas-liquid surface at the top of the pipe should rise quickly as the gas layer starts to ascend. In addition to a slower rise after the gas bubble has formed and some oscillation, as described in section 3.1. The numerical solution however, showed no rise in the discontinuity of the gas-liquid surface at the top of the pipe, figure (5.2 a,b). The loss of the quick increase in the gas-liquid surface may be due to in the experiments, the gas layer was separated from the liquid column by a valve, compared to in the numerical calculation is the gas in the same system as the liquid column initially. This means that the liquid is not forced to rise as the gas is set "free" to ascend. The effect of oscillation and the continued rise after formation of the Taylor bubble may be lost by the assumption of constant densities of the fluids made in the derivation of the model. Therefore, cannot the fluids expand or contract themselves when densities are set to be incompressible, which will eliminate

the oscillation. In the derivation was it seen that the total velocity, u_t, in the system was constant and equal to zero, due to the liquid beneath the gas layer stays still. Hence the superficial velocities of the fluids were equal to each other, equation (4.24). This leads to elimination of the rise since the volume of displaced liquid is always balanced by volume of ascending gas, as indicated in remark 1.

As expected, the height of water column in the pipe will sink with the same hight as the initial gas layer had when it was introduced to the system, figure (5.2 c). This is an effect from the conservation of mass with the assumption of incompressible fluids. A reduction in the gas-liquid surface at the top of the pipe was also observed in the experiments performed by Benja.

5.4 Velocity

From the results of previous experiments on ascending gas bubbles in liquids, it is reasonable to assume that the rise velocity to the gas in a pipe with a diameter of $0,08\,m$ is approximately $u_g \approx 0,3\ m/s$. In table (5.2) are ascend velocities of gas in pipes with diameters close to $0,08\,m$ filled with liquid. These values are either measured and/or calculated by equation (3.1) based on a proposed constant Froude number, Fr [4, 5, 15, 18, 24].

Table 5.2: *Velocity of acending gas slug based on measurements and proposed analytical solution from previous experiments with pipe diameter close to* $0,08\,m$

Researcher	Diameter $[cm]$	Froude constant	Calculated $\nu_b\ [\frac{m}{s}]$ (3.1)	Measured $\nu_b\ [\frac{m}{s}]$
Brown [3][13]	$8,00$	$0,303$	$0,268$	
Dumitrescu [5]	$8,00$	$0,351$	$0,311$	
Davies and Taylor [4]	$7,94$	$0,328$	$0,291$	$0,291$ – $0,306$
Paz [18]	$8,00$			$0,299$ – $0,302$
Viana et al [24]	$7,62$			$0,282$

Figure (5.3) illustrates the superficial gas velocity (red line) and superficial liquid velocity (blue line) as a function of the liquid saturation for the Base case. As shown in the derivation of the model, section 4.2, are the superficial velocities of equal magnitude but

flows in opposite directions due to the constant total velocity that was found to be zero, equation (4.24). Therefore are the superficial velocities in figure (5.3) symmetric around the axis of liquid volume fraction, α_l. The flow of liquid is negative due to positive flow direction is defined to be upwards in the pipe.

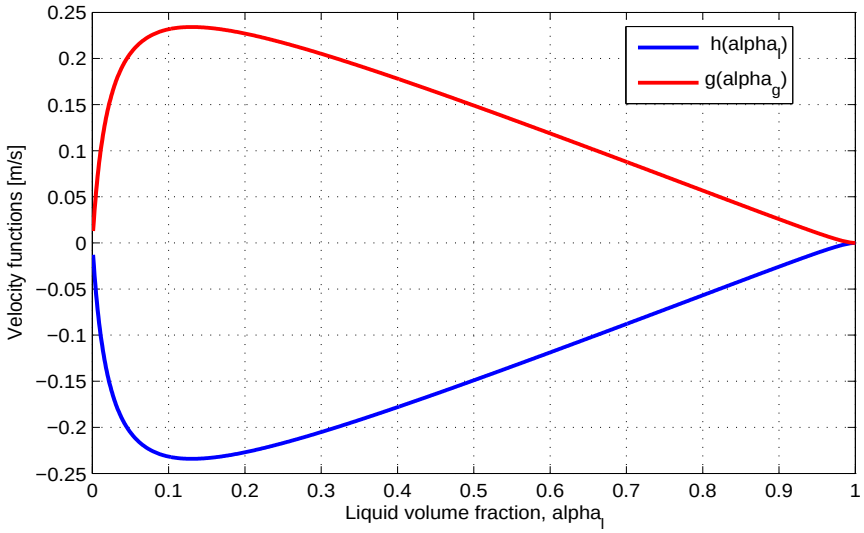

Figure 5.3: *Comparison of the superficial gas velocity, $g(\alpha_g)$, and superficial liquid velocity, $h(\alpha_l)$, for the Base case*

In the model there are several methods to investigate the velocity of the gas slug and there by check if it is correct according to the experimental data. This can be done by either compare the position for the front of the gas slug at different times or by use of the Rankine-Hugoniot jump condition, equation (2.26), which gives the speed to a shock wave solution. By the use of data cursor on the front of the gas slug at different times in figure (5.2 a,b), is the front velocity of the ascending Taylor bubble estimated by the use of fundamental velocity formula, $\nu_b = \frac{\Delta x}{\Delta t}$. The front of the gas slug is evaluated at liquid volume fractions of $\alpha_l = 0,9189$ at time, $T = 8\,s$, and $\alpha_l = 0,9151$ at time, $T = 4\,s$.

$$\frac{\Delta x}{\Delta t} = \frac{(2,856 - 1,664)\,m}{(8-4)\,s} = 0,298\,\frac{m}{s}$$

By use of the Rankine-Hugoniot jump condition, equation (2.26), may the speed to the front of the ascending Taylor bubble be calculated. The position of the shock wave is indicated in the right figure in (5.2 a), where α_l jumps from $0,502$ to 1 at the positions $x \approx 1,624 - 1,681$. Investigation of the liquid velocity function, $h(\alpha_l)$ from the left figure in (5.2 a), are the corresponding function values found to be $h(\alpha_l = 0,502) = -0,1484$ and $h(\alpha_l = 1) = 0$. This gives following speed of the front by Rankin-Hugoniot jump condition:

$$s = \frac{\Delta h(\alpha_l)}{\Delta \alpha_l} = \frac{-0,1484 - 0}{0,502 - 1} = 0,298\,\frac{m}{s}$$

The numbers are found by use of data cursor in MATLAB but some indication can also be obtained by the use of figure (5.2 a). The front velocity of the ascending Taylor bubble at time $T = 8\,s$ is also calculated by the Rankin-Hugoniot jump condition, equation (2.26), and is also found to be $0,298\,\frac{m}{s}$.

Due to the shock wave solution that is present both at the front and the bottom of the ascending Taylor bubble, figure (5.2 a,b), the velocity at the back of the ascending Taylor bubble can be evaluated also at the different times. The velocity at the back of the Taylor bubble is also evaluated by use of the fundamental velocity formula, $\nu_b = \frac{\Delta x}{\Delta t}$. The calculations of the velocities are similar to those illustrated above and the results from the calculations are implemented into table (5.3).

Table 5.3: *Velocities of the ascending gas calculated based on positions of the front of the bubble and Rankin-Hugoniot jump condition, equation* (2.26)

Method	Figure	Positions, either (x,t) or $(\alpha_l, h(\alpha_l))$	Velocity $[\frac{m}{s}]$
$\nu_b = \frac{\Delta x}{\Delta t}$	(5.2 a,b)	(1,664, 4,000) and (2,856, 8,000)	0,298
$\nu_b = \frac{\Delta x}{\Delta t}$	(5.2 a,b)	(1,084, 4,000) and (2,251, 8,000)	0,292
R-H speed s	(5.2 a)	(0,502, −0,1484) and (1,000, 0,000)	0,298
R-H speed s	(5.2 a)	(0,2144, −0,2245) and (0,9252, −0,0182)	0,290
R-H speed s	(5.2 b)	(0,5194, −0,1433) and (1,000, 0,000)	0,298
R-H speed s	(5.2 b)	(0,2725, −0,212) and (0,8813, −0,03163)	0,296

As seen from the table did all evaluations at the front of the Taylor bubble give the same ascend velocity, $0,298\,\frac{m}{s}$. This value is very close to the results from previous experiments, table (5.2). This makes the friction constant used for the Base case a reasonable estimate. The evaluations at the back of the Taylor bubble gave results that did not vary much from the front velocity, but all of them were a little lower than the front velocity. The effect of higher velocity at the front of the ascending bubble compared with the back can also be observed from the liquid velocity function in figure (5.3). By drawing a straight line between the liquid volume fractions (α_l) at approximately $0,5 - 1,0$ (for the front) and $0,2 - 0,9$ (for the back), it is observed that the slope is higher for the front. By the Rankin-Hugoniot jump condition, equation (2.26), this gives a higher speed of the shock wave solutions at the front of the ascending Taylor bubble.

5.5 Liquid film

Indication of the thickness of the liquid film are achieved by the empirical model, equation (3.10), proposed by E. W. Liewellin et al [15] and the correlation proposed by Kang et al, equation (3.9) [13]. In the numerical solution will indications of the thickness of the liquid film, λ, be achieved by the distribution of the liquid volume fraction, α_l, in the pipe.

The dimensionless inverse viscosity is found by equation (3.4).

$$N_f = \frac{1000}{1,2 \times 10^{-3}} \sqrt{9,81 \times 0,08^3} = 59059,292$$

Such high value of the dimensionless inverse viscosity will as described in the theory earlier, section 3.2.1, make the thickness off the liquid film independent of the dimensionless inverse viscosity and will have a dimensionless thickness of the liquid film approximately around $\lambda' = 0,08$ [15]. When the dimensionless inverse viscosity is implemented into the empirical model (3.10) as the calculation below shows it gives out approximately $\lambda' = 0,08$.

$$\lambda' = 0,204 + 0,123 \times tanh(2,66 - 1,15 \times log_{10}(59059,292) = 0,082 \approx 0,08$$

Therefore the thickness of the liquid film can be calculated from the relationship shown in equation (2.14).

$$\lambda = 0,04 \times 0,08 = 0,32\,cm$$

The relation in equation (2.7) gives the volume fraction of gas and liquid by the areas occupied of liquid and gas. This gives a volume fraction of gas at,

$$\alpha_g = \frac{(8 - 2 \times 0,32)^2}{8^2} = 0,846$$

while the liquid volume fraction will be at $\alpha_l = 0,154$ by equation (4.20).

The thickness of the falling liquid film by the correlation from Kang et al where the dimensionless thickness of the film is related to the diameter of the pipe is expressed in equation (3.9) [13].

$$\lambda' = 0,32(59059,292^2)^{-0,1} = 0,036$$

This will give a film thickness of $\lambda = \lambda' \times D = 0,036 \times 0,08 = 0,288\,cm$. The gas volume fraction will be at $\alpha_g = 0,861$ and the liquid volume fraction at $\alpha_l = 0,139$.

It is therefore reasonable to assume that the numerical solution should give the volume fraction of gas at $\alpha_g \approx 0,85$, and the volume fraction of liquid at $\alpha_l \approx 0,15$. The figure

(5.2 a,b) shows that the liquid volume factor at the gas slug will increase as it moves throughout the pipe, which means that the thickness of the liquid film will increase. Previous research shows that ideally should the thickness of the liquid film stay constant after the formation of the gas slug as it depends mainly on the viscosity of the liquid and the interfacial tension between the fluids [10, 13, 15, 17, 21, 27]. However, due to the formation of the tail consisting of dispersed gas bubbles and a small increase in length of the gas slug as it moves upwards, will the liquid volume fraction increase at the body of the gas slug in the numerical solution.

5.6 Accuracy of the numerical solution and stability

As mentioned in section 2.4, it is important to use appropriate size of grid during the numerical simulations and investigations. In addition may stability problems occur from when the stability condition in equation (2.22) is not fulfilled or other effects may cause problems when the numerical solution is to be found.

5.6.1 Comparison of grid

The figure (5.4) illustrates the importance of using appropriate grid during numerical investigations. By comparing the grid of 500 cells ($N = 500$) with the grid of 2000 cells ($N = 2000$) after four seconds it can be seen that the liquid saturation of the front is lower and that the front is more smeared out, in addition to the simulation was very fast with the grid of 500 cells. With the grid of 5000 cells ($N = 5000$) took the simulation long time and by comparing with the grid of 2000 cells is little difference observed. Therefore it is safe to use the number of 2000 cells in order to achieve accurate simulations and to keep the computing time low.

5.6.2 Stability

A too steep liquid velocity function may, as the left image in figure (5.5) illustrates, create stability problems during calculation of the numerical solution of the saturation distribution. From the simulation, it was seen that the numerical solution of the saturation distribution immediately after start gave both unlikely and unphysical values through the pipe. As seen from the right image in figure (5.5) at the lower part of the pipe, does the saturation distribution show a layer of gas with varying saturation instead of a Taylor

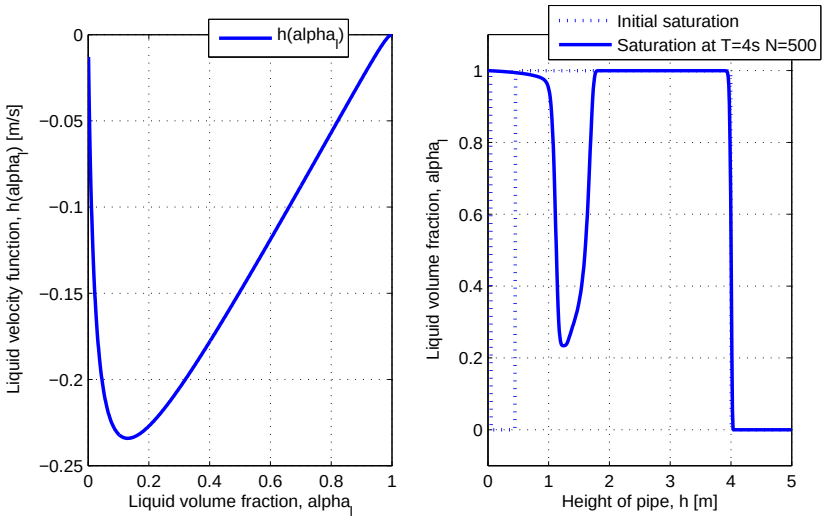

(a) *Grid with 500 cells,* ($N = 500$)

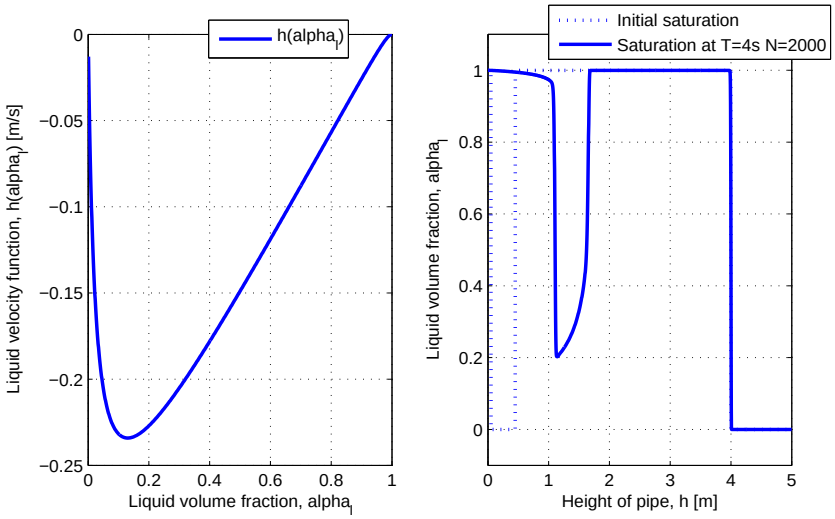

(b) *Grid with 2000 cells,* ($N = 2000$)

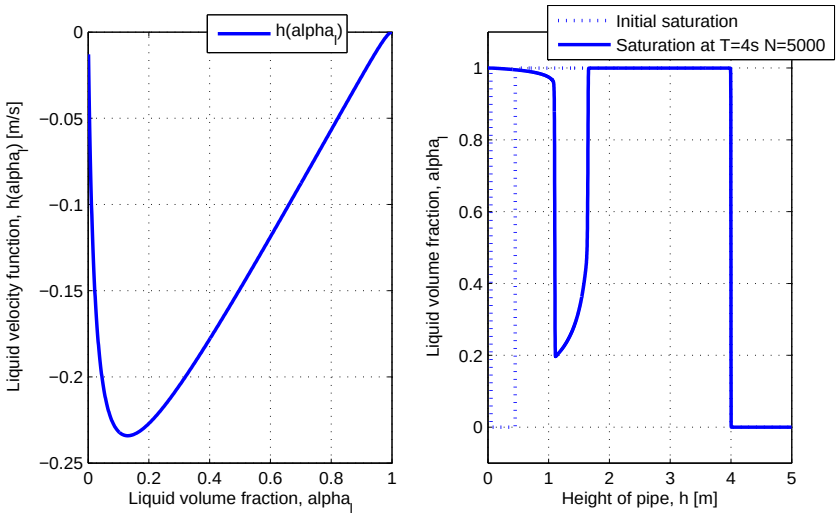

(c) *Grid with 5000 cells,* ($N = 5000$)

Figure 5.4: *Comparison of the number of grid cells,* N*, effects the simulation to make it as accurate as possible*

bubble. At the upper part of the pipe gives an unphysical solution as it shows liquid above the upper gas-liquid surface in the pipe, in addition to liquid saturations above one and below zero. It is also observed that the gas-liquid surface at the top of the pipe has raised upwards approximately the same distance as the layer of gas in the bottom has raised.

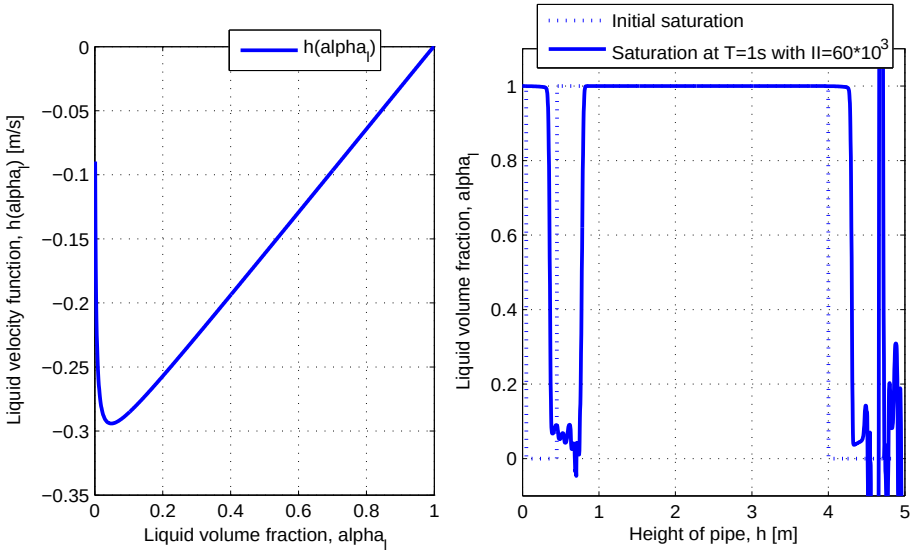

Figure 5.5: *Illustration of an unstable simulation due to steep liquid velocity function,* $h(\alpha_l)$

Stability problems may also occur when the variable a is set to low [7]. When the parameter a is set to low will not the stability condition described earlier in equation (2.22), be satisfied. The right images in figure (5.6 a,b) shows how a too low value of parameter a will affect the numerical solution. The numerical solution in figure (5.6 a) is seen to be within the stability area. Here is the value of parameter a set to be 9. While the numerical solution in figure (5.6 b) shows an unphysical solution, where the liquid volume fraction is above one and below zero in the pipe. That is for a parameter a at 8. In addition it is observed that the gas-liquid surface at the top of the pipe has moved upwards, as it did with too steep velocity curve.

An important observation that was noticed during the simulations with variation in the parameter a were that when a was low the computing time was also low, but when a was high did also the computing time increase. It was therefore kept at a value of $a = 20$ in the rest of the simulations to keep the simulation time low but still accurate.

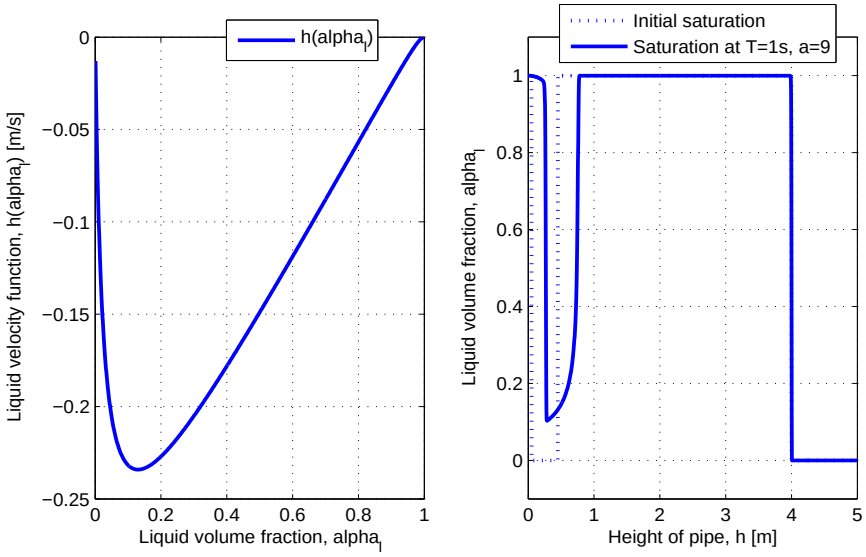

(a) *Stable simulation with* $a = 9$

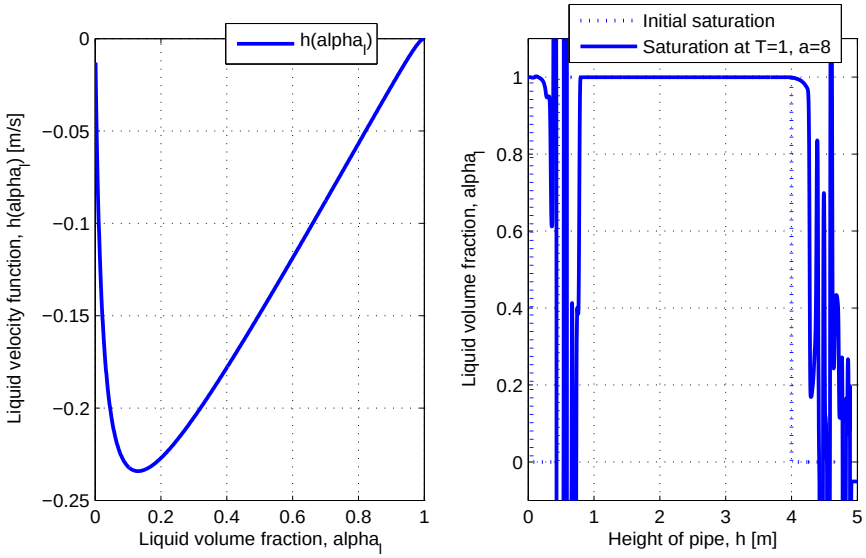

(b) *Unstable simulation with* $a = 8$

Figure 5.6: *Illustration of stability problems during simulation regarding the value of parameter a*

6 THE NUMERICAL SOLUTION

In the previous section was a Base case for the model constructed. In this section is the sensitivity of the numerical solution investigated. The sensitivity is tested by how changes in some of the parameters that are defined for the Base case will affect the numerical solution. In addition the phase and superficial velocities, the pressure and pressure differences will be considered, as well as some new expression for the frictions will also be considered as the friction terms are only proposed expression (remark 2).

6.1 Friction

As indicated in the derived expression of the superficial velocity of liquid, equation (4.48), the superficial velocities will depend on several friction terms. The friction between fluids and wall (f_g and f_l), in addition to the interfacial tension between the two fluids (C). Relations for the friction terms are given in the equations (4.50)-(4.52), and as the relations indicates they will depend on friction constants, I_g, I_l and II. The size of the friction terms will affect the shape of the liquid velocity function.

To determine the friction constants it has to be known how they affect the liquid velocity function, $h(\alpha_l)$. Based on the equation when the expressions of friction terms, equations (4.50)-(4.52), are implemented into the superficial liquid velocity function which gives equation (4.55). The constant for the interfacial tension (II) can be assumed to be the most controlling parameter at the high liquid volume fractions, due to the other terms contain $(1-\alpha_l)$. While at low liquid volume fractions it can be assumed that the constants for interfacial tension (II) and the friction between the liquid and the wall (I_l) are the most controlling parameters since in the term of friction between the gas and wall (I_g) contains α_l, which will reduce its value.

In figure (6.1) are the variation in friction constants illustrated, where one can observe how a change in respectively one of the friction constants, either II, I_l or I_g, while the other two are held constant will affect the liquid velocity function, $h(\alpha_l)$. In the figure represents the blue line the base case while the red line is with a lower value of friction constant and the purple line is with a higher value of friction constant compared with the base case. The values for the constants are included in the legends in each sub-figure.

In the figure (6.1 a), is the friction constant II varied, while the constants I_l and I_g are kept constant. As observed from the figure does the friction constant II mainly

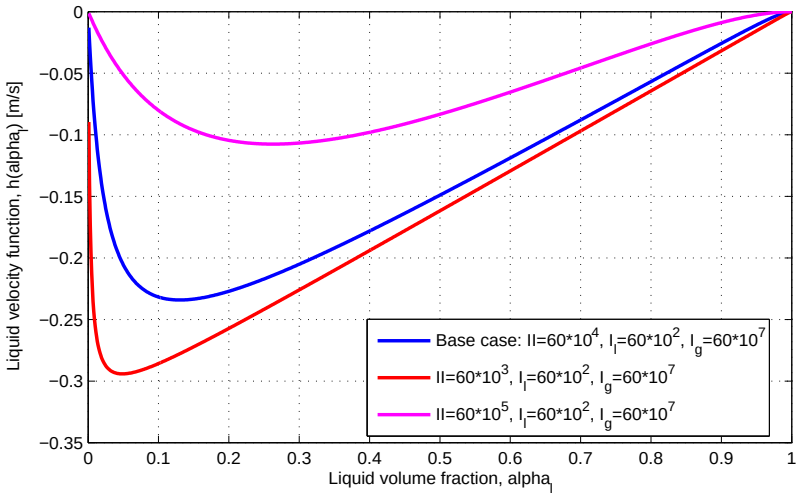

(a) Variation in II

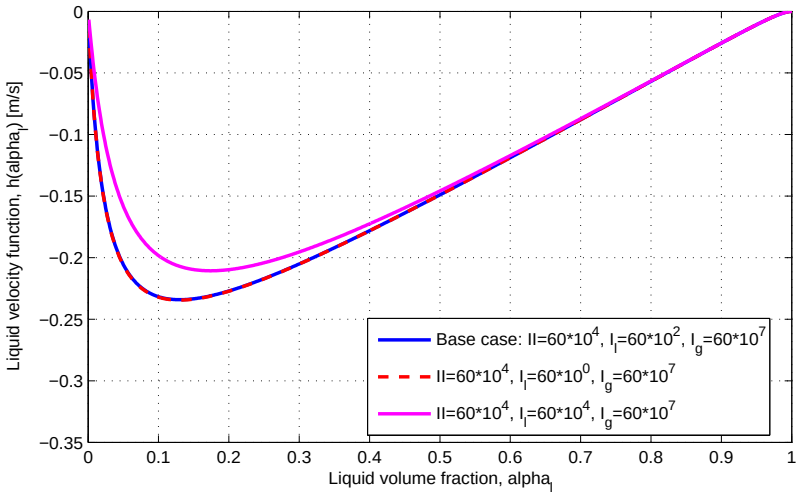

(b) Variation in I_l

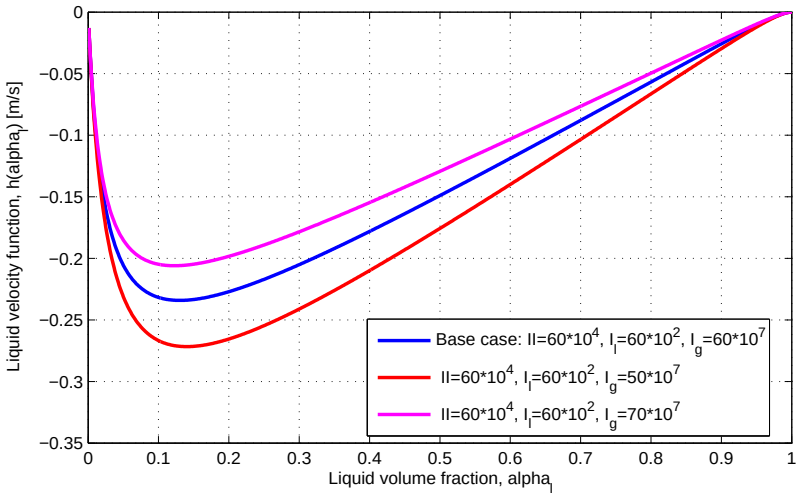

(c) Variation in I_g

Figure 6.1: *Comparison of how the different friction constants* (II, I_l *and* I_g) *affects the liquid velocity functions,* $h(\alpha_l)$

determine how steep the function will be at the low liquid volume fractions and at which liquid saturation the function will turn and rise again. At lower values of II, the curve will be very steep with the turn in the function at lower liquid volume fractions. While at higher values, the curve will be less steep and the turn in the function will take place at higher liquid volume fractions. In addition, the function at higher liquid volume fraction is more curved for higher values of II. This is in agreement with the proposed determining areas based on the expression of the liquid velocity function.

Variation in friction constant I_l is illustrated in figure (6.1 b), and has some similarity with the trend shown in variation in the friction constant II. As the figure indicates will not a lower value of I_l influence the shape of the curve. The reason for this may be due to the value in base case is not high, which means the lowered value is not significantly lowered. At higher values of I_l it is observed that the curve will be less steep than the curve to the base case which was also observed for higher values of the friction constant II. However, it will merge into the base case after the function has started to rise. One can assume that the change in I_l may only affect the velocity function at lower liquid volume fractions, which is in agreement with the proposed effect based on the expression of the superficial liquid velocity.

While with varying the friction constant I_g as shown in figure (6.1 c), has a trend that differs from the others. The steepness of the curve at low liquid volume fractions seems not to be affected by the change in I_g, but how low the function will go before it turns seems to be affected. Therefore the steepness of the curve at higher liquid volume fractions will be affected by change in I_g. As seen will a lower value of I_g lead to a steeper curve at the higher liquid volume fractions, and the opposite applies for higher values of I_g. One should also notice that the curves merge into another at a liquid volume fraction close to zero and one. This indicates that the value of I_g does not affect the liquid velocity function at values of liquid volume fractions close to zero and one, which is in agreement with the suggested of impact based on the expression of the liquid velocity function.

As this section has illustrated, the shape of the liquid velocity function will be sensitive to the changes in values of the friction constants II, I_l and I_g. In section 5.4, was the velocity of the ascending Taylor bubble calculated based on the Rankin-Hugoniot jump condition, equation (2.26). It was seen that the slope of the liquid velocity function after the turn in the function (at $0,5 \leq \alpha_l \leq 1$) was used to estimate the ascend velocity. Therefore, it is important to choose values of the friction constant carefully to achieve as accurate model as possible. It was seen in this section that the friction constants for interfacial tension (II) and friction between the gas and wall (I_g) had the most influence

on the slope of the velocity function. In addition, it is noticed that the liquid volume fraction at the Taylor bubble is mostly dependent of the interfacial tension (II), but also the friction between the liquid and the wall (I_l) has some influence. This is in agreement with the previous research where the interfacial forces is one of the parameters that affects the ascend velocity of the Taylor bubble [24, 26].

6.2 The shape of the liquid velocity function

As mentioned, the velocity is calculated from the slope of the liquid velocity function at the linear part after the turn in the function, and from the previous research is a velocity at approximately $0,3\,\frac{m}{s}$ of interest in a pipe with inner diameter at $0,08\,m$. Therefore is an indication of how low the function should go before a turn based on the interested value of the slope. If the liquid velocity function goes lower before it turn, the velocity of the Taylor bubble will be higher, and the opposite applies for an earlier turn in the function. In addition is the liquid volume fraction at the turn in the liquid velocity function an indication of the liquid volume fraction to expect at the body of the Taylor bubble. From the previous research it was seen that a liquid volume fraction at $\alpha_l \approx 0,15$, is of interest to have at the body of the Taylor bubble. If the turn is located at higher liquid volume fraction, the liquid fraction at the body will be higher. The opposite effect applies for lower liquid volume fractions. As indicated in section 5.6.2, a too steep function will lead to stability problems, (5.5), and thereby restrict the liquid volume fraction at the Taylor bubble in this model. Some steeper function than Base case was investigated but all of them had stability problems.

As previously indicated, a tail of dispersed gas bubbles will follow the Taylor bubble as it ascends. This tail is created by the bend in the liquid velocity function, $h(\alpha_l)$, at the liquid volume fractions close to one. Two different liquid velocity functions are implemented in figure (6.2 a). The blue line represents the Base case and the red line is based on different values of friction constants. It is observed that the function based on the friction constants different from the Base case is approximately linear from the turn in the function and upto $\alpha_l = 1$. All the parameters in table (5.1) except the values of friction constants for interfacial tension and friction between the liquid and the wall is kept constant. The change in the friction constants are implemented into table (6.1).

The numerical solutions after four seconds for each of the liquid velocity functions are illustrated in figure (6.2 b,c). As observed, there is only a shock wave solution at the back of the Taylor bubble for the case with the set of friction constant from table (6.1)

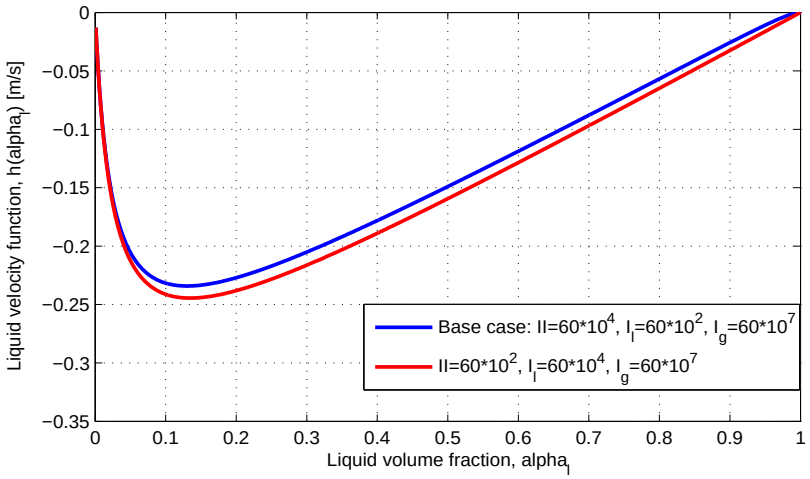

(a) *Comparison of the liquid velocity function, $h(\alpha_l)$ with and without the tail effect*

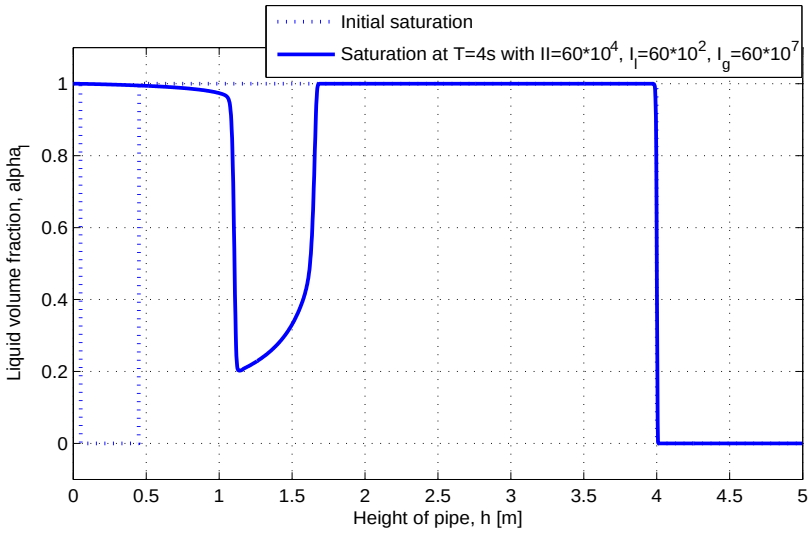

(b) *The base case liquid saturation distribution*

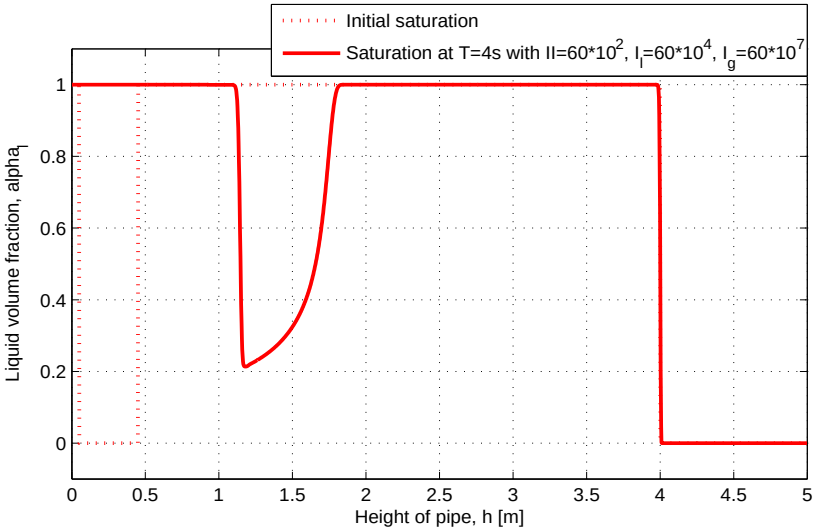

(c) *The liquid saturation distribution for the case without the tail effect*

Figure 6.2: *Illustration of how the tail effects the liquid velocity function, $h(\alpha_l)$ and the simulation after time, $T = 4\,s$*

Table 6.1: *Variation in the values of friction constant to illustrate the tail effect*

Type of friction	Friction constant	Base case $[\frac{1}{m^2}]$	Without the tail effect $[\frac{1}{m^2}]$
Interfacial tension	II	60×10^4	60×10^2
Liquid and wall	I_l	60×10^2	60×10^4
Gas and wall	I_g	60×10^7	60×10^7

compared with the Base case that has a rarefaction wave following the shock wave at the back of the ascending Taylor bubble. The saturation jumps straight to a liquid volume factor of one, and the continuous decrease observed at the Base case is not present.

By this, the tail effect of an ascending Taylor bubble can be related to the interfacial tension as it determines the curvature in at the high liquid volume fractions, figure (6.1). High interfacial tension gives a larger tail while at low interfacial tension may the tail effect disappear.

6.3 Pressure

The pressure changes as the gas slug ascends is of interest. A numerical solution is therefore constructed to measure the pressure difference at some locations in the pipe. The first measuring point is placed $1,1\,m$ above the top of the gas column initially in place. The second and third measuring points are placed above with $1\,m$ space between all of the measuring points.

As the figure (6.3) illustrates, the pressure difference at both locations before start of simulation (time, T=0 s) are $9\,810 Pa$ and will stay at this value until the top of the gas slug reaches the first pressure measuring point. This is due to the measuring points are each placed $1m$ apart from each other and the pressure gradient in the liquid is $9\,810\,\frac{Pa}{m}$ in water, as the following calculation indicates.

$$\frac{\Delta P}{\Delta h} = \rho g = 1000\,\frac{kg}{m^3} 9,81\,\frac{m}{s^2} = 9\,810 \frac{Pa}{m}$$

When the gas slug reaches the first point where pressure is measured (red line), dropped the pressure difference. The reason for this is due to the density of the gas is lower than liquid, hence a lower pressure gradient. The pressure gradient in air is $9,81\,\frac{Pa}{m}$ as the calculation below illustrates.

$$\frac{\Delta P}{\Delta h} = \rho g = 1\,\frac{kg}{m^3} 9,81\,\frac{m}{s^2} = 9,810 \frac{Pa}{m}$$

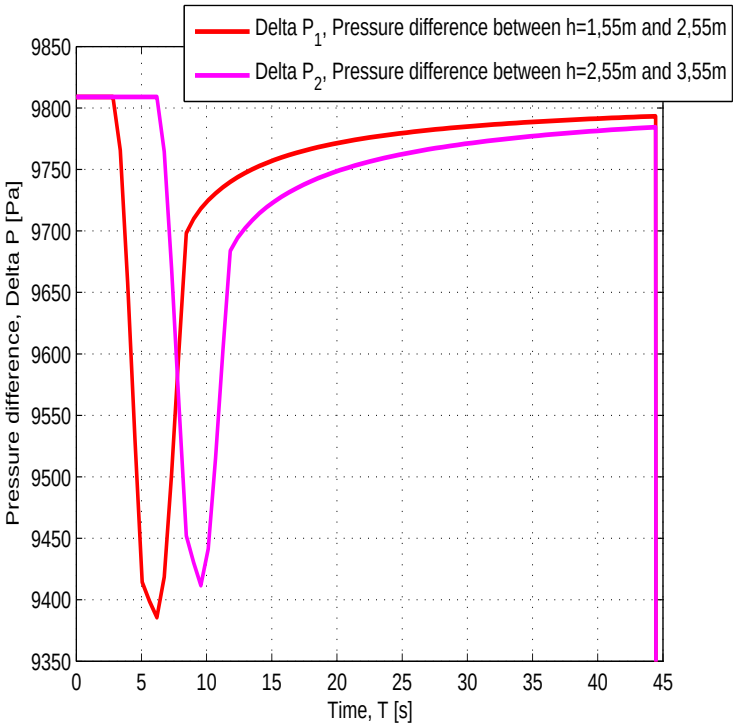

Figure 6.3: *Illustration of how the pressure difference* (ΔP_1 *and* ΔP_2) *changes between two measuring point placed* $1\,m$ *apart as the gas slug ascends up the pipe*

The pressure difference dropped approximately $450\,Pa$ when the gas slug is in the middle of two measuring point. This corresponds well to the pressure drop of around $5\,mbar$ ($500\,Pa$) that Tjelta and Kvamme observed in their experiments of pressure logging for pressure in the gas cap almost equal to pressure in the liquid column with measuring points at the same distance [23]. After the top of the gas slug has passed the second pressure point, the pressure difference between the two first measuring points will start to increase again but it takes long time until it reaches its original value. This is probably due to the tail of dispersed gas bubbles following the Taylor bubble.

Between the second and third measuring points is the same effect of the pressure difference observed, but there are some differences that are important to consider. The drop of pressure difference is not as low and it takes longer time to rise up original value. The cause of this may be due to the growing tail of dispersed gas bubbles that follows the Taylor bubble. This effect is also observed in the experimental data of Tjelta and Kvamme experiments [23]. Figure (6.4) is the result from Tjelta and Kvamme experiments in their bachelor thesis. As seen the plot in the left figure illustrates the pressure difference as the gas slug ascends. They did not release the gas until $8s$ after the start. The trend in the curves are the same as in the numerical solution, figure (6.3). The pressure drop when the gas slug is between two measuring points is $5\,mbar$.

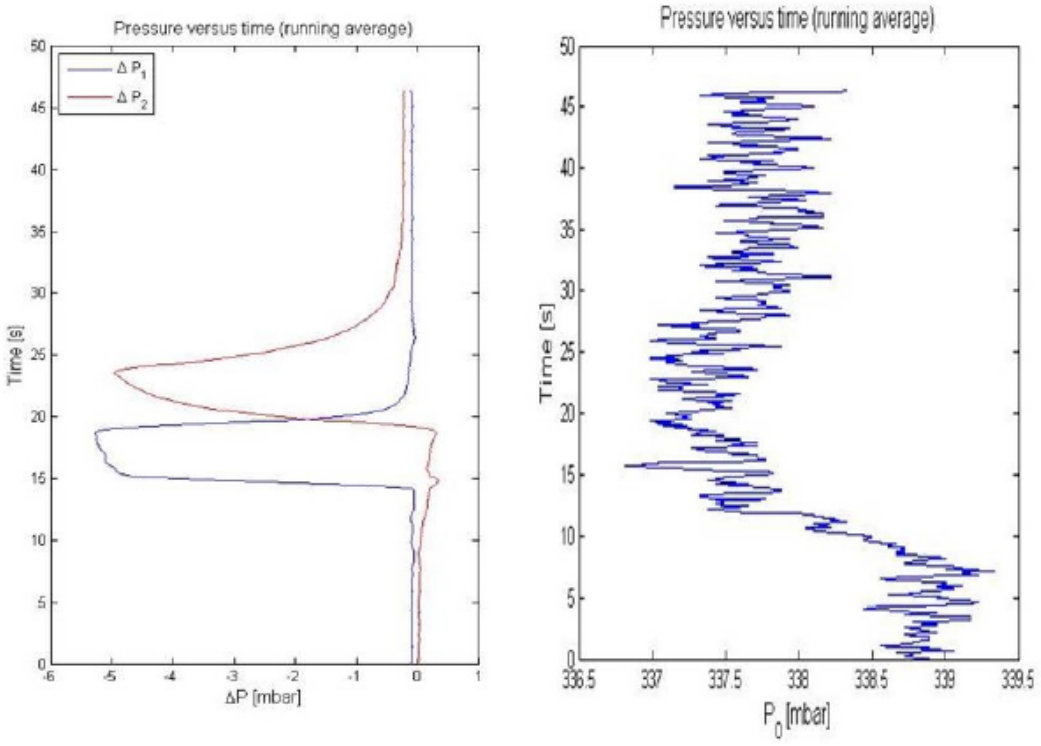

Figure 6.4: *A plot of the difference pressure achieved in the bachelor thesis to Høyland Tjelta and Kvamme [23]*

The gauge pressure $(P(i) - P_{atm})$ as a function of the height in the pipe is illustrated in figure (6.5). From the figure it can be seen that the gauge pressure does not vary much in gas phase (upper part of the pipe, $x > 3,6\,m$). This is due to the low-pressure gradient in gas. For the liquid phase increases the gauge pressure as one moves downwards in the pipe through the liquid column. It has a constant slope, equal to the pressure gradient in liquid (water).

6.4 Length of gas layer

From previous research it is assumed that the length of bubble should not affect the velocity of ascending gas and therefore should not the length of initial gas layer affect the ascending gas velocity [5, 16, 24, 26]. In figure (6.6), the Base case which contain a gas layer with length of $0,4m$ is compared with gas layers of length $0,2m$ and $0,6m$ simulated to see if the length of the gas layer will affect this mathematical model during the simulation.

To investigate the velocity of the ascending Taylor bubbles from the numerical solutions with different length in the initial gas layer is the data cursor function in MATLAB used.

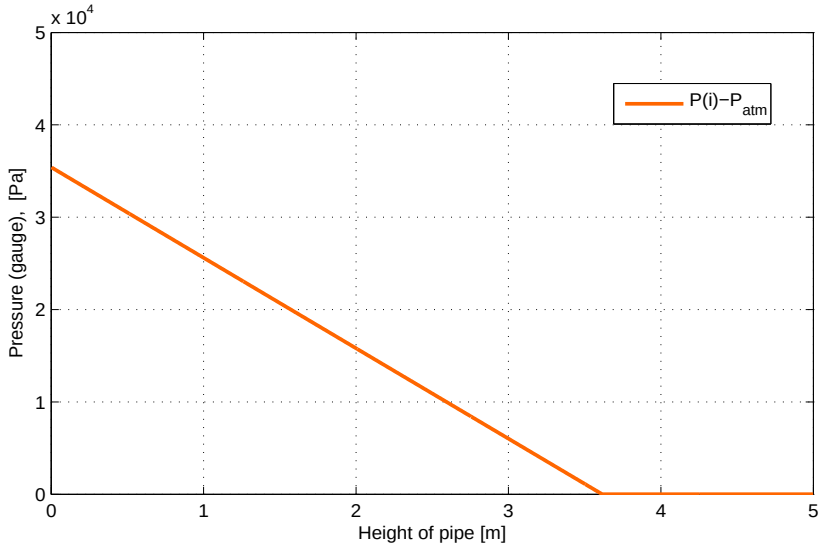

Figure 6.5: *Illustration of the gauge pressure* $(P(i) - P_{atm})$ *as a function of the height of the pipe*

As described in section 5.4, the velocity is estimated by how far the front of the gas slug has reached from start upto four seconds has passed by the fundamental velocity formula, $\nu_b = \frac{\Delta x}{\Delta t}$. The position of the fronts are investigated at the same liquid volume fractions. The calculations for the Base case, shorter layer and longer layer are shown below respectively.

$$\nu_{b,basecase} = \frac{1,661 - 0,45}{4 - 0} = 0,303\,\frac{m}{s}$$

$$\nu_{b,shorter} = \frac{1,461 - 0,25}{4 - 0} = 0,303\,\frac{m}{s}$$

$$\nu_{b,longer} = \frac{1,861 - 0,65}{4 - 0} = 0,303\,\frac{m}{s}$$

These results shows that the length of the initial gas layer does not affect the velocity in the numerical solution.

Since the initial data does not affect the liquid velocity function, $h(\alpha_l)$, should not changes in the initial length of the gas layer affect the ascending velocity of the Taylor bubble.

It is also important to notice how the liquid saturation at the gas slug changed when the length of gas layer changed. This will not occur in laboratory experiments, and as explained earlier the thickness of the liquid film will be dependent on mainly the viscosity of the liquid and the interfacial tension between the fluids [10, 13, 15, 17, 21, 27]. The reason for this effect in the numerical solution is probably due to the friction constant (interfacial tension II), which created the tail effect and as explained earlier the tail will be created by reduction of the saturation height of the Taylor bubble. As the figure (6.6)

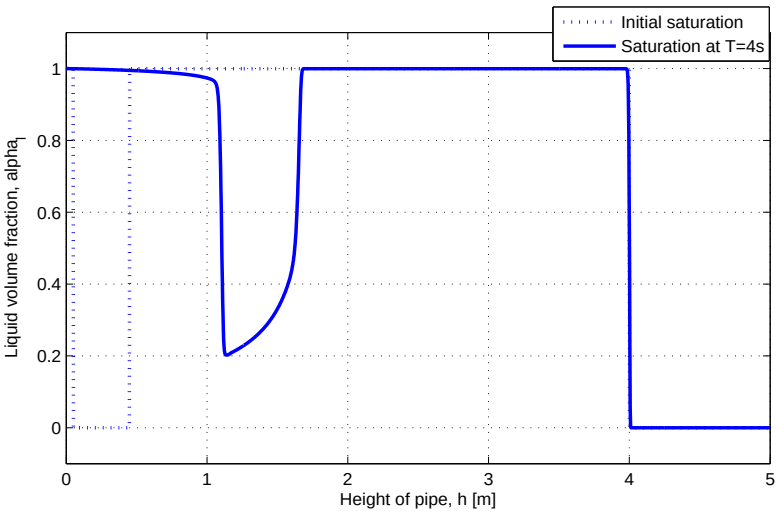

(a) *Base case which contain a gas layer of initial length* $0,4\,m$

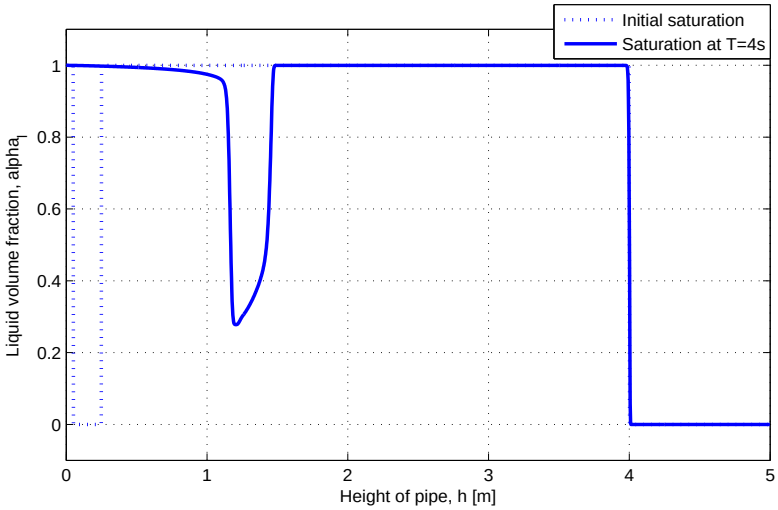

(b) *Shorter layer of gas with initial length of* $0,2\,m$

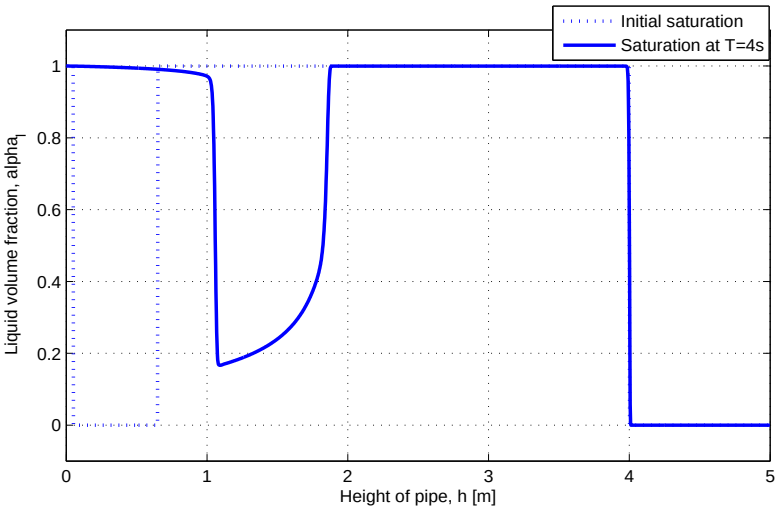

(c) *Longer layer of gas with initial length of* $0,6\,m$

Figure 6.6: *Illustration of the saturation distribution at time* $T = 4\,s$ *with different lengths of the initial gas layer*

indicates are the tails equal for all the different sets of initial data, which means that it will reduce the liquid volume fraction at the smallest layer the most as it has less area to reduce.

6.5 Comparison of phase velocities and superficial velocities

As previously explained, the derivation of the model showed that superficial velocity to liquid and gas are of same magnitude but in opposite direction, equation (4.25). This does not mean that the phase (real) velocity of liquid and gas are of equal magnitude, as indicated in remark 1. Figures (6.7) and (6.8) illustrates the magnitude of the superficial and phase velocity as the gas slug passes through the pipe. Only the superficial velocity to liquid is shown in the figure but the superficial velocity of the gas will as mentioned above be equal of magnitude.

The first figure compare the velocities right after the gas layer is released ($T = 0,01s$) in addition to after it has moved a little up in the pipe ($T = 4s$). As the figure (6.7 a) illustrates, the liquid velocity will be quite high right after the gas layer is released, but it is seen in the simulation that the liquid velocity will sink quickly as a Taylor bubble is formed and starts to move upwards. The reason for such high liquid velocity in the start is due to the little passage for liquid past the ascending gas immediately after the release of gas. As remark 1 indicates, the flow of falling liquid must compensate for the flow of ascending gas, which leads to the need of high liquid velocity in the thin passage. The velocity of the gas and the superficial velocity of the liquid is quite low as the gas slug is released, but by studying figure (6.7 a) are small increase in the velocities at the gas-liquid surfaces detected. The increase at the top of the gas layer may be an indication that the gas layer is about to start ascending. As seen, the peak at the top of the gas layer is a little wider and decreases to zero a little below the surface. The peaks at the other two gas-liquid surfaces may be caused by errors in the numerical solution when the saturation goes from liquid saturated area to gas saturated area and opposite.

The second figure (6.7 b) compares the velocities after $4s$ has passed by. The liquid velocity does not sink as quickly as before, but it still sinks. This is due to the thickness of the liquid film does not increase as quickly as when the gas was released. Meanwhile the gas velocity and the superficial velocities have stabilized at approximately $0,3m/s$ and $0,2m/s$ respectively. A gas velocity of approximately $0,3m/s$ is the value that the model was aimed at. The liquid velocity is lower at the front of the slug and increasing towards the back of the slug. This is logical since as mentioned earlier in section 5.3,

the gas-liquid surface at the top of the pipe will not move at all as the gas slug ascends upwards in the numerical solution. Since the liquid film is thinnest behind the nose of the Taylor bubble, the liquid velocity must increase in order to be displaced fast enough to avoid movement in the gas-liquid surface at the top. There is an opposite tendency observed for the gas velocity. As seen from the figures the gas velocity will be highest at the nose of the Taylor bubble and decrease towards the back. This small decrease was also detected during the estimation of the velocity at the back of the Taylor bubble by Rankin-Hugoniot condition, section 5.4 table (5.3).

The tail of the dispersed gas bubbles is also present in the gas velocity curve. After the Taylor bubble decreases the gas velocity back to the lower part of the pipe. This is the velocity of the gas bubbles in the tail, and as indicated in section 5.2, the velocity of the gas bubbles in the tail are highest for the larger gas bubbles right behind the Taylor bubble, which corresponds well with the observations from performance of the experiments. Also here, is an increase in the gas velocity at the gas-liquid surface at the top of the pipe is detected in the numerical solution. As before may this increase be caused by an error in the numerical solution when there is a transition in saturation from liquid to gas saturated area.

The second figure (6.8) compare the velocities when the gas slug has moved further up the pipe ($T = 8s$) in addition to when it has passed through the pipe ($T = 14s$). By comparing (6.7 b) with (6.8 a) it can be seen that the liquid velocity has decreased further while the gas velocity and the superficial velocity to the gas slug remains the same. The reason to the continued decrease in the liquid velocity is due to the still continued increase in liquid volume fraction in the Taylor bubble as previously mentioned. The thickness on the liquid film increases as the Taylor bubble ascends, hence the liquid velocity at the Taylor bubble must be lower in order to compensate for the rate of gas that displaces the liquid. As previously mentioned, this increase of thickness in the falling liquid film is not in agreement with previous research [10, 13, 15, 17, 21, 27]. It is also noticed that the gas velocity still decreases from the back of the Taylor bubble and all the way to the bottom of the pipe, due to the tail of dispersed gas bubbles.

When considering figure (6.8 b) it is noticed that the Taylor bubble has passed through the pipe, and the liquid velocity and the superficial velocities has decreased to zero. There is still a gas tail with a gas velocity that goes all the way back to the bottom of the pipe which is in agreement with the observed dispersed flow of gas bubbles under the performance of the experiments that still ascended in the pipe for a while after the Taylor bubble had passed through.

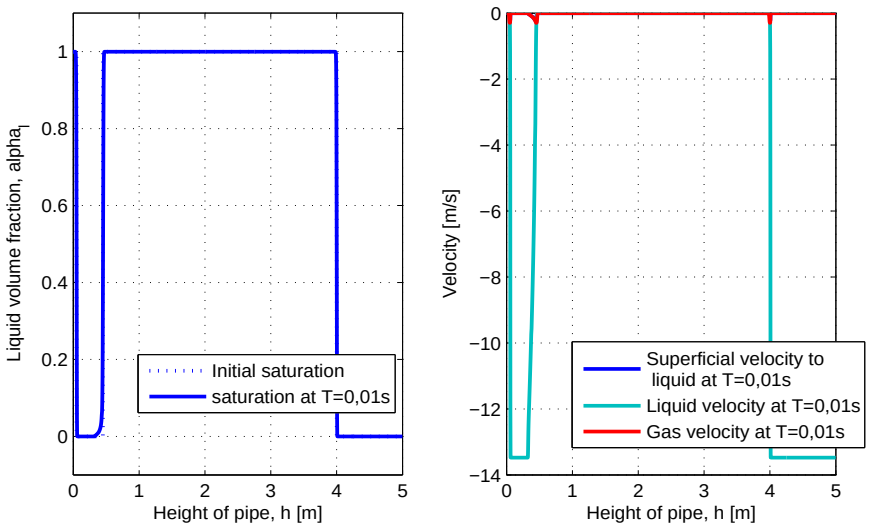

(a) *Time*, $T = 0,01s$

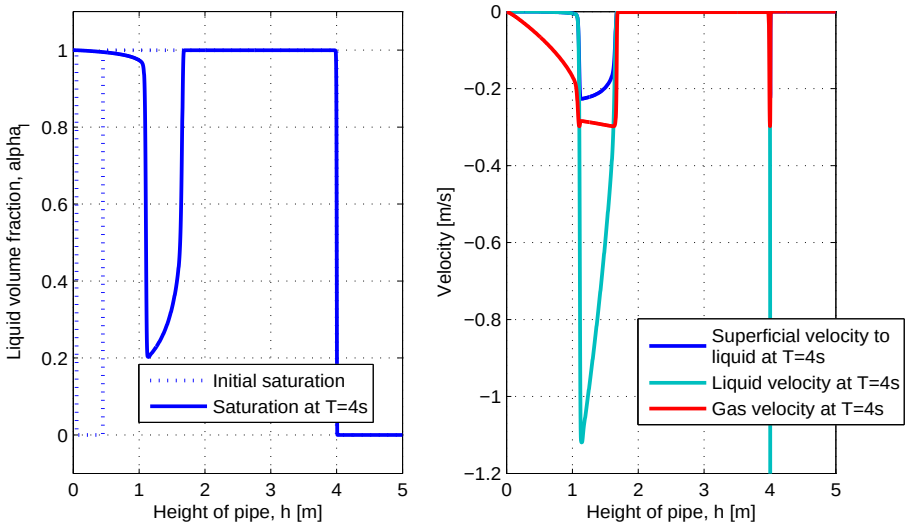

(b) *Time*, $T = 4s$

Figure 6.7: *Illustration of the saturation distribution in the pipe in addition to the superficial and fluid phase velocities to gas and liquid in the pipe at different times* $(T = 0-4s)$

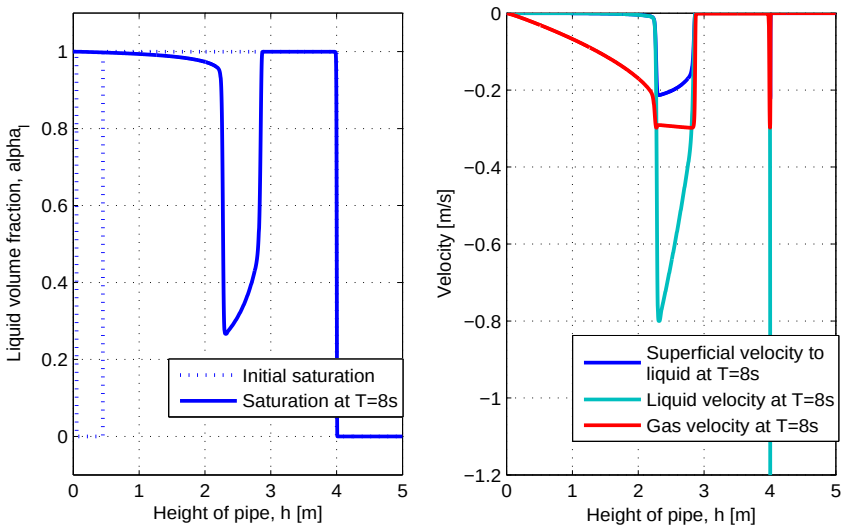

(a) *Time*, $T = 8s$

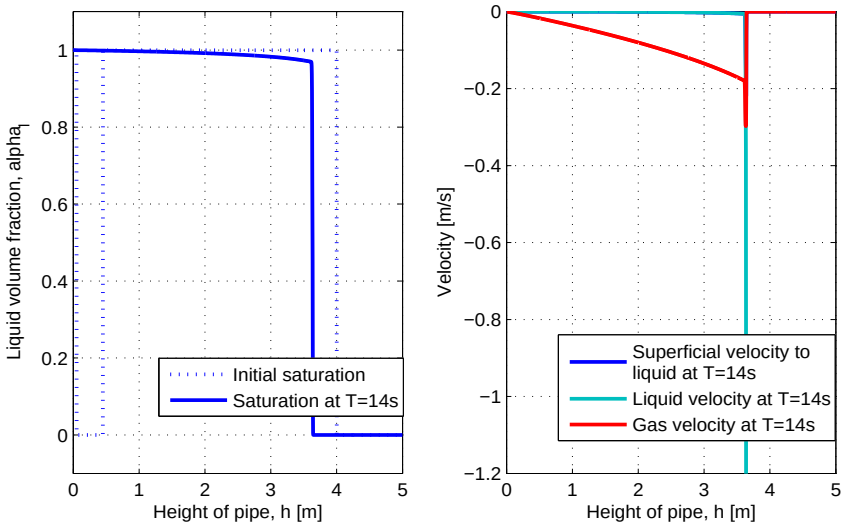

(b) *Time*, $T = 14s$

Figure 6.8: *Illustration of the saturation distribution in the pipe in addition to the superficial and fluid phase velocities to gas and liquid in the pipe at different times*

6.6 Friction terms with exponents on the volume fractions

As previously explained, remark 2, are the expression of the friction terms only a guess/estimate. Therefore it is useful to also look at other expressions for the friction terms f_g, f_l and C.

6.6.1 Volume fraction of gas included in the interfacial tension term

The new expressions are quite similar to the previous ones in equations (4.50)-(4.52). The difference is that the fluid volume fractions have exponents in addition to the gas volume fraction, α_g is included in the expression for interfacial tension. The new expressions are listed in equations (6.1)-(6.3), where the relation between the fluid volume fraction in equation (4.20) is used. To observe what the changes will be are the friction constants, I_g, I_l and II kept at the same value as for the base case ($60 \times 10^7 \frac{1}{m^2}, 60 \times 10^2 \frac{1}{m^2}$ and $60 \times 10^4 \frac{1}{m^2}$ respectively).

$$f_g = I_g \mu_g \alpha_g^{k_g} = I_g \mu_g (1 - \alpha_l)^{k_g} \tag{6.1}$$

$$f_l = I_l \mu_l \alpha_l^{k_l} \tag{6.2}$$

$$C = II \mu_l \alpha_l^{k_l} \alpha_g^{k_g} = II \mu_l \alpha_l^{k_l} (1 - \alpha_l)^{k_g} \tag{6.3}$$

The result of the numerical solution where the liquid velocity function is simulated with the new expressions for friction in addition to the Base case curve is seen in figure (6.9). As seen from this figure varies the result quite much depending on the value of the exponents.

From the figure (6.9 a) it is seen that with the exponents in the new expression, equation (6.1)-(6.3) equal to one ($k_l = k_g = 1$), the velocity curve is quite similar to the Base case. Therefore one can assume that including the gas volume fraction in the expression for friction between the two fluids does not affect the velocity function very much. However, it is important to notice that there are some difference in the new curve. It is more linear and does not bend off at the top as the Base case curve does. As indicated earlier in section 6.2, this will lead to disappearance of the tail following the Taylor bubble. When the exponents are increased further, they differ much from the Base case. As indicated in section 6.2, these types of shapes will not be relevant for the ascending Taylor bubble in this thesis.

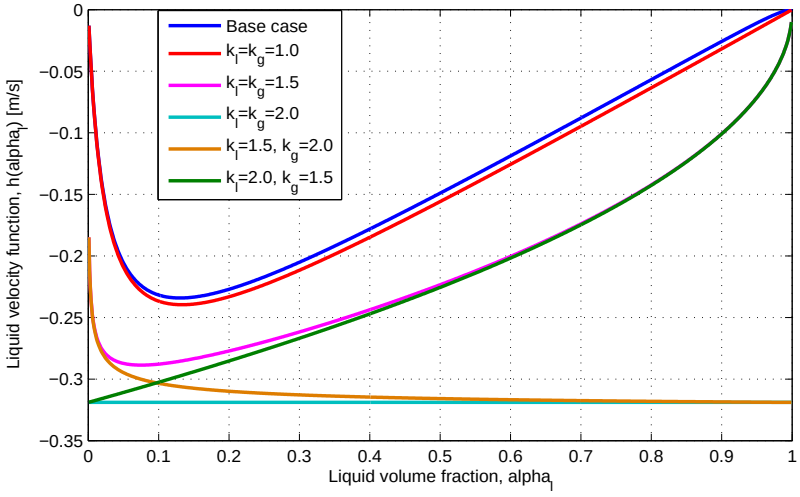

(a) *Base case compared with exponent at* $1 \leq k_l, k_g \leq 2$

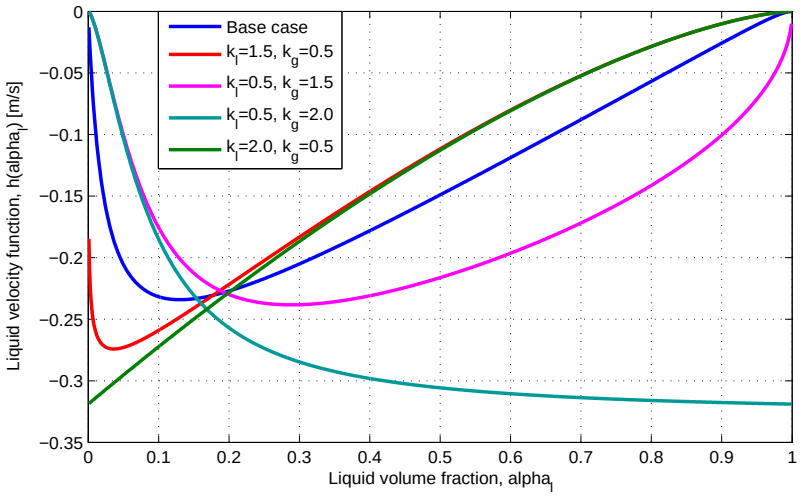

(b) *Base case compared with exponent at* $0,5 \leq k_l, k_g \leq 2$

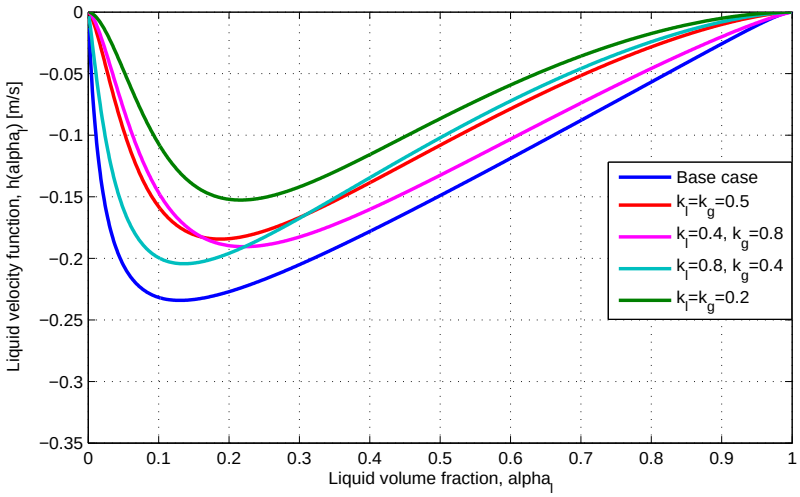

(c) *Base case compared with exponent at* $0,2 \leq k_l, k_g \leq 0,8$

Figure 6.9: *Comparison of the liquid velocity function the new expression for friction with variation in the exponents against the base case* (k_l *and* k_g) *for the fluid volume fraction with the Base case*

The case where both of the exponents are equal to two ($k_l = k_g = 2$) is shown in figure (6.9 a) to be a straight line. In order to understand this result the liquid velocity equation (4.48) need to be considered by inserting the new expressions of friction constants.

$$u_{ls} = -\frac{(\alpha_l - \alpha_l^2)^2}{\alpha_l^2 f_g + (1-\alpha_l)^2 f_l + C}\Delta\rho g \tag{6.4}$$

By using the relation of the fluid volume fraction in equation (4.20) and implementing the new expression for friction, equation (6.1)-(6.3).

$$u_{ls} = -\frac{\alpha_l^2(1-\alpha_l)^2}{\alpha_l^2(1-\alpha_l)^{k_g} I_g\mu_g + (1-\alpha_l)^2\alpha_l^{k_l} I_l\mu_l + \alpha_l^{k_l}(1-\alpha_l)^{k_g} II\mu_l}\Delta\rho g \tag{6.5}$$

If the values of the exponents are equal to $k_l = k_g = 2$

$$u_{ls} = -\frac{\alpha_l^2(1-\alpha_l)^2}{\alpha_l^2(1-\alpha_l)^2 I_g\mu_g + (1-\alpha_l)^2\alpha_l^2 I_l\mu_l + \alpha_l^2(1-\alpha_l)^2 II\mu_l}\Delta\rho g \tag{6.6}$$

$$u_{ls} = -\frac{1}{I_g\mu_g + I_l\mu_l + II\mu_l}\Delta\rho g \tag{6.7}$$

The derived expression, equation (6.7), gives an expression that only depends on parameters that are constant. This explains the straight line observed in the result of the curve figure (6.9 a).

The curves in figure (6.9 b) are results from keeping one of the exponent in the equations (6.1)-(6.3), below one and the other exponent above one. As the resulting curves indicates, does this result also lead to very different shape of the liquid velocity curve compared to the Base case. These types of curves are not of interest in this thesis.

While the curves in figure (6.9 c) are results from keeping both of the exponents in the equations (6.1)-(6.3) below one ($0 < k_l, k_g < 1$). The curves have a similar shape of the liquid velocity function as the Base case, but are little more curved both before and after the turning point of the Base case function. From the result of these curves, one can expect a larger tail due to the larger bend in the curve right before the liquid volume fraction reaches one.

The curves in figure (6.9) will not produce logical numerical solutions of the saturation distribution in the pipe as the time passes by. Either there are problems that gives errors from imaginary parts or one cannot observe the ascending gas passing through the system even with the simulation time set very low, are problems that arises in MATLAB. Therefore cannot the expression of frictions given in equation (6.1)-(6.3), be reasonable expression in this model to calculate numerical solutions.

6.6.2 Volume fraction of gas not included in the interfacial tension term

Since the curves produced from the expressions of frictions defined in equations (6.1)-(6.3), containing exponents less than one have some similarity to the Base case but are more curved are these of interest to investigate further. Some changes needs to be done with the terms in order to get an appropriate numerical solution.

I want to compare the Base case with the expressions of frictions defined in equations (6.8)-(6.10). The difference between these expressions and the expressions in equations (6.1)-(6.3), are that the gas volume fraction with exponent is not introduced into the interfacial tension term. These new expressions are equal to the expressions in the Base case, equation (4.50)-(4.52), but with exponents kept on the volume fractions.

$$f_g = I_g \mu_g \alpha_g^{k_{gfg}} = I_g \mu_g (1 - \alpha_l)^{k_{gfg}} \tag{6.8}$$

$$f_l = I_l \mu_l \alpha_l^{k_{lfl}} \tag{6.9}$$

$$C = II \mu_l \alpha_l^{k_{lcl}} \tag{6.10}$$

These expression of friction terms gives the superficial velocity of liquid, equation (4.48), following form:

$$u_{ls} = -\frac{\alpha_l^2 (1 - \alpha_l)^2}{\alpha_l^2 (1 - \alpha_l)^{k_{gfg}} I_g \mu_g + (1 - \alpha_l)^2 \alpha_l^{k_{lfl}} I_l \mu_l + \alpha_l^{k_{lfl}} II \mu_l} \Delta \rho g \tag{6.11}$$

The figure (6.10) illustrates several quite interesting results. By using the expression in equations (6.8)-(6.10), when the exponents k_{lfl} and k_{gfg} are set equal to $0,5$ while k_{lc} is set equal to one, the resulting curve did overlap with the Base case curve up to approximately a liquid volume fraction of $0,05$. When it reached a liquid volume fraction of approximately $0,6$, it started to overlap with the curve for all exponents set equal to $0,5$. The opposite effect where observed when the exponents k_{lfl} and k_{gfg} are set equal to one while k_{lc} is set to $0,5$. This curve will first overlap with the curve for the Base case with all exponents equal to $0,5$ up to approximately a liquid volume fraction of $0,05$. Afterwards it overlaps with the Base case from approximately liquid volume fraction of $0,6$.

It is of interest to test the same variation as illustrated for the exponent k_{lc} in figure (6.10) for variation in k_{gfg} in addition to k_{lfl}. The resulting curves are shown in figure (6.11) respectively. The curves with variation in k_{gfg}, figure (6.11 a), show similar results

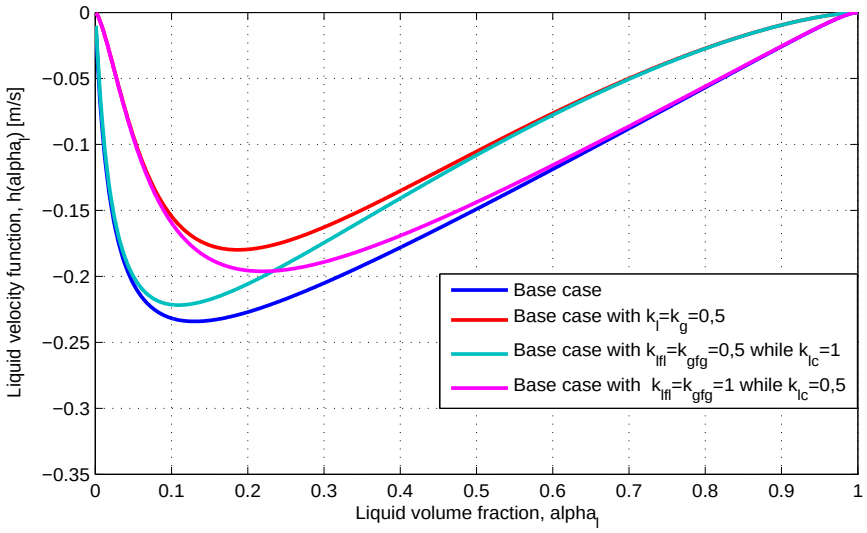

Figure 6.10: *Comparison of the liquid velocity function to the Base case with the liquid velocity function where the expressions of friction is defined in equations (6.8)-(6.10). The exponents k_{lfl} and k_{gfg} are similar while k_{lc} is different from the others*

to the curves in figure (6.10). The curves for the variation in k_{lfl}, figure (6.11 b), show that when k_{gfg} and k_{lc} are equal to one and k_{lfl} is equal to $0,5$, the curve will overlap with the Base case curve for all liquid volume factors. While for k_{gfg} and k_{lc} equal to $0,5$ and k_{lfl} equal to one, the curve will overlap with the curve where all exponents (k_{flf}, k_{gfg} and k_{lc}) are equal to $0,5$.

By this numerical solution it is seen which part of the curve each exponents k_{gfg}, k_{lfl} and k_{lc} determines the curvature of the liquid velocity curve. From the figures (6.10 and 6.11) it seems like the exponent k_{lc} determines the curvature at the lower volume factors since the curves always follows the Base case curve when the value of this exponent is equal to one, while for the value of the exponent at $0,5$, it will follow the curve where all exponents have values at $0,5$. The opposite effect applies for the exponent k_{gfg} where the curve will follow the Base case curve at high liquid volume factors when it has a value of one, while it will follow the other curve which have all the exponents at a value of $0,5$ at high liquid volume fractions when it has a value of $0,5$. While the values of the exponent, k_{lfl}, does not seem to affect the curvature of the liquid velocity function.

It is of interest to see how the curvature of the liquid velocity function in figure (6.10 and 6.11) affects the movement off the gas slug. Figure (6.12) shows how the liquid saturation with the exponents at values of $k_{lfl} = k_{gfg} = 0,5$ and $k_{lc} = 1$ is distributed at different times in the pipe. This is the curve which overlaps with the Base case at low liquid volume fractions and at high liquid volume fraction it will overlap with the curve of all

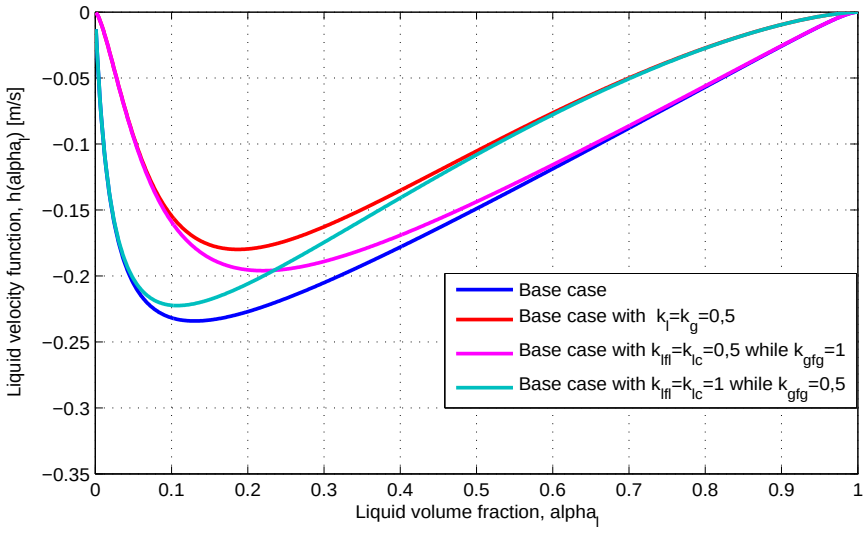

(a) *Different value on the exponent* k_{gfg}

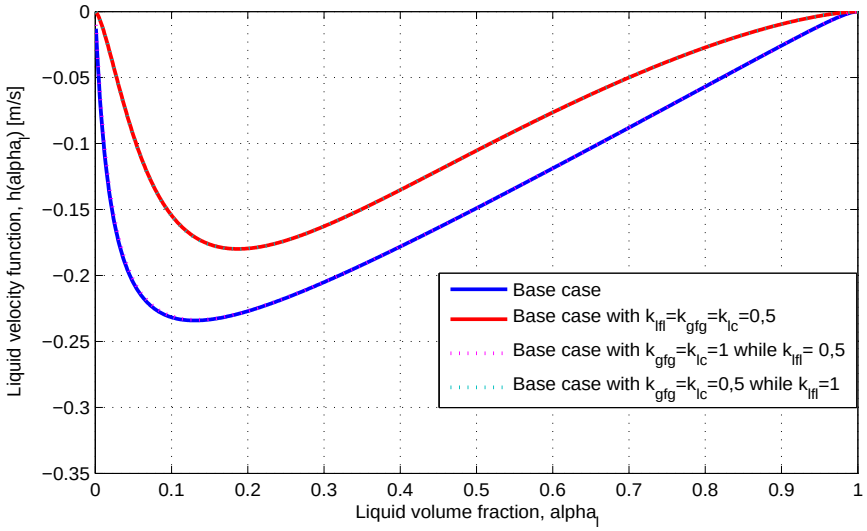

(b) *Different value on the exponent* k_{lfl}

Figure 6.11: *Comparison of the liquid velocity function to base case with the liquid velocity function where the expressions of friction is defined in equations (6.8)-(6.10). The exponents* k_{lfl} *and* k_{lc} *are similar while* k_{gfg} *is different from the others*

exponents at the value of $0,5$. When the liquid saturation distribution is compared with the Base case, figure (5.2) there are a lot of effects to investigate. The tail is larger and the velocity of the gas slug is lower in figure (6.12). This was expected based on the large bend of the curve at high liquid volume fractions and the slopes of the curve indicated that the velocity at the front of the Taylor bubble will slower (slope at the higher liquid volume fractions), while the velocity at the bottom of the Taylor bubble (slope at the transition between the two curves, figure (6.10), will be larger than the front velocity. Hence the Taylor will be dissolved as the shock wave at the bottom of the bubble catches up with the front of the bubble, figure (6.12). In addition it is seen that the curved part, characteristic curve for the nose of the Taylor bubble, in figure (5.2 a,b) is not present in figure (6.12 a,b) where a linear part connects the front and the bottom of the bubble.

Figure (6.13) illustrates the liquid saturation distribution at different times when the exponents have a value of $k_{lfl} = k_{gfg} = 1$ and $k_{lc} = 0,5$. This were the case in figure (6.10) where the curve overlapped with base case at high liquid volume fractions and with the curve containing all exponents at the value of $0,5$ at low liquid volume fractions. The numerical solution from this case gives a better estimate to the base case then the numerical solution in figure (6.12).

An important effect to observe is that the length of the bubble is increased in this case. This increase in length is created from increase in the liquid volume fraction in the Taylor bubble. As seen from the result of the simulation in figure (6.13), the liquid volume fraction at the Taylor bubble will as before, increase as the time passes by, but it increases more than for the Base case, figure (5.2), hence the increase in length. Since the curvature of the liquid velocity function overlaps with the curve of the Base case at high liquid volume fractions, figure (6.10), is an equal size of the tail expected. The numerical solution in figure (6.13), shows that the tail corresponds to the tail in the numerical solution of the Base case, figure (5.2). The velocity of the ascending Taylor bubble, figure (6.13), is a little lower than for the Base case, figure (5.2). This is caused by the lower slope in the liquid velocity function as the turn in the function takes place, figure (6.10).

From these results it is seen that with the new expressions of friction terms, equations (6.8)-(6.10), will not give as accurate model as the Base case. Either problems as to high velocity at the bottom of the Taylor bubble or too much reduction of the gas volume fraction at the Taylor bubble occurs.

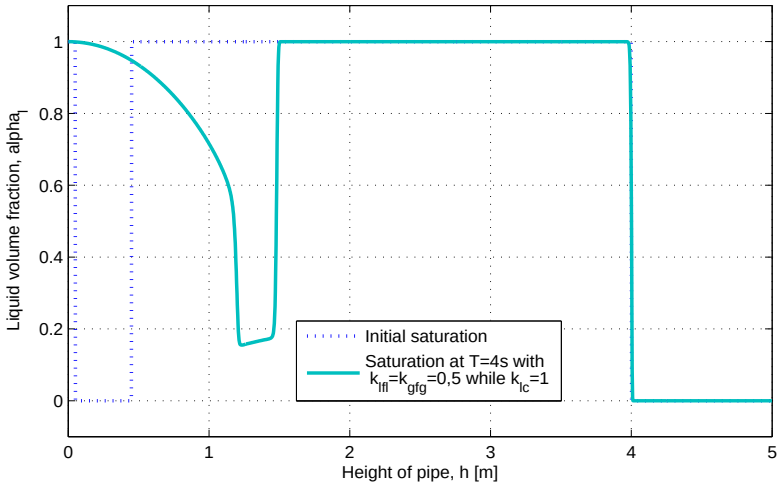

(a) *Time*, $T = 4s$

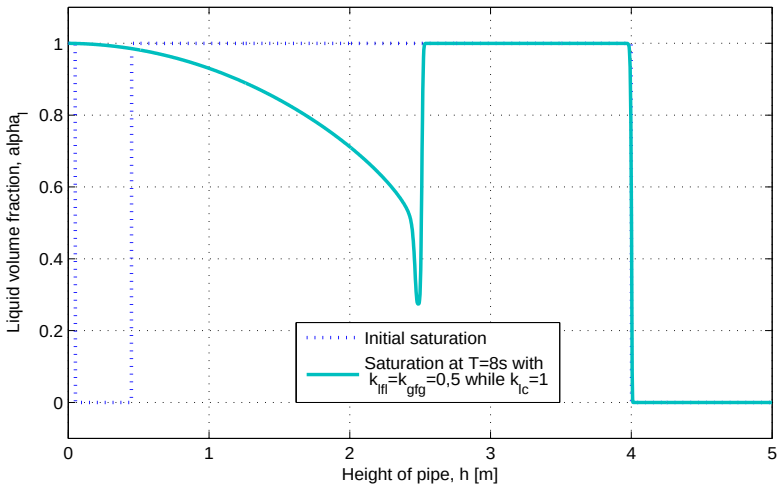

(b) *Time*, $T = 8s$

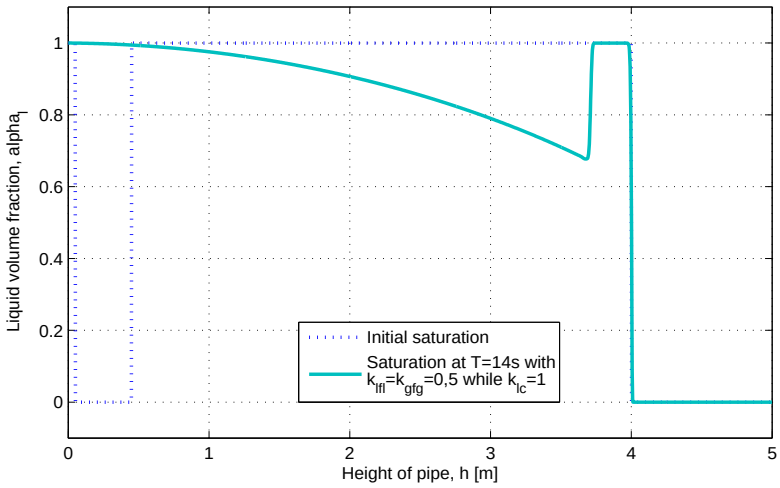

(c) *Time*, $T = 14s$

Figure 6.12: *Illustration of the liquid saturation distribution at different times when the exponents defined in equation (6.11) holds the following values* $k_{lfl} = k_{gfg} = 0,5$ *and* $k_{lc} = 1$

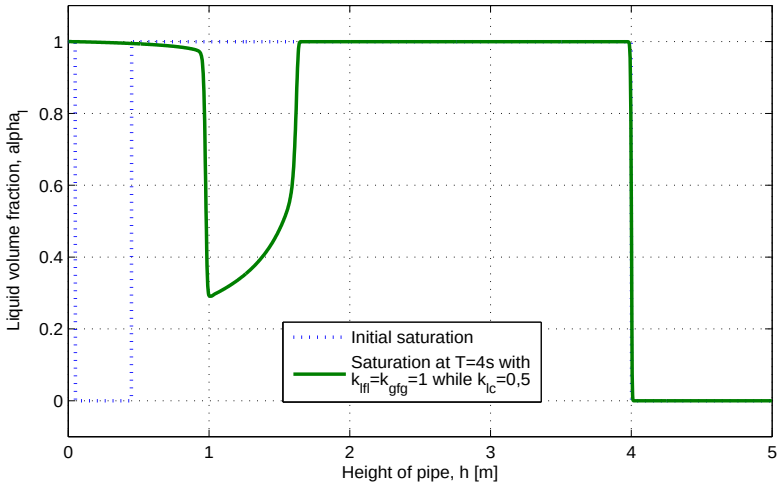

(a) *Time*, $T = 4s$

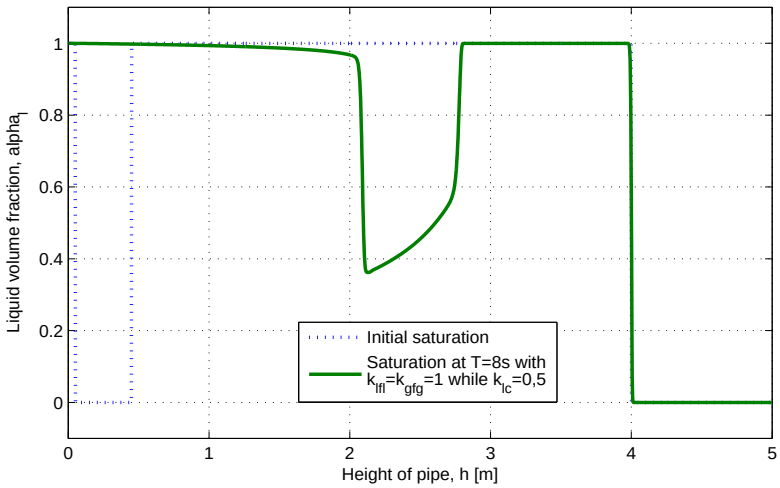

(b) *Time*, $T = 8s$

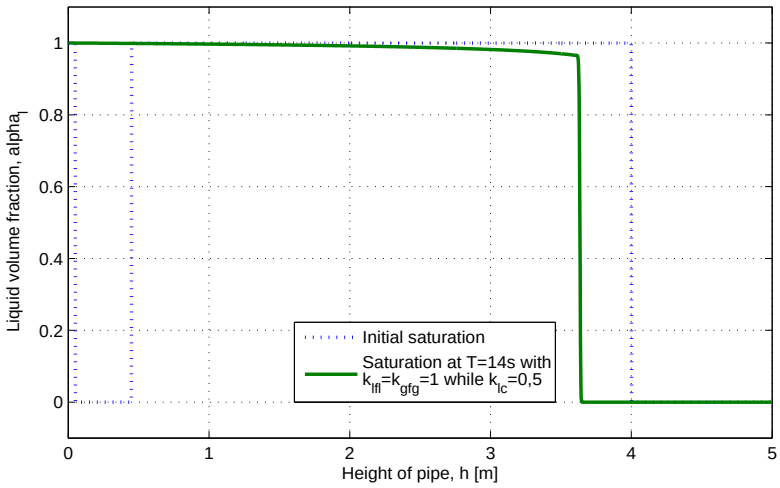

(c) *Time*, $T = 14s$

Figure 6.13: *Illustration of the liquid saturation distribution at different times when the exponents defined in equation (6.11) holds the following values* $k_{lfl} = k_{gfg} = 1$ *and* $k_{lc} = 0,5$

6.7 Diameter of the pipe

Previous research has shown that the velocity of the ascending Taylor bubble depends strongly on the diameter of the pipe [4, 5, 26]. An expression relating the diameter of the pipe is therefore included in the superficial velocity of liquid, equation (4.48). Since the Base case is designed with friction constants based on flow in a pipe with diameter of $0,08\,m$, is the relation defined by Dumitrescu, equation (3.7), which has proven to give good estimate of the ascending velocity of Taylor bubbles, used to relate the superficial velocity of liquid to pipes consisting of other diameters.

$$\frac{u_{ls,new}}{u_{ls,Basecase}} = \frac{u_{gs,new}}{u_{gs,Basecase}} = \frac{\frac{\nu_{b,new}}{\alpha_g}}{\frac{\nu_{b,basecase}}{\alpha_g}} = \frac{0,351 \times \sqrt{9,81 \times D_{new}}}{0,351 \times \sqrt{9,81 \times D}} = \sqrt{\frac{D_{new}}{0,08}}$$

The new expression of the superficial liquid velocity is given by equation (6.12).

$$u_{ls} = -\frac{\alpha_l^2(1-\alpha_l)^2}{\alpha_l^2 f_g + (1-\alpha_l)^2 f_l + C}\Delta\rho g\sqrt{\frac{D_{new}}{0,08}} \tag{6.12}$$

From this expression is the numerical solution of the superficial velocity function for liquid found for pipes with diameter $0,04\,m$, $0,06\,m$, $0,08\,m$ (The Base case) and $0,10\,m$, and the results are shown in figure (6.14). As the figure illustrate, the shape of the different curves will be very similar. When the diameter is increased, the liquid velocity function will be steeper at the low liquid volume fractions, which gives a steeper slope at the linear part, hence larger velocity as the diameter of the pipe increases.

The same method as described in section 5.4, the slope of the function $(\frac{\Delta h(\alpha_l)}{\Delta\alpha_l})$ defined by the Rankin-Hugoniot jump condition, equation (2.26), is used to find the velocity of ascending gas from figure (6.14). The results are implemented into table (6.2), where also the velocities calculated by the relation defined by Dumitrescu are included.

Table 6.2: *Relationship between the diameter of the pipe and velocities of ascending Taylor bubbles from Dumitrescu's relation in equation (3.7), and the velocity estimated from the Rankin-Hugoniot jump condition, equation (2.26), on the slope of the liquid velocity function in the numerical solution*

Diameter of pipe [m]	Velocity based on (3.7) $[\frac{m}{s}]$	Velocity from slope $[\frac{m}{s}]$
$0,04$	$0,220$	$0,211$
$0,6$	$0,269$	$0,258$
$0,08$ (Base case)	$0,311$	$0,298$
$0,10$	$0,348$	$0,333$

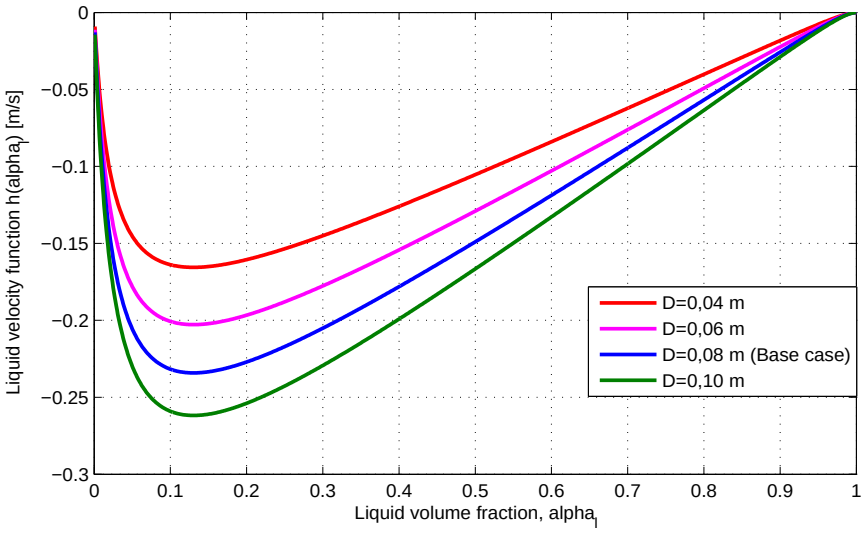

Figure 6.14: *Illustration of how the liquid velocity function, $h(\alpha_l)$, changes when diameter of the tube is changed*

As seen from the table (6.2) does this approach to find the ascend velocity of a Taylor bubble in pipes of other diameter than the Base case give a good estimate. Other relationship between the diameter and velocity may also be used and inserted into the expression in the same way as Dumitrescu's relation is.

7 CONCLUSION

A mathematical model for the ascend velocity of gas in a two-phase flow in a vertical pipe have been derived. The model is based on the fundamental conservation laws, the conservation mass and momentum. In the introduction it was mentioned that the ascending gas will depend on diameter, density and viscosity of the liquid, interfacial tension and gravitational acceleration. Throughout this thesis this statement have been proven to be correct. The model is investigated at laboratory scale where assumptions as incompressible fluids, no viscous terms, no acceleration effects and equal phase pressure are made. In addition, the total velocity (u_{mix}) was found to be constant and equal to zero, which lead an equal superficial velocity of liquid (u_{ls}) and gas (u_{gs}). The derivation lead to an expression of the superficial velocity of liquid as indicated below where it is dependent on liquid volume fraction (α_l), friction terms between gas and wall and between liquid and wall (f_g and f_l), interfacial tension (C), density difference between liquid and gas ($\Delta\rho$) and gravitational acceleration (g).

$$h(\alpha_l) = u_{ls} = -\frac{\alpha_l^2(1-\alpha_l)^2}{\alpha_l^2 f_g + (1-\alpha_l)^2 f_l + C}\Delta\rho g$$

With the simplified conservation of mass of liquid indicated in the following expression.

$$\partial_t \alpha_l + \partial_x h(\alpha_l) = 0$$

The numerical solutions are found by implementing the derived model of the superficial velocity of liquid into a MATLAB script, with a layer of gas approximately at the bottom of the pipe as given in the initial condition in equation (5.1). An ascending gas velocity of approximately $0,3\,\frac{m}{s}$ and a liquid volume fraction (α_l) and gas volume fraction (α_g) at approximately $0,15$ and $0,85$ at the body of the Taylor bubble were aimed at respectively, based on previous research on ascending gas in pipes with diameter at $D = 0,08\,m$ filled with liquid. A Base case was created, with input parameters as described in table (5.1) and friction terms as equations (4.50)-(4.52).

The numerical solutions depends on choices made for the friction terms (f_l, f_g and C) and the value set for the friction constants (I_l, I_g and II). These choices determines the shape of the superficial liquid velocity function, which gives the phase- and superficial velocities of gas and liquid and the volume fraction distribution in the pipe as the gas ascends. Based on the volume fraction distribution, an indication of thickness of falling liquid film, the shape of the tail consisting of dispersed gas bubbles and the pressure distribution in the pipe are achieved.

The numerical solutions sensitivity to changes in friction terms were therefore investigated, figure (6.1) and the results showed:

- When the interfacial tension increased did the numerical solution give a lower ascend velocity of the Taylor bubble (lower slope from $\alpha_l \epsilon [0,5,\ 1]$), a larger tail (given by larger curvature at $\alpha_l \approx 1$) and thicker falling liquid film around the bubble (the turn in the function located at higher α_l). This effect corresponds well with observations from previous research by Zheng et al [27]

- The numerical solution showed that the friction between liquid and wall had an influence on the thickness of the liquid film. Higher values of the friction gave thicker liquid film.

- The friction between the gas and wall had an influence on the ascend velocity of the Taylor bubble. The larger friction the slower ascend velocity.

Overall, the numerical solution of the model gives a good illustration of effects that are observed during performance of laboratory experiments and corresponds well with the previous research.

- A tail of dispersed gas bubble following the ascending Taylor bubble is clearly indicated in the numerical solution.

- The length of the initial gas layer is observed to not affect the velocity of the ascending Taylor bubble. This corresponds well with previous research [20, 24, 26]. However, the length of the initial gas layer has an effect on the thickness of the falling liquid film. It is observed that shorter initial gas layer gave thicker liquid films and vice versa. This is caused by the tail of dispersed gas bubbles that increases the thickness of the liquid film.

- The differential pressure between pressure measuring points placed one meter apart corresponds well with previous similar measurements of the differential pressure [23].

The model shows excellent agreement with the phase velocity of gas at $0,3\,\frac{m}{s}$ as the numerical solution was aimed at, but as shown in section 6.7 it can also be related to other pipe diameters by use of velocity relations. As previous research has shown will the velocity of the ascending Taylor bubble decrease when the diameter of the pipe is decreased.

The main problem with the model is that the liquid volume fraction does not seem to hold a constant value as the Taylor bubble ascends through the pipe, as shown to be the case in laboratory experiments in previous research as it depends mainly on the viscosity of the liquid and the interfacial tension between the fluids [10, 13, 15, 17, 21, 27].

Recommendation for further work

- Gas kicks often occur when there is flow of liquid in the pipe during drilling, not in stagnant liquid. A model with flow of liquid is therefore of large interest in the industry as research have shown that flow in the liquid affect the ascend velocity of the gas [16, 20].

- As the model in this thesis applies for laboratory-scale, is a model that applies for field scale of interest. In field-scale models there may be temperature and pressure changes that can affect the densities, viscosities and the friction forces. This will give a more complicated model where several of the assumptions used to define this model needs to be neglected. A model that applies on field scale will be quite relevant for the industry.

- The previous researchers have looked into different regimes where the flow may be dominated by either viscous forces, interfacial tension, inertia or different combinations of them. The model developed in this thesis was the viscous terms neglected. It may therefore be of interest to develop a model where the viscous terms are included in the model.

References

[1] M. Ben-Artzi and J. Falcovitz, *Generalized Riemann Problems in computational fluid dynamics*, Cambridge: Cambridge University Press, 2003.

[2] C.E. Brennen, *Fundamentals of Multiphase Flow*. Cambridge: Cambridge University Press, 2005.

[3] R.A.S. Brown, "The mechanics of large gas bubbles in tubes: I. Bubble velocities in stagnant liquids", *The Canadian Journal of Chemical Engineering*, vol. 43(5), pp. 217-223, 1965. DOI:10.1002/cjce.5450430501

[4] R.M. Davies and G. Taylor, "The mechanics of large bubbles rising through extended liquids and through liquids in tubes", *Proceedings of the Royal Society of London. Series A, Mathematical and Physical Sciences*, vol. 200(1062), pp. 375-390, 1950. DOI:10.1098/rspa.1950.0023

[5] D.T. Dumitrescu, "Strömung an einer Luftblase im senkrechten Rohr", *Zeitschrift für angewandte Mathematik und Mechanik*, vol. 23(3), pp. 139-149, 1943. DOI:10.1002/zamm.19430230303

[6] S. Evje and T. Flåtten, "Hybrid central upwind schemes for numerical resolution of two-phase flows", *ESAIM: Mathematical Modelling and Numerical Analysis*, vol. 39(2), pp. 253-273, 2005. DOI:10.1051/m2an:2005011

[7] S. Evje, A linear two-phase transport equation, University of Stavanger, Lecture notes PET510:Computational reservoir and well modelling, 2013

[8] S. Evje, Some basic theory for nonlinear conservation laws+exercises, University of Stavanger, Lecture notes PET565:Core scale modelling and interpretation, 2014

[9] S. Evje, The Buckley-Leverett model: Analytical and numerical solution, University of Stavanger, Lecture notes PET565:Core scale modelling and interpretation, 2014

[10] J.Q. Feng, "Buoyancy-driven motion of a gas bubble through viscous liquid in a round tube", *Journal of Fluid Mechanics*, vol. 609, pp.377-410, 2008. DOI:10.1017/S0022112008002516

[11] K.K. Fjelde, Drilling programs and drilling problems, Lecture notes in the course PET505:Directional drilling and flowing well engineering, University of Stavanger, 2013.

[12] T. Funada, D.D. Joseph, T Maehara, S. Yamashita, "Ellipsoidal model of the rise of a Taylor bubble in a round tube", *International Journal of Multiphase Flow*, vol. 31(4), pp. 473-491, 2005. DOI:10.1016/j.ijmultiphaseflow.2004.11.010

[13] C.W. Kang, S. Quan, J. Lou, "Numerical study of a Taylor bubble rising in stagnant liquids", *Physical Review E*, vol. 81(6), pp.066308-(1-11), 2010. DOI:10.1103/PhysRevE.81.066308

[14] H. Kleppe, RESERVOIR SIMULATION, One phase, 1D, flow, Numerical solution (Course compendium). University of Stavanger, Stavanger, 2010

[15] E.W. Llewellin, E. Del Bello, J. Taddeucci, P. Scarlato and S.J. Lane, "The thickness of the falling film of liquid around a Taylor bubble", *Proceedings Of The Royal Society A-Mathematical Physical And Engineering Sc*, vol. 468(2140), pp. 1041-1064, 2012. DOI:10.1098/rspa.2011.0476

[16] D.J. Nicklin, J.O. Wilkes and J.F. Davidson, "Two-phase flow in vertical tubes", *Trans. Instn Chem. Engers*, vol. 40, pp. 61-68, 1962.

[17] S. Nogueira, M.L. Riethmuler, J.B.L.M. Campos, A.M.F.R. Pinto, "Flow in the nose region and annular film around a Taylor bubble rising through vertical columns of stagnant and flowing Newtonian liquids", *Chemical Engineering Science*, vol. 61(2), pp. 845-857, 2006. DOI:10.1016/j.ces.2005.07.038

[18] T. Paz, "Expanding bubbles in non-newtonian fluid in a vertical pipe, An experimental gas-kick study", Bachelor thesis, Faculty of Science and Technology, University of Stavanger, Stavanger, 2011.

[19] A. Prosperetti and G. Tryggvason, *Computational methods for multiphase flow*, Cambridge: Cambridge University Press, 2007.

[20] D.W. Rader, A.T. Bourgoyne and R.H. Ward, "Factors Affecting Bubble-Rise Velocity Of Gas Kicks", *Journal of Petroleum Technology*, vol. 27, pp. 571-584, 1975. DOI:http://dx.doi.org/10.2118/4647-PA document id:SPE-4647-PA

[21] T. Taha and Z.F. Cui, "CFD modelling of slug flow in vertical tubes", *Chemical Engineering Science*, vol. 61(2), pp. 676-687, 2006. DOI:10.1016/j.ces.2005.07.022

[22] R. Time, Two-phase flow in pipelines (Course compendium), University of Stavanger, Stavanger, 2009

[23] K. Høyland Tjelta and I. Kvamme, "Interfacial Waves of Taylor Bubbles in Vertical Two-phase Flow", Bachelor thesis, Faculty of Science and Technology, University of Stavanger, Stavanger, 2013.

[24] F. Viana, R. Pardo, R. Yanez, J. Trallero and D.D. Joseph, "Universal correlation for the rise velocity of long bubbles in round pipes", *Journal of Fluid Mechanics*, vol. 494, pp. 379-398, 2003. DOI:10.1017/S0022112003006165

[25] J. R. Welty, C.E Wickes, R. E. Wilson and G. L. Rorrer, *Fundamentals of Momentum, Heat and Mass Transfer*, Hoboken, N.J: John Wiley and Sons, Ink, 5 edition, c2008.

[26] E.T. White and R.H. Beardmore, "The velocity of rise of single cylindrical air bubbles through liquids contained in vertical tubes", *Chemical Engineering Science*, vol. 17, pp. 351-361, 1962.

[27] D. Zheng, X. He, D. Che, "CFD simulations of hydrodynamic characteristics in a gas-liquid vertical upward slug flow", *International Journal of Heat and Mass Transfer*, vol. 50, pp. 4151-4165, 2007. DOI:10.1016/j.ijheatmasstransfer.2007.02.041

8 NOMENCLATURE

ρ	Density, kg/m^3
g	Gravitational acceleration, m/s^2
P	Fluid phase pressure, $Pa = kg/ms^2$
α	Fluid volume fraction
u	Phase velocity, m/s
u_s	Superficial phase velocity, m/s
u_{mix}	Mixture velocity, m/s
q	Volumetric flow rate, m^3/s
A	Cross sectional area/area of flow, m^2
A_f	Area of flow containing fluid f, m^2
x	Height, m
D	Diameter, m
r	Radius, m
μ	Viscosity, $Pa \times s = kg/ms$
λ	Thickness of the falling liquid film, m
λ'	Dimensionless thickness of the falling liquid film
Ω	Source/sink term, kg/m^3s
β	Rate of mass transfer to the fluid phase, kg/m^3s
C or σ_{gl}	Interfacial tension, kg/m^3s
f_l	Friction between liquid and wall, kg/m^3s
f_g	Friction between gas and wall, kg/m^3s
II	Friction constant for interfacial tension, $1/m^2$
I_l	Friction constant for friction between liquid and wall, $1/m^2$
I_g	Friction constant for friction between gas and wall, $1/m^2$
a	Sound velocity, m/s
N_f	Inverse dimensionless viscosity
a, b, c, d	Constants
Fr	Froude number (dimensionless velocity)
Eo	Eötvös number (ratio of buoyancy and interfacial tension forces),
Mo	Morton number (ratio of viscous and interfacial tension forces),
Re_b	Reynolds bubble number (ratio of inertial and viscous forces)

Subscriptions:	
t	Total
l	Liquid
g	Gas
f	Fluid phase f

9 APPENDIX

DERIVATION OF THE SIMPLIFIED MODEL

The full derivation of the simplified model is included to achieve full understanding of how the simplified model in section 4.2, is developed.

9.1 Derivation of phase velocities

The derivation in section 4.2.2, is described in more details in this section. Here are the reduced momentum conservation equations, (4.26)and (4.27):

$$\alpha_g \partial_x P = -f_g u_g - C(u_g - u_l) - \rho_g \alpha_g g$$

$$\alpha_l \partial_x P = -f_l u_l + C(u_g - u_l) - \rho_l \alpha_l g$$

Solving them for u_g and u_l respectively gives equations (4.28) and (4.29):

$$u_g = -\frac{\alpha_g \partial_x P + \rho_g \alpha_g g - C u_l}{C + f_g}$$

$$u_l = -\frac{\alpha_l \partial_x P + \rho_l \alpha_l g - C u_g}{C + f_l}$$

Inserting for u_l and u_g respectively to reduce the amount of unknowns:

$$u_g = -\frac{\alpha_g \partial_x P + \rho_g \alpha_g g + C\frac{\alpha_l \partial_x P + \rho_l \alpha_l g - C u_g}{C + f_l}}{C + f_g}$$

$$u_l = -\frac{\alpha_l \partial_x P + \rho_l \alpha_l g + C\frac{\alpha_g \partial_x P + \rho_g \alpha_g g - C u_l}{C + f_g}}{C + f_l}$$

Solve for u_g and u_l:

$$u_g(1 - \frac{C^2}{(C + f_l)(C + f_g)}) = -\frac{\alpha_g \partial_x P + \rho_g \alpha_g g + C\frac{\alpha_l \partial_x P + \rho_l \alpha_l g}{C + f_l}}{C + f_g}$$

$$u_g = -\frac{\alpha_g \partial_x P + \rho_g \alpha_g g + C\frac{\alpha_l \partial_x P + \rho_l \alpha_l g}{C + f_l}}{(C + f_g)(1 - \frac{C^2}{(C + f_l)(C + f_g)})}$$

Which gives equation (4.30):

$$u_g = -\frac{\alpha_g \partial_x P + \rho_g \alpha_g g + C\frac{\alpha_l \partial_x P + \rho_l \alpha_l g}{C + f_l}}{C + f_g - \frac{C^2}{C + f_l}}$$

$$u_l(1 - \frac{C^2}{(C+f_l)(C+f_g)}) = -\frac{\alpha_l \partial_x P + \rho_l \alpha_l g + C\frac{\alpha_g \partial_x P + \rho_g \alpha_g g}{C+f_g}}{C+f_l}$$

$$u_l = -\frac{\alpha_l \partial_x P + \rho_l \alpha_l g + C\frac{\alpha_g \partial_x P + \rho_g \alpha_g g}{C+f_g}}{(C+f_l)(1 - \frac{C^2}{(C+f_l)(C+f_g)})}$$

As for the liquid gives equation (4.31):

$$u_l = -\frac{\alpha_l \partial_x P + \rho_l \alpha_l g + C\frac{\alpha_g \partial_x P + \rho_g \alpha_g g}{C+f_g}}{C+f_l - \frac{C^2}{C+f_g}}$$

As seen in the expressions above, they consist of two parts. One pressure dependent part and one gravity dependent part.

$$u_g = -\frac{\alpha_g \partial_x P + \frac{C\alpha_l \partial_x P}{C+f_l} + \rho_g \alpha_g g + \frac{C\rho_l \alpha_l g}{C+f_l}}{C+f_g - \frac{C^2}{C+f_l}}$$

$$u_l = -\frac{\alpha_l \partial_x P + \frac{C\alpha_g \partial_x P}{C+f_g} + \rho_l \alpha_l g + \frac{C\rho_g \alpha_g g}{C+f_g}}{C+f_l - \frac{C^2}{C+f_g}}$$

Rearrange and reduce some of the fractions in the expression by multiplying with $\frac{C+f_l}{C+f_l}$ in u_g and $\frac{C+f_g}{C+f_g}$ in u_l on the right hand side:

$$u_g = -\frac{(\alpha_g + \frac{C\alpha_l}{C+f_l})(C+f_l)\partial_x P + (\rho_g \alpha_g + \frac{C\rho_l \alpha_l}{C+f_l})(C+f_l)g}{(C+f_g - \frac{C^2}{C+f_l})(C+f_l)}$$

$$u_l = -\frac{(\alpha_l + \frac{C\alpha_g}{C+f_g})(C+f_g)\partial_x P + (\rho_l \alpha_l + \frac{C\rho_g \alpha_g}{C+f_g})(C+f_g)g}{(C+f_l - \frac{C^2}{C+f_g})(C+f_g)}$$

which gives:

$$u_g = -\frac{[\alpha_g(C+f_l) + C\alpha_l]\partial_x P + [\rho_g \alpha_g(C+f_l) + C\rho_l \alpha_l]g}{C(C+f_l) + f_g(C+f_l) - C^2}$$

$$u_l = -\frac{[\alpha_l(C+f_g) + C\alpha_g]\partial_x P + [\rho_l \alpha_l(C+f_g) + C\rho_g \alpha_g]g}{C(C+f_g) + f_l(C+f_g) - C^2}$$

Rearranging:

$$u_g = -\frac{[\alpha_g f_l + C(\alpha_g + \alpha_l)]\partial_x P + [\rho_g \alpha_g f_l + C(\rho_l \alpha_l + \rho_g \alpha_g]g}{Cf_l + f_g C + f_g f_l}$$

$$u_l = -\frac{[\alpha_l f_g + C(\alpha_l + \alpha_g)]\partial_x P + [\rho_l \alpha_l f_g) + C(\rho_g \alpha_g + \rho_l \alpha_l]g}{Cf_g + f_l C + f_g f_l}$$

By use of the constraint $\alpha_g + \alpha_l = 1$ can it be rewritten to equations (4.32) and (4.33):

$$u_g = -\frac{\alpha_g f_l + C}{Cf_g + Cf_l + f_g f_l}\partial_x P - \frac{\alpha_g \rho_g f_l + (\alpha_l \rho_l + \alpha_g \rho_g)C}{Cf_g + Cf_l + f_g f_l}g$$

$$u_l = -\frac{\alpha_l f_g + C}{Cf_g + Cf_l + f_g f_l}\partial_x P - \frac{\alpha_l \rho_l f_g + (\alpha_l \rho_l + \alpha_g \rho_g)C}{Cf_g + Cf_l + f_g f_l} g$$

The relation between the superficial and phase velocity, $u_{gs} = u_g \alpha_g$ and $u_{ls} = u_l \alpha_l$ gives:

$$u_{gs} = \alpha_g u_g = -\frac{\alpha_g f_l + C}{Cf_g + Cf_l + f_g f_l}\alpha_g \partial_x P - \frac{\alpha_g \rho_g f_l + (\alpha_l \rho_l + \alpha_g \rho_g)C}{Cf_g + Cf_l + f_g f_l}\alpha_g g$$

$$u_{ls} = \alpha_l u_l = -\frac{\alpha_l f_g + C}{Cf_g + Cf_l + f_g f_l}\alpha_l \partial_x P - \frac{\alpha_l \rho_l f_g + (\alpha_l \rho_l + \alpha_g \rho_g)C}{Cf_g + Cf_l + f_g f_l}\alpha_l g$$

Which leads to:

$$u_{gs} = -\frac{\alpha_g^2 f_l + \alpha_g C}{Cf_g + Cf_l + f_g f_l}\partial_x P - \frac{\alpha_g^2 \rho_g f_l + (\alpha_g \alpha_l \rho_l + \alpha_g^2 \rho_g)C}{Cf_g + Cf_l + f_g f_l} g$$

$$u_{ls} = -\frac{\alpha_l^2 f_g + \alpha_l C}{Cf_g + Cf_l + f_g f_l}\partial_x P - \frac{\alpha_l^2 \rho_l f_g + (\alpha_l^2 \rho_l + \alpha_g \alpha_l \rho_g)C}{Cf_g + Cf_l + f_g f_l}\rho_l g$$

By again using the constraint $\alpha_g + \alpha_l = 1$ gives that:

$$\alpha_g^2 \rho_g = \alpha_g(1 - \alpha_l)\rho_g = \alpha_g \rho_g - \alpha_g \alpha_l \rho_g$$

$$\alpha_l^2 \rho_l = \alpha_l(1 - \alpha_g)\rho_l = \alpha_l \rho_l - \alpha_g \alpha_l \rho_l$$

By inserting and some rearranging are equations (4.34) and (4.35) obtained:

$$u_{gs} = -\frac{\alpha_g^2 f_l + \alpha_g C}{Cf_g + Cf_l + f_g f_l}\partial_x P - \frac{\alpha_g^2 f_l + \alpha_g C}{Cf_g + Cf_l + f_g f_l}\rho_g g - \frac{\alpha_g \alpha_l(\rho_l - \rho_g)C}{Cf_g + Cf_l + f_g f_l} g$$

$$u_{ls} = -\frac{\alpha_l^2 f_g + \alpha_l C}{Cf_g + Cf_l + f_g f_l}\partial_x P - \frac{\alpha_l^2 f_g + \alpha_l C}{Cf_g + Cf_l + f_g f_l}\rho_l g + \frac{\alpha_g \alpha_l(\rho_l - \rho_g)C}{Cf_g + Cf_l + f_g f_l} g$$

9.2 Derivation of the pressure expression

An expression for $\partial_x P$ is found by adding the superficial velocities together and assuming that the total velocity is zero, $u_t = u_{gs} + u_{ls} = 0$:

$$u_{gs} + u_{ls} = (-\frac{\alpha_g^2 f_l + \alpha_g C}{Cf_g + Cf_l + f_g f_l}\partial_x P - \frac{\alpha_g^2 f_l + \alpha_g C}{Cf_g + Cf_l + f_g f_l}\rho_g g - \frac{\alpha_g \alpha_l(\rho_l - \rho_g)C}{Cf_g + Cf_l + f_g f_l} g)$$

$$+(-\frac{\alpha_l^2 f_g + \alpha_l C}{Cf_g + Cf_l + f_g f_l}\partial_x P - \frac{\alpha_l^2 f_g + \alpha_l C}{Cf_g + Cf_l + f_g f_l}\rho_l g + \frac{\alpha_g \alpha_l(\rho_l - \rho_g)C}{Cf_g + Cf_l + f_g f_l} g) = 0$$

Observe that the last term of u_{gs} and u_{ls} cancel each other and put the pressure terms on left side of the expression:

$$\partial_x P(\frac{\alpha_g^2 f_l + \alpha_g C}{Cf_g + Cf_l + f_g f_l} + \frac{\alpha_l^2 f_g + \alpha_l C}{Cf_g + Cf_l + f_g f_l}) = -\frac{\alpha_g^2 f_l + \alpha_g C}{Cf_g + Cf_l + f_g f_l}\rho_g g - -\frac{\alpha_l^2 f_g + \alpha_l C}{Cf_g + Cf_l + f_g f_l}\rho_l g$$

By some rearranging is following expression, equation (4.36), achieved for pressure:

$$\partial_x P = -\frac{\frac{\alpha_g^2 f_l + \alpha_g C}{Cf_g + Cf_l + f_g f_l}\rho_g + \frac{\alpha_l^2 f_g + \alpha_l C}{Cf_g + Cf_l + f_g f_l}\rho_l}{\frac{\alpha_g^2 f_l + \alpha_g C}{Cf_g + Cf_l + f_g f_l} + \frac{\alpha_l^2 f_g + \alpha_l C}{Cf_g + Cf_l + f_g f_l}} g$$

Which by defining some variables can be rewritten to equation (4.37):

$$\partial_x P = -\frac{\lambda_g \rho_g + \lambda_l \rho_l}{\lambda_g + \lambda_l} g = -\frac{\lambda_g \rho_g + \lambda_l \rho_l}{\lambda_t} g$$

where λ_g, λ_l and λ_t are defined respectively as, equations (4.38)-(4.40):

$$\lambda_g = \frac{\alpha_g^2 f_l + \alpha_g C}{Cf_g + Cf_l + f_g f_l}$$

$$\lambda_l = \frac{\alpha_l^2 f_g + \alpha_l C}{Cf_g + Cf_l + f_g f_l}$$

$$\lambda_t = \lambda_g + \lambda_l = \frac{\alpha_g^2 f_l + \alpha_l^2 f_g + C}{Cf_g + Cf_l + f_g f_l}$$

9.3 Derivation of the superficial velocities

By implementing the expressions for λ_g, λ_l and λ_t into the superficial velocity expressions, equation (4.34) and (4.35), are following achieved:

$$u_{gs} = -\lambda_g \partial_x P - \lambda_g \rho_g g - \frac{\alpha_g \alpha_l (\rho_l - \rho_g) C}{Cf_g + Cf_l + f_g f_l} g$$

$$u_{ls} = \lambda_l \partial_x P - \lambda_l \rho_l g + \frac{\alpha_g \alpha_l (\rho_l - \rho_g) C}{Cf_g + Cf_l + f_g f_l} g$$

When implementing the expression for pressure, equation (4.37) are following expressions obtained:

$$u_{gs} = \frac{\lambda_g \rho_g + \lambda_l \rho_l}{\lambda_t} \lambda_g g - \lambda_g \rho_g g - \frac{\alpha_g \alpha_l (\rho_l - \rho_g) C}{Cf_g + Cf_l + f_g f_l} g$$

$$u_{ls} = \frac{\lambda_g \rho_g + \lambda_l \rho_l}{\lambda_t} \lambda_l g - \lambda_l \rho_l g + \frac{\alpha_g \alpha_l (\rho_l - \rho_g) C}{Cf_g + Cf_l + f_g f_l} g$$

which corresponds to (4.43). By using the relation between λ_g, λ_l and λ_t: $\lambda_t = \lambda_g + \lambda_l$ which means that:

$$\lambda_g = \lambda_t - \lambda_l$$

$$\lambda_l = \lambda_t - \lambda_g$$

Makes the expression rewritten to:

$$u_{gs} = \frac{(\lambda_t - \lambda_l)\rho_g + \lambda_l \rho_l}{\lambda_t} \lambda_g g - \lambda_g \rho_g g - \frac{\alpha_l \alpha_g (\rho_l - \rho_g) C}{Cf_g + Cf_l + f_g f_l} g$$

$$u_{ls} = \frac{\lambda_g \rho_g - (\lambda_t - \lambda_g)\rho_l}{\lambda_t}\lambda_l g - g\rho_l\lambda_l + \frac{\alpha_l\alpha_g(\rho_l - \rho_g)C}{Cf_g + Cf_l + f_g f_l}g$$

This can be reduced by take the part with λ_t out of the fraction, equation (4.44):

$$u_{gs} = \frac{\lambda_l(\rho_l - \rho_g)}{\lambda_t}\lambda_g g + \lambda_g\rho_g g - \lambda_g\rho_g g - \frac{\alpha_l\alpha_g(\rho_l - \rho_g)C}{Cf_g + Cf_l + f_g f_l}g$$

$$u_{ls} = \frac{\lambda_g(\rho_g - \rho_l)}{\lambda_t}\lambda_l g + \lambda_l\rho_l g - \lambda_l\rho_l g + \frac{\alpha_l\alpha_g(\rho_l - \rho_g)C}{Cf_g + Cf_l + f_g f_l}g$$

Set $\Delta\rho = \rho_l - \rho_g$, which leads to, equation (4.45):

$$u_{gs} = \frac{\lambda_l\lambda_g}{\lambda_t}\Delta\rho g - \frac{\alpha_l\alpha_g C}{Cf_g + Cf_l + f_g f_l}\Delta\rho$$

$$u_{ls} = -\frac{\lambda_l\lambda_g}{\lambda_t}\Delta\rho g + \frac{\alpha_l\alpha_g C}{Cf_g + Cf_l + f_g f_l}\Delta\rho g$$

By implementing the relations for λ_g, λ_l and λ_t in order to reduce the expression further, equation (4.46).

$$u_{gs} = \frac{\frac{(\alpha_l^2 f_g + \alpha_l C)(\alpha_g^2 f_l + \alpha_g C)}{(Cf_g + Cf_l + f_g f_l)^2}}{\frac{\alpha_l^2 f_g + \alpha_g^2 f_l + C}{Cf_g + Cf_l + f_g f_l}}\Delta\rho g - \frac{\alpha_l\alpha_g C}{Cf_g + Cf_l + f_g f_l}\Delta\rho g$$

$$u_{ls} = -\frac{\frac{(\alpha_l^2 f_g + \alpha_l C)(\alpha_g^2 f_l + \alpha_g C)}{(Cf_g + Cf_l + f_g f_l)^2}}{\frac{\alpha_l^2 f_g + \alpha_g^2 f_l + C}{Cf_g + Cf_l + f_g f_l}}\Delta\rho g + \frac{\alpha_l\alpha_g C}{Cf_g + Cf_l + f_g f_l}\Delta\rho g$$

As seen is $Cf_g + Cf_l + f_g f_l$ a common term in the first fraction reducing these equations to:

$$u_{gs} = \frac{(\alpha_l^2 f_g + \alpha_l C)(\alpha_g^2 f_l + \alpha_g C)}{(Cf_g + Cf_l + f_g f_l)(\alpha_l^2 f_g + \alpha_g^2 f_l + C)}\Delta\rho g - \frac{\alpha_l\alpha_g C}{Cf_g + Cf_l + f_g f_l}\Delta\rho g$$

$$u_{ls} = -\frac{(\alpha_l^2 f_g + \alpha_l C)(\alpha_g^2 f_l + \alpha_g C)}{(Cf_g + Cf_l + f_g f_l)(\alpha_l^2 f_g + \alpha_g^2 f_l + C)}\Delta\rho g + \frac{\alpha_l\alpha_g C}{Cf_g + Cf_l + f_g f_l}\Delta\rho g$$

A common denominator for the fractions is seen to be $(Cf_g + Cf_l + f_g f_l)(\alpha_l^2 f_g + \alpha_g^2 f_l + C)$, which is used to simplify the expressions:

$$u_{gs} = \frac{(\alpha_l^2 f_g + \alpha_l C)(\alpha_g^2 f_l + \alpha_g C)}{(Cf_g + Cf_l + f_g f_l)(\alpha_l^2 f_g + \alpha_g^2 f_l + C)}\Delta\rho g - \frac{\alpha_l\alpha_g C(\alpha_l^2 f_g + \alpha_g^2 f_l + C)}{(Cf_g + Cf_l + f_g f_l)(\alpha_l^2 f_g + \alpha_g^2 f_l + C)}\Delta\rho g$$

$$u_{ls} = -\frac{(\alpha_l^2 f_g + \alpha_l C)(\alpha_g^2 f_l + \alpha_g C)}{(Cf_g + Cf_l + f_g f_l)(\alpha_l^2 f_g + \alpha_g^2 f_l + C)}\Delta\rho g + \frac{\alpha_l\alpha_g C(\alpha_l^2 f_g + \alpha_g^2 f_l + C)}{(Cf_g + Cf_l + f_g f_l)(\alpha_l^2 f_g + \alpha_g^2 f_l + C)}\Delta\rho g$$

leads to:

$$u_{gs} = \frac{\alpha_l^2\alpha_g^2 f_l f_g + \alpha_l^2\alpha_g f_g C + \alpha_l\alpha_g^2 f_l C + \alpha_l\alpha_g C^2}{(Cf_g + Cf_l + f_g f_l)(\alpha_l^2 f_g + \alpha_g^2 f_l + C)}\Delta\rho g - \frac{\alpha_l^3\alpha_g f_g C + \alpha_l\alpha_g^3 f_l C + \alpha_l\alpha_g C^2}{(Cf_g + Cf_l + f_g f_l)(\alpha_l^2 f_g + \alpha_g^2 f_l + C)}\Delta\rho g$$

$$u_{ls} = -\frac{\alpha_l^2\alpha_g^2 f_l f_g + \alpha_l^2\alpha_g f_g C + \alpha_l\alpha_g^2 f_l C + \alpha_l\alpha_g C^2}{(Cf_g + Cf_l + f_g f_l)(\alpha_l^2 f_g + \alpha_g^2 f_l + C)}\Delta\rho g + \frac{\alpha_l^3\alpha_g f_g C + \alpha_l\alpha_g^3 f_l C + \alpha_l\alpha_g C^2}{(Cf_g + Cf_l + f_g f_l)(\alpha_l^2 f_g + \alpha_g^2 f_l + C)}\Delta\rho g$$

Rearrange the expression and see that $\alpha_l\alpha_g C$ falls out.

$$u_{gs} = \frac{\alpha_l\alpha_g(\alpha_l\alpha_g f_l f_g + \alpha_g(1-\alpha_g)f_l C + \alpha_l(1-\alpha_l)f_g C}{(Cf_g + Cf_l + f_g f_l)(\alpha_l^2 f_g + \alpha_g^2 f_l + C)}\Delta\rho g$$

$$u_{ls} = -\frac{\alpha_l\alpha_g(\alpha_l\alpha_g f_l f_g + \alpha_g(1-\alpha_g)f_l C + \alpha_l(1-\alpha_l)f_g C}{(Cf_g + Cf_l + f_g f_l)(\alpha_l^2 f_g + \alpha_g^2 f_l + C)}\Delta\rho g$$

Again is the constrain of $\alpha_l + \alpha_g = 1$:

$$u_{gs} = \frac{\alpha_l^2\alpha_g^2(Cf_g + Cf_l + f_g f_l)}{(Cf_g + Cf_l + f_g f_l)(\alpha_l^2 f_g + \alpha_g^2 f_l + C)}\Delta\rho g$$

$$u_{ls} = -\frac{\alpha_l^2\alpha_g^2(Cf_g + Cf_l + f_g f_l)}{(Cf_g + Cf_l + f_g f_l)(\alpha_l^2 f_g + \alpha_g^2 f_l + C)}\Delta\rho g$$

$Cf_g + Cf_l + f_g f_l$ is a common term gives equation (4.47):

$$u_{gs} = \frac{\alpha_l^2\alpha_g^2}{\alpha_l^2 f_g + \alpha_g^2 f_l + C}\Delta\rho g$$

$$u_{ls} = -\frac{\alpha_l^2\alpha_g^2}{\alpha_l^2 f_g + \alpha_g^2 f_l + C}\Delta\rho g$$

By using the constrain of volume fractions again can the superficial phase velocity be expressed with only its own phase volume fraction, equations (4.48) and (4.49).

$$u_{gs} = \frac{\alpha_g^2(1-\alpha_g)^2}{(1-\alpha_g)^2 f_g + \alpha_g^2 f_l + C}\Delta\rho g$$

$$u_{ls} = -\frac{\alpha_l^2(1-\alpha_l)^2}{\alpha_l^2 f_g + (1-\alpha_l)^2 f_l + C}\Delta\rho g$$

Which may also be written as:

$$u_{gs} = \frac{(\alpha_g - \alpha_g^2)^2}{(1-\alpha_g)^2 f_g + \alpha_g^2 f_l + C}\Delta\rho g$$

$$u_{ls} = -\frac{(\alpha_l - \alpha_l^2)^2}{\alpha_l^2 f_g + (1-\alpha_l)^2 f_l + C}\Delta\rho g$$